# Edgetones and Acoustic Resonances in a Duct

Thesis by
Kim Maynard Aaron

In Partial Fulfillment
of the Requirements for the Degree of
Doctor of Philosophy

California Institute of Technology
Pasadena, California

1985
(submitted May 24th, 1985)

For my parents, who gave me the desire to learn

## ACKNOWLEDGMENTS

This work was supported by the Air Force Office of Scientific Research under grant AFOSR-84-0286 and by the California Institute of Technology.

I would like to thank my advisor, Dr. F.E.C. Culick, from whom I learned a great deal throughout the course of this work. The suggestions of my committee members, Drs. A. Acosta, T. Kubota, F.E. Marble, A. Roshko and E.E. Zukoski, were very useful. In particular, Dr. Kubota laid the foundation on which the model was built and inspired me to tackle that part of the project with renewed vigor.

The expert counseling of Ms. Manya Jiannino kept me going during the last few months.

Mr. Larry Chew assisted with a few of the experiments and with the preparation of the graphs, while Mrs. Betty Wood used her expertise to create most of the line drawings.

Discussion of ideas with Mr. Lorenz Sigurdson and Mr. Thomas H. Sobota were very helpful.

Mr. Duncan Still and Dr. Alan A. Vetter loaned me some of their personal equipment to make the work easier.

The support of Ms. Camille Kunze throughout was invaluable.

Many others helped in some way. Thank you all.

## ABSTRACT

Undesirable sound generation in the combustion chamber of segmented solid propellant rocket motors has been attributed to vortex shedding from obstructions that are uncovered as the propellant burns back. This phenomenon has been investigated experimentally and the mechanism explained.

A pair of aluminum baffles within a lucite duct through which air is drawn models the important aspects which enable the sound generation mechanism to operate. The baffles form an edgetone system which interacts with the longitudinal acoustic modes of the chamber. Acoustic tones occur spontaneously, at frequencies determined by the acoustic resonances, when the spacing between the baffles satisfies certain criteria.

Flow visualization using smoke and a strobe light triggered by the pressure oscillations indicate that vortex shedding occurs at the first baffle in phase with the acoustic velocity oscillations there. The interaction of these vortices with the downstream baffle drives the acoustic resonance which, in turn, triggers the formation of new vortices at the upstream separation point.

The phase relations for this feedback to operate require that there be close to an integral number of wavelengths, or vortices, from the separation point to the impingement point.

A model has been developed which predicts the experimentally observed behaviour well. Pressure amplitudes are predicted within an order of magnitude. Mean flow rates and baffle spacings yielding maximum response are determined correctly by the model.

# TABLE OF CONTENTS

## LIST OF SYMBOLS

| Symbol | Description |
|---|---|
| $a$ | Radius of half-round baffle (m) |
| $A$ | Amplitude of resonator |
| $A_1$, $A_2$ | Amplitudes of acoustic waves (m) |
| $B_1$, $B_2$ | Amplitudes of acoustic waves (m) |
| $B$ | Proportionality constant between response velocity and driving force for resonator |
| $B_s$ | Saturated driving amplitude for resonator |
| $c$ | Speed of sound (m/s) |
| $f$ | Frequency (Hz) |
| $f_1$, $f_2$ | frequencies at which response power is half the maximum value |
| $f(\dot{\eta})$ | Forcing function |
| $F$ | Force of baffle on air in duct |
| $G$ | Dimensionless forcing pressure in duct |
| $h$ | Height of baffles (m) |
| $k$ | Wavenumber (radians/m) |
| $L$ | Length of duct (m) |
| $p$ | Pressure ($N/m^2$) |
| $p'$ | Acoustic pressure ($N/m^2$) |
| $Q$ | Quality factor of a resonator |
| $r_d$ | Radius of circle with same area as duct (m) |
| $S$ | Strouhal number (non-dimensional frequency), $f\Delta x/U_\infty$ |
| $S_\theta$ | Strouhal number based on momentum thickness, $f\theta/\Delta U$ |
| $S$ | Cross-sectional area of duct |
| $t$ | Time (s) |
| $T$ | Period of resonator (s) |
| $u$ | Velocity (m/s) |
| $u'$ | Acoustic Velocity (m/s) |

| | |
|---|---|
| $u_1$ | Fluctuating velocity on low speed side of shear layer (m/s) |
| $u_2$ | Fluctuating velocity on high speed side of shear layer (m/s) |
| $u_m$ | Mean of peak fluctuating velocities on two sides of shear layer, $(u_1 + u_2)/2$ (m/s) |
| $u_v$ | x component of $U_v$ |
| U | Freestream velocity in potential flow calculation |
| $U_\infty$ | Freestream velocity between baffles (m/s) |
| $U_c$ | Convection velocity of vortices (m/s) |
| $U_v$ | Velocity of vortex in potential flow calculation |
| $U_1$ | Mean velocity on low speed side of shear layer (m/s) |
| $U_2$ | Mean velocity on high speed side of shear layer (m/s) |
| $\Delta U$ | Velocity difference across shear layer, $U_2 - U_1$ (m/s) |
| $v_v$ | y component of $U_v$ |
| w | Complex potential function |
| x | Streamwise coordinate measured downstream from inlet (m) |
| $x_1$ | Location of upstream baffle (m) |
| $x_2$ | Location of downstream baffle (m) |
| $\Delta x$ | Baffle spacing, $x_2 - x_1$ (m) |
| X | Drag on baffle (N/m) |
| y | Streamwise coordinate measured upstream from exit, L-x (m) |
| y | Coordinate across duct (m) |
| Y | Lift on baffle (N/m) |
| z | Complex coordinate in potential flow calculation |
| $z_o$ | Location of vortex |
| $z^*$ | Complex conjugate of z |
| Z | Dimensionless impedance, $p'/\rho u'c$ |

| | |
|---|---|
| $\alpha$ | Exponential growth rate constant |
| $\eta$ | Displacement of resonator |
| $\dot{\eta}$ | Velocity of resonator |
| $\dot{\eta}_{o-p}$ | Zero to peak amplitude of velocity |
| $\theta$ | Momentum thickness of shear layer (m) |
| $\lambda$ | Wavelength; distance between consecutive vortices (m) |
| $\xi$ | Acoustic displacement (m) |
| $\rho$ | Density ($kg/m^3$) |
| $\bar{\rho}$ | Mean density ($kg/m^3$) |
| $\rho'$ | Acoustic density ($kg/m^3$) |
| $\tau$ | Time lag between response and driving of resonator (s) |
| $\phi$ | Phase between forcing and response of resonator (radians) |
| $\phi$ | Potential function |
| $\psi$ | Stream function |
| $\omega$ | Circular frequency, $2\pi f$ (radians/s) |
| $\omega_o$ | Resonant frequency (radians/s) |
| $\Delta\omega$ | Shift in resonant frequency (radians/s) |
| $\Gamma$ | Strength of vortex (circulation/$2\pi$) |
| $\dot{x}$ | Dot represents time derivative of quantity, x |
| $\bar{x}$ | Bar denotes mean of quantity, x |
| $x'$ | Prime denotes fluctuating component of quantity, x |

## LIST OF FIGURES

# Chapter 1
# INTRODUCTION

Undesirable spontaneous acoustic oscillations have been observed in segmented solid propellant rocket motors at frequencies equal to the longitudinal acoustic organ pipe modes of the combustion chambers. Since the cause was not known, limiting amplitudes could not be predicted. Such oscillations occurred in the space shuttle boosters at 15Hz. While it is unlikely that the pressure amplitude could grow to a level that could cause failure of the motor case, previous experience has shown that vibrations of this sort could cause other structural damage or failure of equipment with a mechanical resonance at a nearby frequency. This frequency is also close to the resonant frequency of the human eyeball and although the amplitudes have never reached sufficiently high levels to impair reading of instruments, the vibrations have been noticeable to the astronauts. Further increases in the amplitude could cause difficulties.

These oscillations occur in a class of rockets which are constructed with the solid propellant in large segments which are loaded into the case individually. This procedure is mainly for ease of casting and handling the large blocks of propellant. A large retaining ring is installed between each segment and bonded to the ends of the propellant grain segments to inhibit burning other than on the lateral surfaces. This configuration is depicted schematically in Figure 1.1 on page 5. These inhibitors are made of a material that burns more slowly than the propellant and thus they protrude into the mean flow as the propellant

burns back.

In 1975, Flandro and Jacobs (1) first suggested that vortex shedding from these protrusions may be driving the acoustic resonances to produce the unwanted oscillations. This finding now appears correct but the actual mechanism by which the vortex shedding interacts with the acoustic resonances was not well understood at that time.

The aim of the present investigation has been to understand this interaction mechanism by performing laboratory experiments. Based on the understanding gained from these experiments and from the work of others, a mechanism has been proposed and is described below. From the postulated mechanism, a model has been developed which predicts the behaviour observed experimentally.

### 1.1. Postulated Mechanism.

The postulated mechanism is as follows. The protruding inhibitors act as separation points resulting in the formation of shear layers. In such a shear layer, vortices grow due to the instability of the flow as investigated by Freymuth (2) and Michalke (3,4,5). The vortices initially grow exponentially in the streamwise direction, but eventually their strengths reach a saturated value. This saturation process is the amplitude limiting aspect of the entire interaction. As the vortices are convected downstream by the mean flow, they pass another protruding inhibitor resulting in a fluctuation of the drag force acting on this obstacle. By Newton's second law, since the fluid is applying a fluctuating force on the obstacle, the obstacle applies an equal and opposite force on the fluid. This

oscillating force drives the acoustic resonance of the chamber at a frequency equal to that of the passage of the vortices. The acoustic velocity at the location of the separation point acts as a perturbation which triggers the formation of new vortices in phase with the acoustic response. Thus, there is a closed feedback loop and the whole process can be self-excited. This is the main idea to be investigated and has not been advanced in previous investigations of oscillations in rocket motors.

Since the proposed mechanism does not involve the burning processes, a cold flow apparatus is used. Difficulties associated with instrumenting hot flows are thus avoided. Other experimental investigations of this type of oscillation confirm that the mechanism operates in the absence of burning (6,7,8,9,10,11).

## 1.2. Examples of Self-Excited Oscillations.

In their book, "Theory of Oscillations," Andronow and Chaikin (12) define a self-oscillatory system as one that generates a periodic process from a non-periodic source. Stoker, in his book, "Nonlinear Vibrations," (13) includes the oscillations of the Tacoma bridge and flutter of aircraft wings in the class of self-excited oscillations since the vibration results through partial conversion of energy from a steady flow (in these cases the wind) into oscillations. Both books include clocks and electronic oscillators as examples. Such autonomous systems spontaneously undergo oscillations at frequencies and amplitudes determined by their physical characteristics. In the rocket motors, the energy of oscillation comes from the free stream and ultimately from the chemical energy of

combustion.

A few examples of self-excited systems which are more closely related to the combustion chamber type of oscillation are presented in Figure 1.1. It will be recognized that the cavity flow, which is a type of edgetone, constitutes part of the system that contributes to the self-sustained oscillation in the combustion chamber. In an edgetone, as the vortices in the shear layer interact with the downstream obstacle, they induce a velocity at the separation point upstream, which triggers the further formation of vortices. In one version of a tea-kettle whistle, this phenomenon is put to good use. Escaping steam is made to pass through two consecutive concentric disks forming a hole-tone. A tube-like shear layer forms in which ring vortices grow, much like smoke rings, before colliding with the second disk. In addition to triggering the continued formation of vortices, the disturbances due to the passage of the ring vortices through the hole in the second disk are also heard as the tone announcing that the water is boiling.

## 1.3. Shear Layer Instability.

A shear layer forms when there is a region in which two streams of fluid moving parallel to one another have different velocities. Shear layers are unstable to disturbances in a range of frequencies dependent upon the thinness of the layer and the velocity difference across the layer. This instability has been investigated extensively (2,3,4,5) and remarkable agreement has been found between theory and experiment. In order to make the frequency dimensionless, a Strouhal number is formed based on

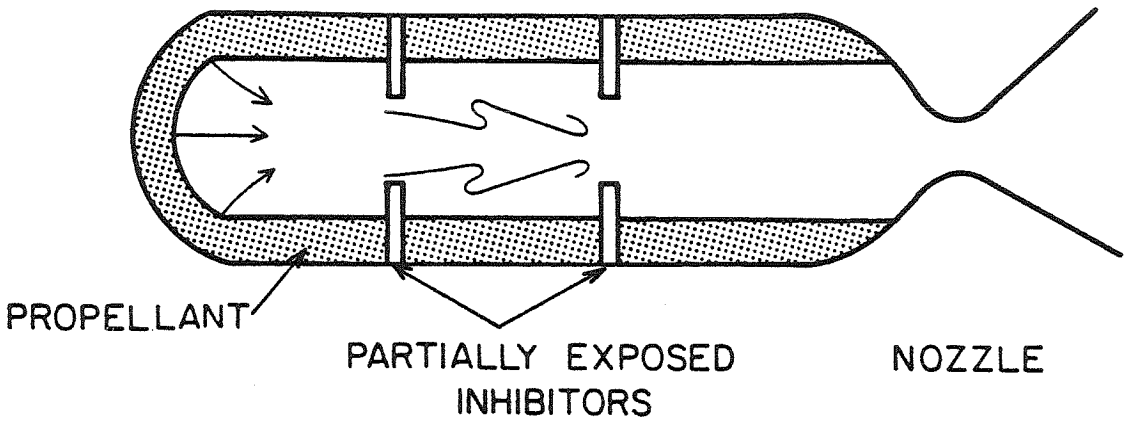


SEGMENTED SOLID PROPELLANT ROCKET

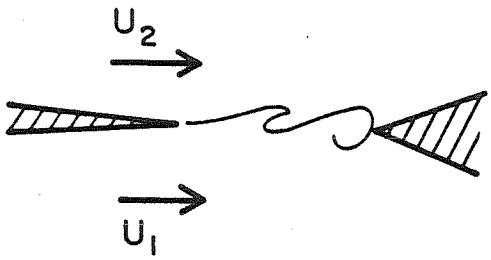


EDGE TONE

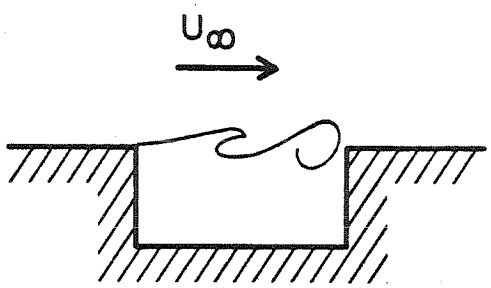


CAVITY FLOW

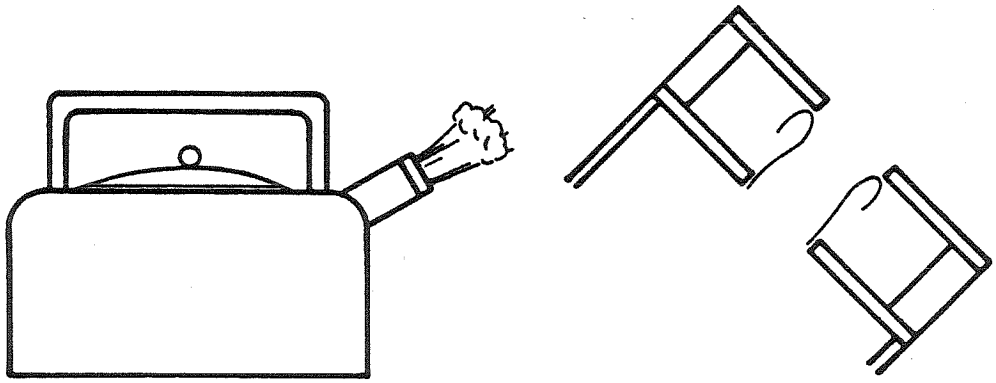

TEA-KETTLE WHISTLE (HOLE TONE)

FIGURE 1.1 CONFIGURATIONS IN WHICH SELF-EXCITED OSCILLATIONS OCCUR

appropriate parameters describing the shear layer: its momentum thickness, $\theta$, and the velocity difference across the shear layer, $\Delta U = U_2 - U_1$:

$$S_\theta = \frac{f\theta}{\Delta U} \qquad (1.1)$$

$$\theta = \int_{-\infty}^{\infty} \frac{u-U_1}{\Delta U} \frac{U_2-u}{\Delta U}\, dy \qquad (1.2)$$

where $U_1$ and $U_2$ are the velocities on either side of the layer. The instability properties of the shear layer are found to depend only on $S_\theta$ to a good approximation. If a wavy disturbance is present with a frequency in the amplified range then this disturbance will grow and form vortices at the same frequency. Since the shear layer selectively amplifies velocity fluctuations, in the absence of any significant disturbance, vortices will tend to grow at the frequency with the largest growth rate for the particular conditions of the shear layer. Experiment and theory agree that this corresponds to a Strouhal number of about 0.017 (5).

The vortices grow exponentially in the streamwise direction according to the growth rate, $\alpha$, corresponding to the Strouhal number. Eventually, non-linearity not included in the theory limits the growth and the amplitude saturates at a value which can be determined experimentally as a function of Strouhal number. Although Freymuth (2) concentrates on the growth region, his data indicate the saturation values. This saturation of the strengths of the vortices is the amplitude limiting process in the self-excited mechanism being investigated here.

## 1.4. The Edgetone.

An edgetone is created when an edge is placed in the path of a shear layer. As the vortices are convected past the edge, velocity fluctuations are induced at the origin of the shear layer resulting in the formation of subsequent vortices. This is part of the overall mechanism being investigated and several extensive reviews (8,14,15) have been written describing the edgetone in detail.

Although no tone is generated, an edgetone can operate in water. Such a flow has been investigated in detail by Ziada and Rockwell (18) with a shear layer in a water channel impinging on a wedge downstream. For flows with mean velocities much smaller than the speed of sound, as in the experiments of Ziada and Rockwell, the time for the vortex to travel from the separation point to the impingement point is much greater than the time for the acoustic signal to travel back to the separation point to induce the next vortex. Thus the time between successive vortices is equal to the time of flight from separation to impingement. The frequency is therefore proportional to the velocity and inversely proportional to the spacing between the separation and impingement points. This frequency can be made non-dimensional by multiplying it by the spacing, $\Delta x$, and dividing by the mean velocity, U. The resultant number is also a Strouhal number:

$$S = \frac{f\Delta x}{U} \qquad (1.3)$$

For an edgetone, this Strouhal number remains constant as the spacing and velocity are changed.

It is possible to have more than one vortex between separation and impingement. Each vortex still triggers a new vortex, but there are now other vortices in between the two. The number of vortices is referred to as the stage of operation. Transitions from one stage to another occur abruptly as either the velocity or the spacing is gradually changed. Accompanying the transition, there is a jump in the Strouhal number to a new value that remains essentially constant throughout the new stage.

Experimentally, it has been observed that the spacing, $\Delta x$, corresponds to approximately an integral number of wavelengths (the distance from one vortex to the next) and that the vortices convect at a speed close to the mean of the two freestreams of fluid flowing past the edgetone system. Since the frequency multiplied by the wavelength is defined as the convection velocity, these results suggest a value for S of approximately n/2, where n is the stage number. Experimentally measured values generally fall in the range of about 0.2 - 2.0 for edgetones in a variety of configurations (6,7,8,9,10,11,14,15,16,17).

Since the shear layer responds with different growth rates to different frequencies (or wavelengths) there is usually one stage which has the largest growth rate. If one considers slowly increasing the edgetone distance, $\Delta x$, one expects the wavelength to increase proportionately. Eventually a point is reached at which the next stage is preferred. The operating stage continues, however, since it has a much stronger perturbation than the new frequency. As $\Delta x$ is increased further, the amplification of the existing stage reduces to the point that random fluctuations at the frequency corresponding to the next stage can grow to a sufficient level that the old stage of operation is

replaced by the new frequency. The transition occurs rapidly and the number of vortices increases by one.

If the $\Delta x$ is now reduced, the new stage will remain dominant for some distance until the old stage becomes sufficiently strong that random fluctuations at its frequency permit it to overcome the existing stage. Thus there is a range of spacing over which either of two stages can operate, depending upon the direction of approach. This behaviour is referred to as "hysteresis" and is common in systems with edgetones. Why the existence of vortices at one frequency inhibits the formation of vortices at another is not understood; the description above is simply an explanation of how this inhibition results in hysteresis in edgetones.

### 1.5. Coupled Edgetone and Resonator.

If an edgetone is placed inside an acoustic resonator, it may interact with the acoustic oscillations as mentioned above. In the absence of a resonator an edgetone can oscillate over a range of frequencies. When a resonator is coupled with the edgetone, it is observed that the frequency remains nearly constant and equal to the natural frequency of the resonator. Thus, it is reasonable to assume that the perturbations to which the shear layer is responding are due to the resonator instead of due to the hydrodynamically-induced velocity of the vortices passing the downstream point. The formation of each vortex is triggered by the response of the resonator rather than directly by the motion of the previous vortices downstream.

The oscillation occurs at any one of a series of discrete natural frequencies (that is, harmonics) of the resonator. Since the formation of vortices is triggered by the resonator, each vortex is initiated at the same point in the cycle. The frequency remains essentially constant so changing the velocity or spacing must cause the vortices to arrive at the downstream impingement point at different phases in the cycle of the oscillator. Thus, there must be a phase difference between the forcing and the response of the oscillator which changes with flowrate or separation distance. For a simple damped linear oscillator treated in many elementary texts (19) it is well known that there is such a phase difference which depends upon the driving frequency. For a lightly damped system, the phase varies considerably for a small change in the driving frequency in the neighbourhood of resonance. Thus, if a phase difference is imposed, the frequency will differ very little from the natural frequency.

## 1.6. Edgetones in Combustion Chambers - Previous Work.

From investigations made during the past decade, it is now known that the phenomenon termed the edgetone is one source of acoustic oscillations in solid rocket motors. Although edgetones have been observed for more than a century, their connection with unexpected oscillations in combustion chambers was not made until quite recently. As previously mentioned, the first suggestion that vortex shedding from discontinuities within the chamber could couple with acoustic resonances came from Flandro and Jacobs (1) in 1975. They did not make the direct association with the edgetone at that time, however. In their paper, a model is suggested in which vortices form at geometric

disturbances and then interact with the acoustic resonances of the chamber. In their formulation, there is no downstream impingement point critical to the operation of an edgetone system. We quote from reference (1), "acoustic waves are produced in a manner analogous to the well-known Aeolian tone resulting from a Karman vortex street." This implies that the resultant acoustic disturbances are due to reaction forces on the body from which the vortices are shed rather than from some other body that the vortices pass later. Their model correctly assumes, based on experimental results, that the shedding of vortices is dominated by the acoustic waves present and therefore that they form at the same frequency. It incorrectly assumes that the strength of the vortical disturbance is proportional to the amplitude of the acoustic pressure. This leads to the conclusion that greater growth rates will occur if the geometric discontinuity is near a pressure antinode. This has since been shown to be incorrect by the experiments of Dunlap and Brown (10) described below, and also in the present work. In fact the strongest response occurs when the edges are near a velocity antinode, the point at which the pressure amplitude is minimum.

It was first demonstrated by Culick and Magiawala (6) that two discontinuities are necessary for the existence of spontaneous oscillations with any significant amplitude. For a very restricted range of baffle location near the midpoint of the duct they observed weak oscillations with a single baffle. Their apparatus consisted of a lucite tube containing a pair of annular baffles through which air was forced by a blower. Only frequencies at resonant modes of the tube were observed and the corresponding Strouhal numbers ranged from 0.4 to 1. They found that the location of the baffle pair within the duct was important in

determining whether or not oscillations would occur but it seems they did not recognize that the strongest response would occur if the baffles were placed at a velocity antinode.

In response to the findings of Culick and Magiawala (6), a more realistic cold-flow scale model of a solid rocket motor was studied theoretically and experimentally by Brown et al. (8,9). Spontaneous oscillations occurred only at frequencies corresponding to longitudinal resonant modes of the combustion chamber of the Titan rocket modeled, confirming that coincidence between vortex shedding and resonant frequencies is required. Strouhal numbers in the range of 0.5 to 2 were measured, Conventional stability calculations for the configuration modeled predicted strongly negative growth rates ($\alpha < -10$ for most of the burn) implying that the observed oscillations should not have arisen. Brown et al. (9) report without reference that similar discrepancies between predicted and actual behavior have been observed for the Space Shuttle Booster and by ONERA in one of their large solid propellant motors. They concluded that vortex shedding is indeed a significant source of acoustic energy not included in the stability prediction. While they conclude that feedback from the acoustic field to the growing vortices occurs, the effect of feedback is ignored in the analysis developed. They confirmed experimentally that at least two restrictors are necessary for sustained oscillations and assume that the effect of the downstream baffle is to disrupt the vortices in the shear layer, preventing their driving the acoustic field further. The same assumption is made by Flandro and Finlayson (20). While it is very unlikely for vortices to collide with a solid object and not be disrupted, it seems that the interaction itself will produce a much larger

driving force than the weak interaction of the growing vortices upstream with the acoustic field.

In a much simpler apparatus, Dunlap and Brown (10) then demonstrated that with nitrogen flowing past a pair of restrictors within a tube, only acoustic modes with velocity antinodes (pressure nodes) near the location of the restrictor pair were excited. Modes with a pressure antinode there did not respond at all. Their apparatus consisted of a tube with a small inlet and an exhaust port at the ends which otherwise were closed. Restrictors made of two washers mounted close together, near the midpoint of the tube, constituted the edgetone part of the system. Both the fundamental resonance and the third mode have acoustic velocity antinodes at that point, but the second mode has a node there. They were unable to excite the second mode at all, but could easily observe the first and third modes at appropriate mean velocities. In order to cause the third mode to oscillate spontaneously they had to triple the mean velocity at which the first mode was excited. This is consistent with the idea that, since the period of a cycle of the third mode is one third of the period of the fundamental, the vortices must travel with three times the speed to cover the distance between the baffles.

The apparatus used in the present investigation was first designed by Nomoto in order to perform experiments for his Engineer's thesis (7). His results are discussed in a more readily available article by Nomoto and Culick (11). By synchronizing a strobe light to flash at the same frequency as the oscillation, Nomoto was able to take photographs of the vortices, made visible using smoke, which clearly demonstrate that vortex shedding is associated with

the oscillation. The frequencies of operation were observed to be almost constant over large velocity ranges and were dictated by the organ-pipe resonances of the duct.

Following the analysis of Rossiter (16) dealing with flow over cavities, Nomoto (7) assumed that the acoustic disturbance generated by the collision of a vortex with the downstream baffle travels upstream and directly triggers the formation of another vortex as in an isolated edgetone. He was thus unable to explain why oscillations occur over ranges of velocity and baffle spacing rather than just at the intersections of lines of constant Strouhal number for the edgetone with lines of constant frequency for the acoustic resonator, as depicted in Figure 1.2. He suggested that some interaction between the two systems was occurring and that the location of the baffles with respect to the acoustic modes may be important, but was not more specific than that.

A similar flow was investigated by Schachenmann and Rockwell (21,22,23). In their apparatus, air is blown through a long tube terminated by a hole-tone cavity which interacts with the organ pipe resonances of the tube. The mean flow rate and distance from separation to the edge are variable. As in Nomoto's apparatus (also used in the present work) the oscillations occur predominantly at the resonant frequencies of the resonator. They find that the resonance is strongest when there is a phase difference of $2n\pi$ between the fluctuating velocities at separation and impingement, meaning that there is an integral number of wavelengths or vortices between the two points. As the mean velocity or spacing is changed, this phase difference varies up to 50° according to the results reported (22). This is in agreement with the model postulated here.

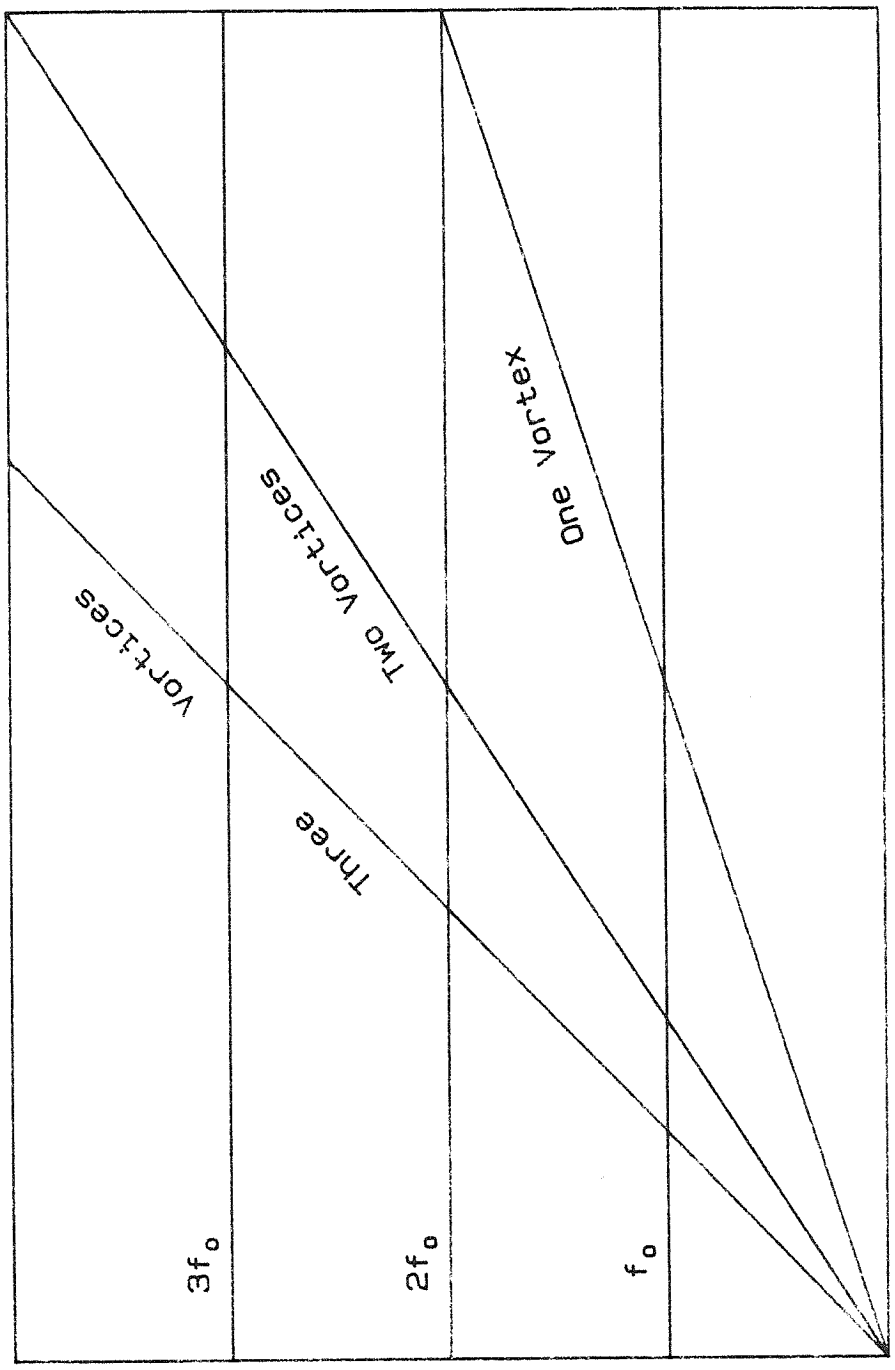


Figure 1.2 Edgetone and Resonator Coincidence Points (after Nomoto (7))

## 1.7. Summary.

A mechanism is postulated which explains the occurrence of self-excited oscillations at resonant frequencies in a duct. This mechanism is probably applicable in the combustion chambers of segmented solid propellant rocket motors. Based on this physical explanation, a model is developed which correctly predicts the behaviour observed in the apparatus and gives amplitudes with the correct order of magnitude.

In the next chapter, the apparatus and instrumentation will be described. Following that, in Chapter 3, the physical model postulated will be quantitatively analyzed. In Chapter 4, the results of the experiments and the analyses will be presented and compared, with final conclusions summarized in Chapter 5.

# Chapter 2
# EXPERIMENTAL APPARATUS

The main part of the experimental apparatus is a rectangular lucite duct through which air flows. This chamber models the aspects of a rocket combustion chamber that are important to the operation of the sound generation mechanism being studied. The duct and various attachments are mounted on a framework of Ames angle iron to raise it to a convenient height above the floor of the laboratory.

Two pairs of baffles can be placed at almost any location inside the duct and are connected by rectangular brass bars which fit in four grooves in the walls of the duct. The baffles act as the separation and impingement points necessary to form an edgetone system. They are modeled after the geometry that occurs in the combustion chamber of a solid propellant rocket when inhibitors protrude into the flowfield as the propellant burns back. A diagram of the apparatus is given in Figure 2.1.

## 2.1. The Flow System.

The duct is 50cm long and has a rectangular cross-section, 5cm x 15cm, which makes flow visualization easier. Air is drawn through the duct by a blower located downstream and driven by a 1.5 HP Gould Century DC motor whose speed can be adjusted using a Minirik Blue Chip II constant speed motor controller. Since the air enters directly from the room, the outlet of the central air conditioning is sealed using a large canvas sheet in order to reduce

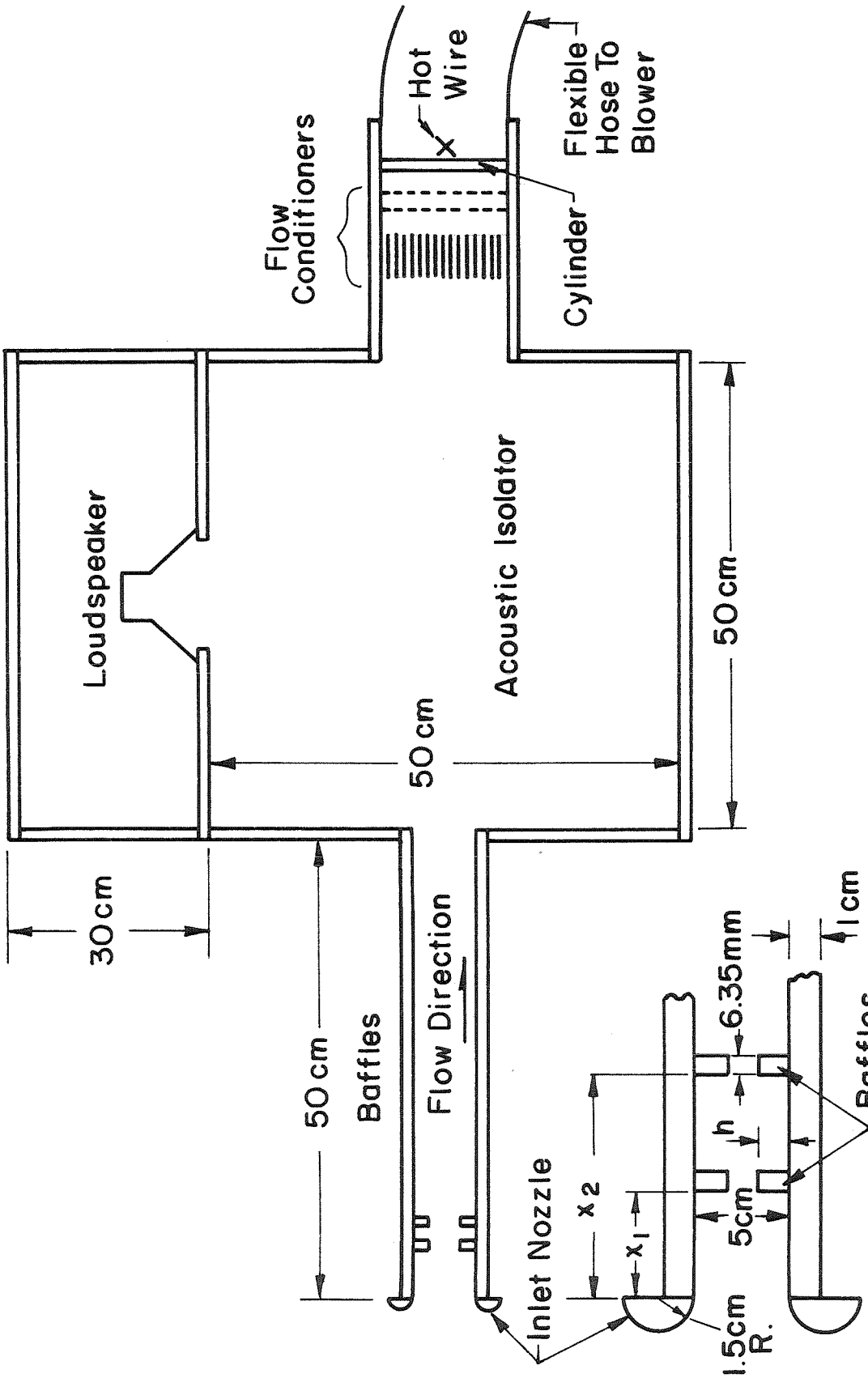


FIGURE 2.1 EXPERIMENTAL APPARATUS

disturbances. An inlet nozzle constructed from wooden half-round dowels is used to round the otherwise sharp inlet. This short nozzle does not significantly affect the acoustic response of the duct.

Immediately downstream of the duct, the air discharges into a wooden cubic box 50cm on a side which acts as an acoustic isolator. Originally, the blower was connected directly to this box. Since this arrangement allowed vibrations to be transmitted to the test section, the blower was moved into the hallway outside the room, the air being carried in a flexible hose 20cm in diameter and about 7m long. This has the added advantage of eliminating the disturbance due to the exhaust of the blower being in the same room as the inlet.

## 2.2. Baffles.

The aluminum baffles are all 0.635cm (0.25in) thick and 15cm long to span the width of the duct. Four sets are used with the following heights: 0.635cm, 1.04cm, 1.27cm, and 1.524cm (0.25in, 0.41in, 0.5in, 0.6in). Another set of baffles was machined from aluminum stock 2.54cm (1.0in) in diameter to form an almost semi-circular cross-section. The mounting screw is in the center of the rod so the flat surface, which rests against the wall, is off-center by 0.317cm (0.125in). A single pair of baffles 2.54cm (1.0in) tall demonstrate that the resonance being investigated operates with just one set of baffles. A few sets of baffles were crudely made from balsa wood to try ideas before having them machined from aluminum. Generally, no significant differences in the behaviour of the system were detected using the balsa baffles.

## 2.3. Velocity Measurement.

Velocity measurements within the test section are made using a TSI 1210 hotwire in the constant temperature mode with a Matilde bridge anemometer. This combination is used to measure both mean velocity profiles and fluctuating velocities in the vicinity of the baffles.

Mean velocity measurements are also made based on the relationship between the periodic shedding of vortices from cylinders and the wind speed. A box containing flow straighteners and turbulence screens is installed between the acoustic isolator and the hose leading to the blower. The downstream portion of this box contains three cylinders, of different diameters, perpendicular to the flow. A constant current hotwire, which can be positioned behind the desired cylinder from outside the box, is used to measure the velocity fluctuations due to the passage of successive vortices. After amplification and filtering, the frequency of this signal is measured using a Fluke 8060A multimeter. The output of this measurement system was calibrated against the velocity in the test section as measured by a pitot-static tube, the pressure difference being measured by a Barocel 570 strain gauge pressure transducer. The shedding frequency was found to be very linear in velocity but was reliably so for a relatively small range (corresponding to cylinder Reynolds numbers in the range 50 - 100). Thus the cylinder diameters were chosen to double successively, yielding an overall range of test section velocities from 1 m/s to 8 m/s. The advantages of this method of measuring the velocity are that no probe is required in the test section and that there is no dependence on the hotwire calibration, which tends to drift with time. Furthermore, disturbances due to changes in the

geometry within the test section do not affect the reading since it is the average flowrate that is measured. Any air that passes through the duct must also pass through the box containing this instrumentation.

## 2.4. Pressure Measurements.

Acoustic pressures are measured using Brüel & Kjaer half inch diameter type 4133 and 4134 capacitance microphones. Microphone mounting ports are located at the midpoint and at the three quarter point of the duct. Acoustic pressure distributions are taken using a B&K type 4002 trolley containing a microphone with a tube extension so that the fluctuating pressure can be measured at any point within the duct.

## 2.5. Flow Visualization.

In order to make the vortices visible, a smoke generator and a General Radio type 1531-A Strobotac strobe light are used. The smoke is generated by dripping mineral oil over a pair of soldering iron elements within a Pyrex jar. The smoke is then blown through a 2cm diameter tube to a contraction made of copper which is positioned in the vicinity of the duct entrance. Zero-crossings of the output of the pressure signal are used to trigger a variable delay which, in turn, triggers the flashes of the strobe light. This results in an image which appears stationary. By changing the time delay, different times in the cycle can be viewed. Since it is difficult to obtain good photographic exposures, the technique is most useful for visualization in real time.

## 2.6. Loudspeaker.

To measure the acoustic response and to investigate external forcing of the vortex shedding, a 100 Watt Phillips AD12250/W loudspeaker is mounted on the acoustic isolater. In order to sweep the frequency through a range to determine Q for the duct, the output from a Wavetek model 185 sweep function generator, amplified by a 75 Watt McIntosh MI-75 power amplifier having excellent linearity, is used to drive the speaker. When a specific frequency is desired, a Waketek model 171 function generator, whose frequency can be set digitally, is used instead of the model 185.

# Chapter 3
# MATHEMATICAL MODELS

A mathematical model has been developed based on the mechanism postulated in the introduction. Since the mathematical model yields results consistent with the behaviour observed in the experiments, it is felt that model is a reasonable (and therefore useful) approximation to reality.

A simpler mathematical model has also been developed, which describes some of the gross features of the mechanism rather well. The analysis associated with the simple model was originally performed to verify that the behaviour of the more complicated model would be as expected. The results of the simple model are so useful for such little investment that it has been decided to include it. Furthermore, it serves as an introduction to the analysis associated with the more detailed model to follow. First the elements of the models will be related to the physical ideas on which they are based.

## 3.1. Features of the Mathematical Model.

The mathematical model is based on a physical explanation of the mechanism that has grown from exploratory experiments and from results reported by other investigators. The model consists of several blocks which can be considered separately, but which, when linked together, explain the behaviour observed experimentally.

One major component is the acoustic duct resonator. Its response can be modeled quite well using one-dimensional acoustics, which neglects any variation across the width of the duct. Its response to a localized sinusoidal forcing at an arbitrary location in the duct (corresponding to the location of the downstream baffle) is calculated.

The other major component is the edgetone system, but its components are also treated separately: the shear layer which forms at the first baffle, the subsequent growth of vortices due to the shear layer instability, and the resultant force on the second baffle due to the passage of the vortices.

Shear layers are known to be susceptible velocity disturbances that may be present in the mean flow (2). In the present case, acoustic waves are present due to the acoustic resonator. It is simply assumed that vortices form in phase with these disturbances. The growth of the vortices is then determined from the growth rate data of Freymuth (2), using a Strouhal number, $S_\theta$, based on the acoustic frequency, the freestream velocity between the baffles and the experimentally measured momentum thickness just downstream of first baffle. Freymuth finds that the momentum thickness remains essentially constant in the region of exponential growth of the velocity fluctuations, so the actual location at which the measurement is made is not too critical. Since the measurement of this quantity is not very accurate, it is assumed to vary with the inverse of the square root of the mean velocity between the baffles. A single measurement of the momentum thickness which was felt to be reliable is used as a reference:

$$\theta = 0.5\text{mm} \times \left(\frac{13.0\ \text{m/s}}{U_\infty}\right)^{1/2} \qquad (3.1)$$

At some downstream point, the amplitude saturates due to non-linearity and the momentum thickness starts to grow at that point. The mean velocity is assumed to be known a priori. The same Strouhal number used to determine the growth rate is used to find the saturation level of the velocity fluctuations from Freymuth's data (2).

The final part involves the calculation of the force on the second baffle due to passage of the vortices. This is done using nonsteady potential flow with point vortices of strength determined by the saturated velocity fluctuations mentioned above. The details of this calculation are in Appendix E. As each vortex travels past the second baffle, it induces pressures on the surface which then drive the acoustic response of the duct.

Each of the contributions mentioned is treated independently, but when they are joined together and allowed to interact they result in the type of behaviour observed in the experiments: spontaneous acoustic standing waves at frequencies near the resonant frequencies of the oscillator and vortex formation with exponential growth to saturated constant amplitudes which depend on the mean velocity and on the baffles spacing and location within the duct. The loop is closed by assuming that the acoustic response velocity measured at the location of the first baffle is equal to the initial perturbation in the shear layer that triggers the formation of vortices.

## 3.2. Simple Mathematical Model.

The simple model simulates some of the behaviour of the more complicated analysis but the results are far more easily interpreted to yield general conclusions. This model is based on the idea that in the vicinity of one of its resonances, an acoustic resonator behaves in a manner which is very analogous to a damped linear oscillator. The spontaneous growth of the amplitude occurs when feedback is added.

When a damped linear oscillator is driven by a constant amplitude sinusoidal driving force, after the initial transients have decayed the response is also sinusoidal and at the same frequency as the driving force. The amplitude of the response is greatest when the frequency of driving is very nearly equal to $f_o$, the resonant frequency of the oscillator. It is the sinusoidal velocity which has a maximum exactly at this frequency. The displacement has its maximum at $f_o(1 - \frac{1}{2Q^2})^{1/2}$.

Typical response curves, for systems with different quality factors, Q, are plotted in Figure 3.1. The quality factor is high for systems with low damping and is defined as $\Delta f/f_o$, where $\Delta f$ is the width of the peak at half the maximum power. For the duct used in the experiments, the value of Q is about 20, as described in Chapter 4.

A resonator can be made into a self-excited oscillator by adding appropriate feedback. Instead of using a forcing function such as F cos $\omega t$, one might use a force proportional to the displacement at an earlier phase in the cycle, for example. This can result in growing

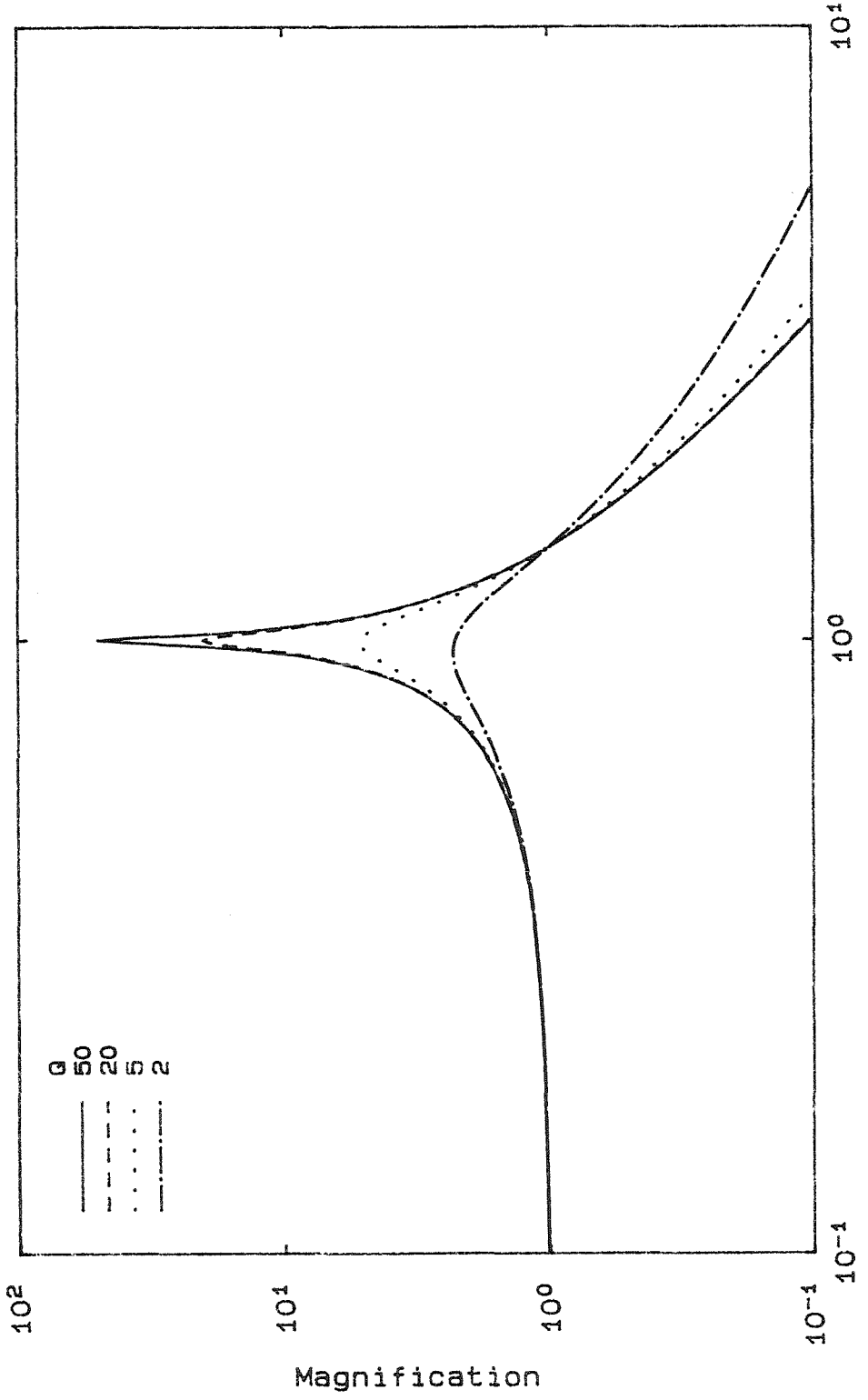


Figure 3.1 Response of Damped Linear Oscillator

oscillations depending upon the time lag and the constant of proportionality. The time lag is important since without the time lag, forcing proportional to displacement is equivalent to modifying the spring constant, possibly making it negative. The effect is to change the natural frequency if the effective spring constant is positive or else to produce exponential growth of the displacement without oscillation if the effective spring constant is negative.

In modeling the duct as a simple damped oscillator, the forcing is due to the interaction of the vortices with the downstream baffle. The vortices are assumed to be initiated when the acoustic response velocity of the duct is maximum at the upstream baffle. The forcing occurs at a later time equal to the time of flight of the vortices from the point of initiation at the first baffle to impingement on the second baffle. The idea central to the simple model, then, is that the forcing function is dependent on the velocity of the resonator at an earlier time, $\tau$. It is the response velocity which is important since the shear layer reacts to fluctuating velocities, as will be discussed in Section 4.5. It is anticipated that the greatest response will occur when $\tau$ is close to an integral number of periods at the natural frequency of the resonator since then the force is in phase with the velocity and the maximum amount of energy is being added to the system in unit time. Since the time lag, $\tau$, corresponds to the time of flight of a vortex from the first baffle to the second, increasing the baffle spacing while keeping everything else fixed, corresponds to increasing $\tau$ proportionately. The assumption is made that the convection velocity of the vortex does not change as the spacing is varied.

There are two phases of operation that it is desired to model. The first is the period during which the response amplitude grows from a small level. The second is the region of saturated amplitude during which the oscillation persists at constant amplitude and frequency.

The forcing is due to the passage of vortices past the second baffle. These vortices are initiated at the first baffle with an initial strength proportional to the response velocity at that time. As they convect downstream, they grow exponentially until they reach a saturated level dependent on the Strouhal number, $S_\theta$. For low enough initial levels, the vortices do not reach their saturated value before arriving at the second baffle and the force on the baffle is proportional to the initial level. Exponential growth of p' and u' with time is then expected. This is the first phase of interest mentioned above.

If the initial amplitude of the vortices, as determined by the response of the resonator, is large enough, then the vortices do reach a saturated level before impinging upon the downstream baffle. In this case the force has a constant amplitude, but its phase with respect to the response cycle is still determined by the time lag. A key element, then, is the frequency-dependent phase difference between the driving force and the response for a resonator. The response is similar to that of an oscillator driven by a constant amplitude driving force in that the amplitude exponentially approaches a constant value. The frequency, however, is determined by the time lag imposed by the system. The frequency adjusts itself to produce a phase difference between driving and response equal to the phase difference imposed. This is the second phase of operation

for which the response characteristics are wanted. The calculations for the above two phases are shown in detail in Appendix B which makes use of the method of time averaging developed by Kryloff and Bogoliuboff (24) and presented in Appendix A.

The simple model describes some of the essential features of the self-excited resonance under investigation. In particular, for the steady-state case, the relative amplitude and frequency behaviour is predicted correctly for different baffle spacing near the peak response condition. The model predicts the exponential growth anticipated for the first case but comparison with experiment is not feasible since the experimental time records do not have well defined, repeatable, growth periods. The transition period between the two cases is not modeled.

### 3.3. Details of Shear Layer Development.

An investigation of shear layers was not undertaken in the present work. Instead the results of other workers are used. The model of the shear layer development in based heavily on the experimental results of Freymuth (2) which seem to have been measured carefully and completely. The assumptions that have been made in order to couple with the other sections of the model will be presented here.

The first assumption is that the initial perturbation is equal to the acoustic velocity present at the location of the upstream baffle. Any effects of an acoustic boundary layer in the transmission of the oscillating velocity to the sensitive separation point are ignored. That the separation point is the correct location to apply the

matching is justified since elsewhere the acoustic field is irrotational. That is, the fluid moves back and forth with the acoustic wave equally in the neighbourhood of any point, thus no vorticity is generated. At the separation point, however, the velocity fluctuation is felt on the high speed side of the shear layer above the sharp lip of the baffle, whereas the low speed side is shielded from oscillations by the physical presence of the baffle. The fluctuating vorticity is superimposed on the mean vorticity being shed there and is amplified downstream by the shear layer instability.

The growth of the fluctuating velocity in the shear layer is exponential in the streamwise direction, with a growth rate determined from the Strouhal number based on the initial momentum thickness. The growth rate as a function of Strouhal number is approximated by a sixth order polynomial fit to the spatial growth curve below $S_\theta = 0.010$ and the temporal growth curve above that value. These are theoretical curves predicted by Michalke (3,4) and reported along with measured growth rates by Freymuth (2). The temporal theory is a calculation of the timewise development of instability waves on the interface between two infinite bodies of fluid moving in opposite directions. The spatial theory is similar, but accounts for variations in the streamwise direction and is more representative of shear flows that can be generated in the laboratory. Below $S_\theta = 0.010$, Freymuth's growth rate data (2) fit the spatial curve best, and above that they follow the temporal theory well. The choice of using a polynomial fit is simply for computational ease. The actual curve used is plotted in Figure 3.2 along with Michalke's predictions. The agreement is at least as good as with the experimental data and is considered adequate for the present purposes.

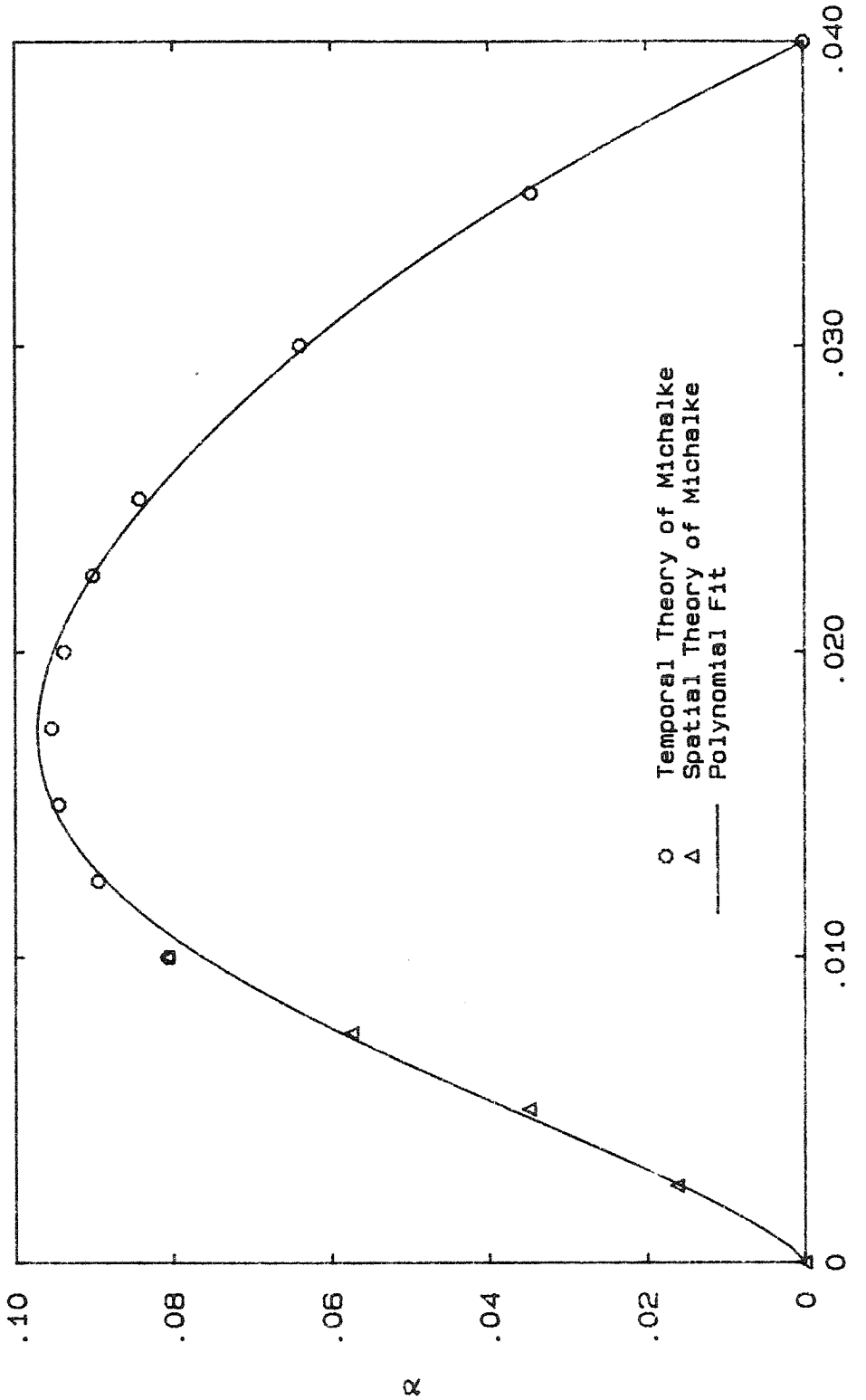


Figure 3.2 Growth Rate

From Figure 15 in Freymuth's report (2) it can be seen that after the region with exponential growth the fluctuating velocity reaches a saturated value downstream. The peak values were measured from the graphs and replotted versus Strouhal number. These data are presented in Figure 3.3 along with another least squares fit polynomial. In this case, the fit was performed using the logarithm of the experimental points, so the antilog must be taken of the polynomial evaluation in order to determine the actual saturation value of the velocity oscillation. In the model, the amplitude of the fluctuating velocity in the shear layer is permitted to grow with the appropriate growth rate until it reaches the value determined by this second polynomial. From that point onward, the velocity is assumed to remain saturated at that value.

### 3.4. Vortex Strength.

In order to calculate the changing drag on the downstream baffle due to the passage of this shear layer with superimposed velocity fluctuations, point vortices are used at the streamwise locations with the greatest velocity fluctuation. Once a strength is assigned to these vortices, the oscillating drag on the second baffle is calculated using potential flow, as shown in Appendix E.

The oscillating drag on the downstream baffle is due to the oscillating component of the vorticity in the shear layer. The magnitude of this vorticity fluctuation is quite small in comparison with the mean vorticity in the shear layer. In order to use the point vortex drag calculation (Appendix E), it is necessary to replace the sinusoidally varying vorticity with point vortices of

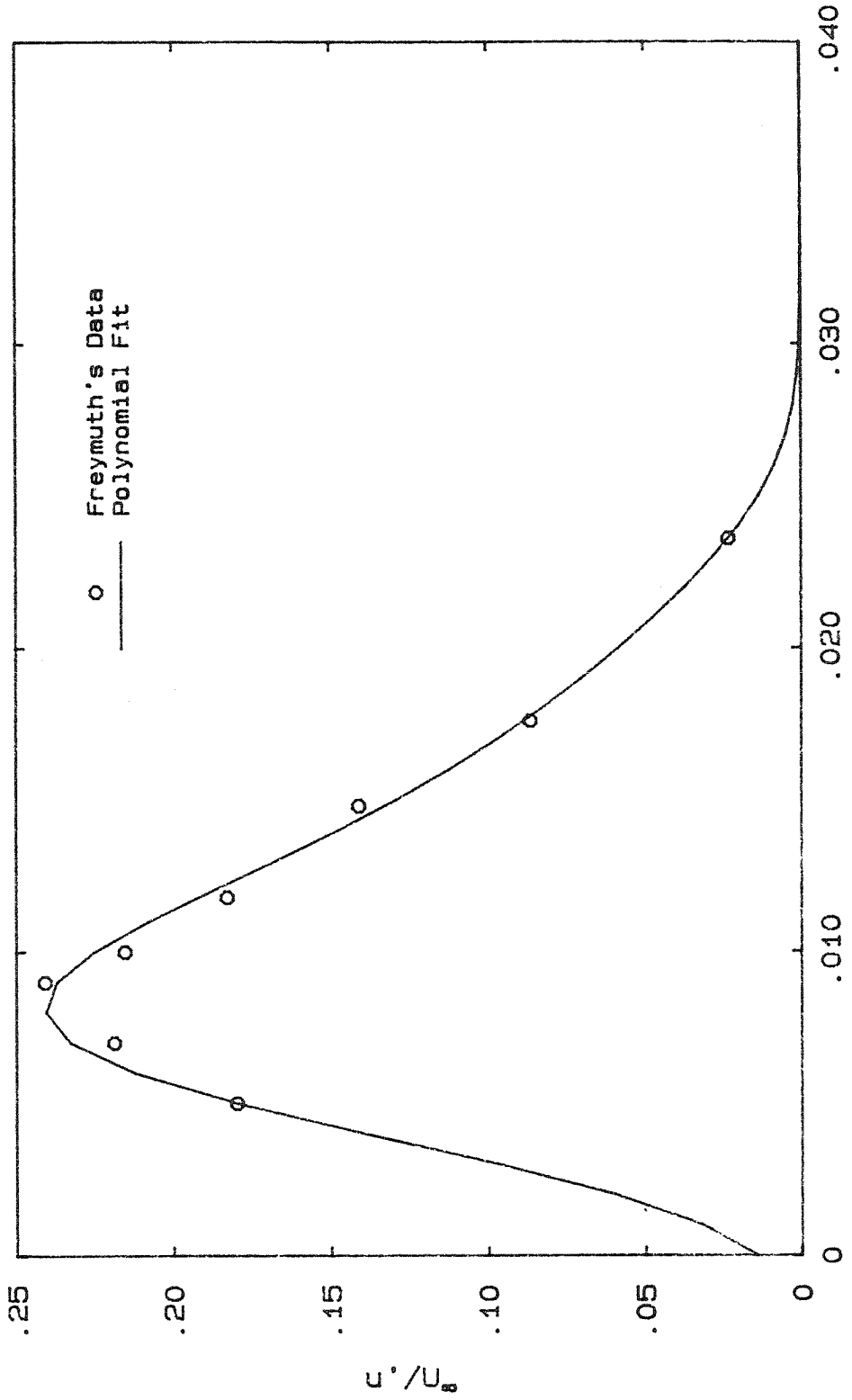


Figure 3.3 Saturated Velocity Amplitude on High Speed side of Shear Layer

appropriate strength and location. The natural choice is to place a vortex once each wavelength at the point with maximum positive vorticity. An alternative approach is to place an additional vortex with opposite strength at the points with maximum negative vorticity. In that case, it is clear that the strength for each vortex should be set equal to the integral of the vorticity over the corresponding half-wavelength. Since the negative vortex would produce an equal but opposite force 180° out of phase, the same effect can be produced using a single positive vortex with twice the strength. Thus, a vortex with circulation $2u_m\lambda/\pi$ is released each cycle at the lip of the upstream baffle at the time of greatest positive acoustic velocity. The vortex strength, $\Gamma$, used in Appendix E is normalized by dividing the circulation by $2\pi$ to eliminate repeated factors of $2\pi$ in the analysis. Therefore, the value for $\Gamma$ is $u_m\lambda/\pi^2$. The wavelength, $\lambda$, is found using the frequency and the convection velocity, $U_c$. Freymuth's data show that the peak velocity on the upper and lower sides of his shear layer, which are 180° out of phase, are of unequal magnitudes. On the low speed side, he finds the peak velocity to be lower than on the high speed side by a factor depending on Strouhal number once again. In the current model, a third polynomial fit (Figure 3.4) is used to calculate the ratio of these two velocities from which the value of the peak velocity on the low speed side can be evaluated once the value on the high speed side is known. The velocity, $u_m$, used in the expression for $\Gamma$ above is taken to be the arithmetic mean of the amplitudes of these two fluctuating velocities.

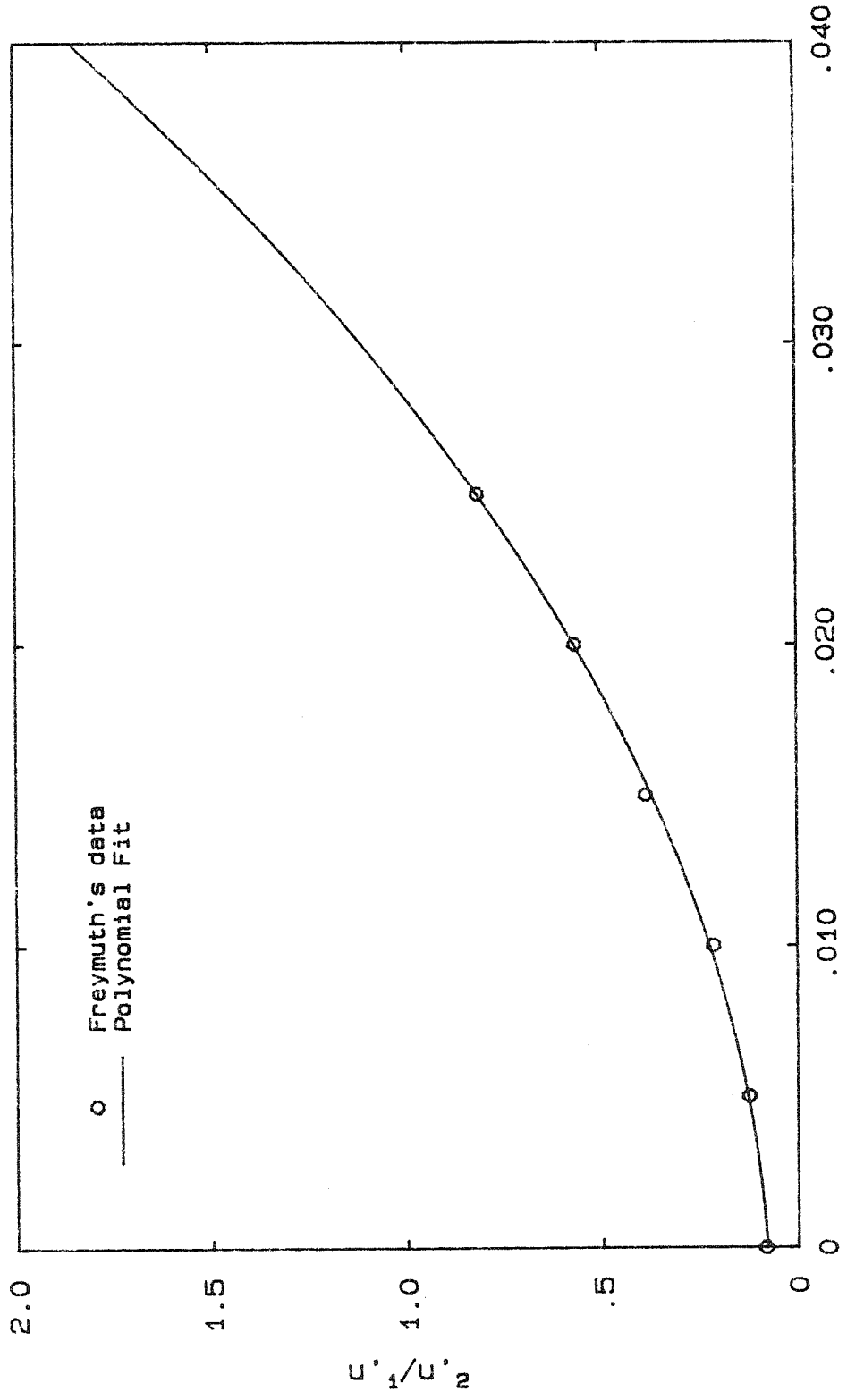


Figure 3.4 Ratio of Velocity Amplitudes across Shear Layer

## 3.5. Drag Calculation.

Experimental measurements indicate that pressure amplitudes differ by factors of at most two when half-round baffles or rectangular baffles are used. The assumption is therefore made that the drag can be calculated on a semi-circular baffles rather than on a rectangular baffle. This is a matter of convenience. The calculation is easier with the semi-circular geometry since no transformations are necessary. Since any potential flow approximation to such a separated unsteady flow can only be expected to yield forces with the correct order of magnitude, this approximation is deemed acceptable. Similar calculations of the interaction of point vortices with downstream obstacles have been made by Holger et al. (25,26) and Panaras (27).

In the potential flow calculation of the drag on the downstream baffle (Appendix E), the upstream baffle does not exist, as can be seen in Figure 3.5 which shows the geometry used for the calculation. Naturally, this leads to some lack of reality in the model. The results of the potential flow calculation indicate that vortices with strengths determined by the technique described in the previous section are so small that the vortices follow trajectories very close to the path that would be traversed by a point of fluid with no circulation. This is because the induced velocity due to the image vortices is negligible compared with the freestream velocity. In the real flow, due to the large body of essentially stationary fluid behind the first baffle and below the shear layer, the vortices actually travel at a convection velocity close to one half of the free steam velocity measured above the baffles. To account for this discrepancy, the free stream value used in the potential flow calculation of the drag is set equal

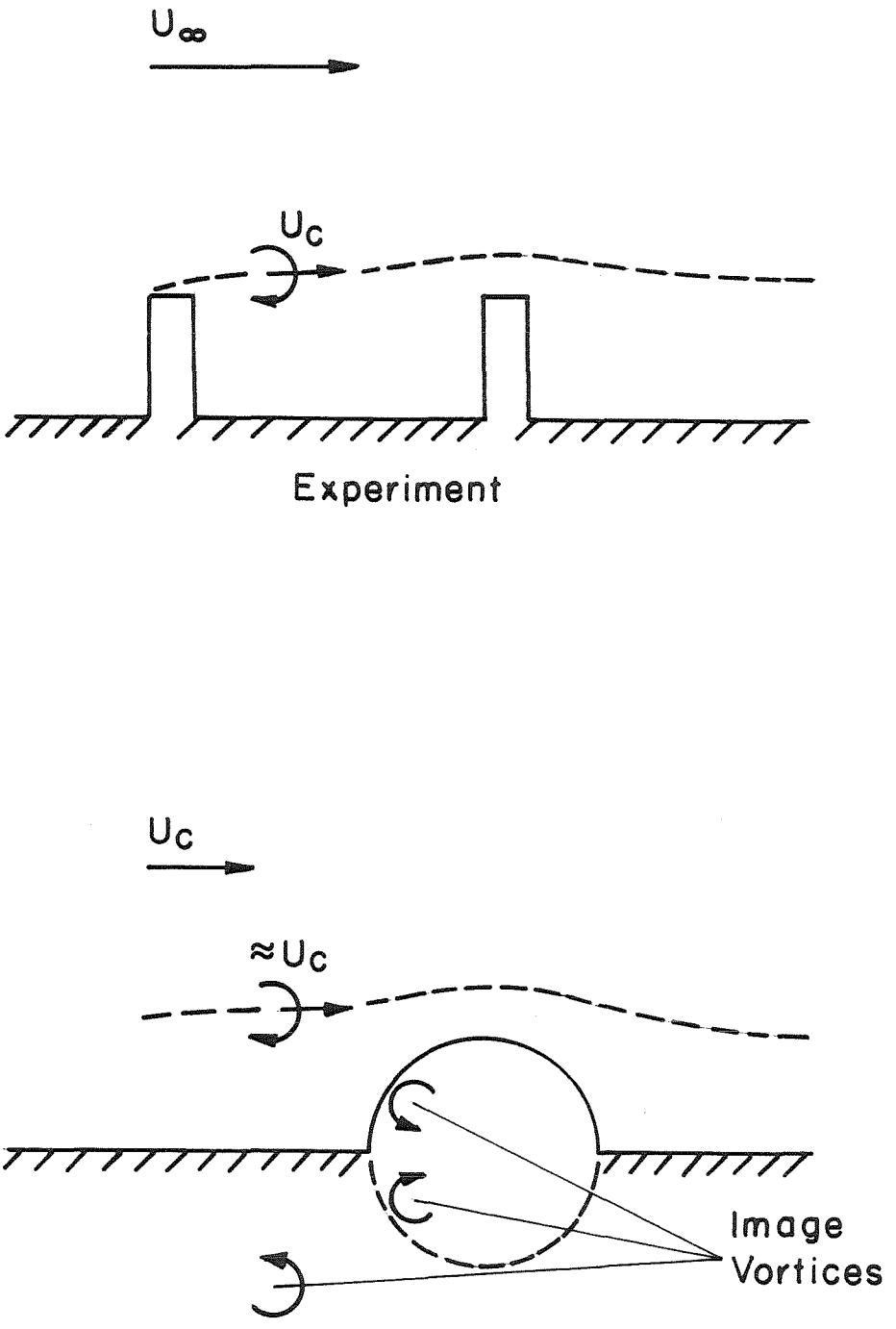


FIGURE 3.5 COMPARISON OF EXPERIMENTAL AND THEORETICAL GEOMETRIES

to the convection velocity as determined below. The speed of the vortices should then correspond to the experimental situation with the same flowrate above the baffles. Part of the effect of the wake of the first baffle is, thus, accounted for by artificially using the convection velocity in place of the free stream velocity in the calculation of the drag on the downstream baffle. The point of release of the vortices is taken to coincide with the location of the separation point on the upstream baffle which is not modeled in the potential flow calculation.

Freymuth's data, as reported by Michalke (4), indicate a dependence of the convection velocity on Strouhal number as plotted in Figure 3.6. A fourth and final polynomial fit is used to include this effect in the model. In order to avoid spurious behaviour in the Strouhal number range with no data, three points were used corresponding to the theoretical prediction of Michalke, towards which the data clearly tend. This procedure has minimal effect on the fit in the region with data.

Once the fluctuating drag is found, it is used as the driving force for the acoustic field. As each vortex moves past the baffle, the fluid exerts a force on the baffle. By Newton's second law, the baffle must therefore exert an equal force on the fluid, but in the opposite direction. There is thus a drop in the pressure across the baffle from the upstream side to the downstream side equal to the drag force divided by the duct area. When the "drag" is negative, the sign of the pressure drop is also negative. It is the oscillating component of the drag and the resultant pressure difference that is important; the mean drag is not considered and does not contribute to the acoustic response. The oscillating pressure difference across the

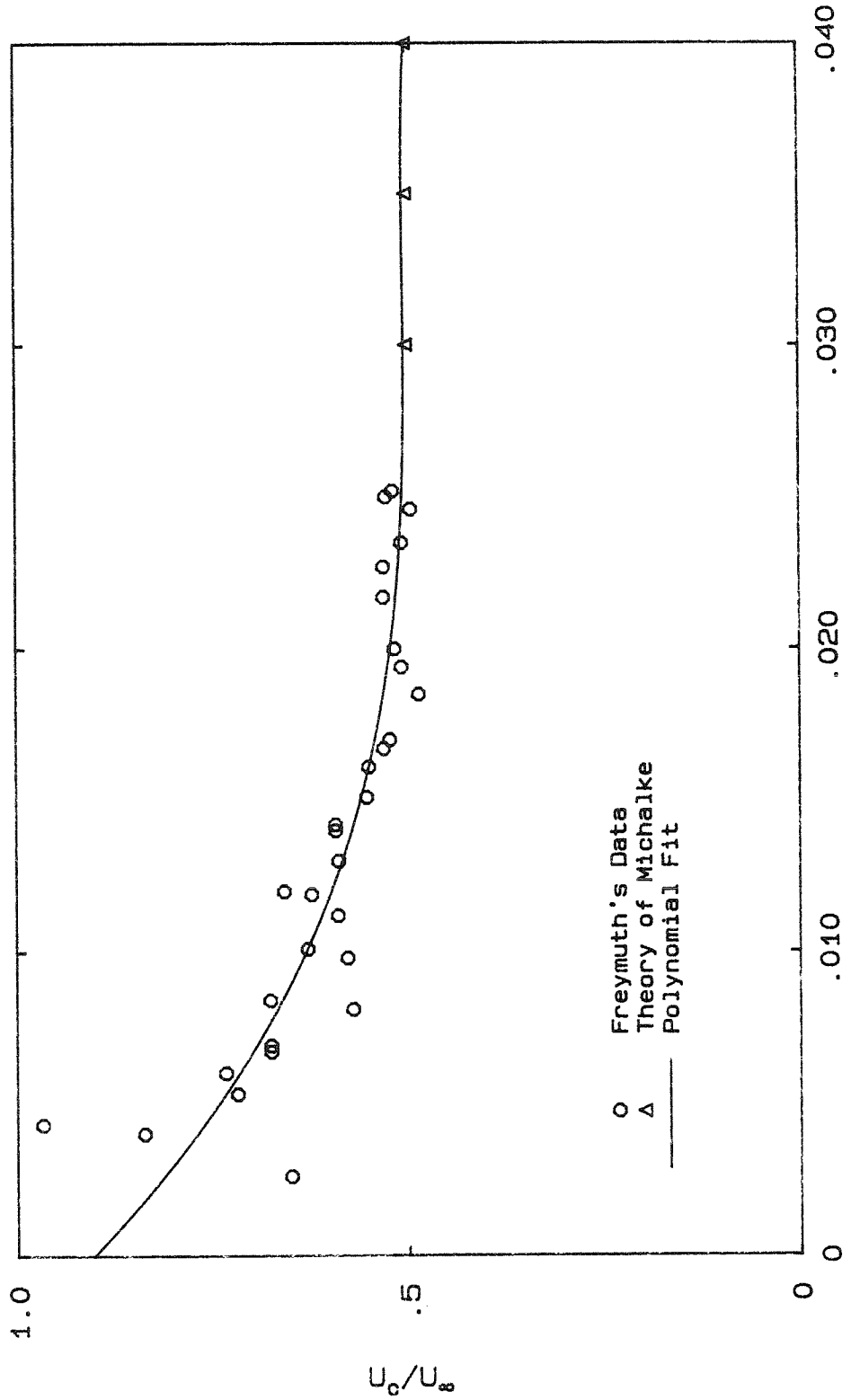


Figure 3.6 Phase Velocity

baffle is used as the driving force in the acoustic model by imposing it as a boundary condition at $x_2$, the location of the downstream baffle.

### 3.6. Calculation Algorithm.

The calculations associated with the various parts of the model are performed in a Fortran program. A description will be given here of how the various parts of the model are treated in the computer code. Originally, it was intended to use the model to predict the quasi-steady behaviour of the system during the growth or decay phases of operation. Results obtained during the development of the program indicated that the assumption of quasi-steady behaviour is grossly violated except very close to the final saturated amplitude. Therefore, the program was developed to calculate only the steady-state behaviour. This restricted goal permitted some simplification in the the further development of the program.

In the algorithm used, an initial frequency and perturbation velocity at separation are assumed. Iteration is performed alternately on each of these two quantities until either a solution is obtained or else divergence occurs, indicating that no solution exists. The convergence criteria will be described in the next section along with a description of the actual iteration scheme used. In this section, the way in which the model is implemented as code will be described. The algorithm described is essentially what happens each time through the iteration loop.

Using the initial values of frequency and the perturbation velocity at separation, along with other input, such as mean velocity and baffle locations, a vortex is initiated at the separation point. As the vortex is followed in the streamwise direction, its strength is determined using the polynomial approximations to Freymuth's data, as described in Sections 3.3 and 3.4. At each position, the resulting instantaneous drag on the downstream baffle is found using the results of the potential flow calculation. As the vortex moves downstream, the drag decreases gradually from zero (the force is upstream) and then rises very abruptly as the vortex passes over the baffle. The force reverses sign and continues to rise to a maximum positive drag, then gradually approaches zero again. If the vortex had constant strength throughout, the shape would be antisymmetric as in Figure E.1. This is not quite the case since the vortex strength is allowed to change here, but the variation is quite similar even so. Clearly, the variation in force is not sinusoidal. The acoustic model, which uses this result, assumes the forcing function is sinusoidal. It is necessary, therefore, to determine the amplitude of a sinewave which would be equivalent to the sum of an infinite succession of such plots, each separated from the next by a period at the assumed frequency of operation. In other words, the first term is required in each of the Fourier sine and cosine series of the function representing the drag. This operation is performed by multiplying the instantaneous drag at each time step by $ie^{-i\omega t}$ and integrating over the lifetime of the vortex. This lifetime is chosen to be two periods of the oscillation. Since the vortex traverses the distance between the two baffles in approximately one period, the vortex is extinguished at a location roughly as far downstream of the second baffle as the release point is upstream. The use of

complex notation is convenient for keeping track of the phase information which is important in this formulation. Finding the Fourier components is thus accomplished in one operation. The phase angle is measured with respect to the time of release of the vortex at the upstream baffle, which occurs at the instant of maximum acoustic velocity.

The drag, manipulated as a complex quantity, is then converted into an average pressure acting on the cross-section of the duct and used as the forcing function in the acoustic model of Appendix C. The location of this forcing is equal to the location of the downstream baffle, $x_2$. Using this drag force acting at $x_2$, the acoustic response velocity at $x_1$, the location of the upstream baffle, is then calculated using the results of the acoustic model. This velocity fluctuation at $x_1$ is assumed to be the perturbation which triggers the formation of the next vortex. For a steady state to exist, this value must be exactly equal to the guess which was used at the start of the current iteration. This equality includes the phase angle as well as the magnitude. Since the various quantities are maintained in complex form in the program, this is equivalent to requiring that the two complex values be equal. When this criterion is satisfied, within some preselected tolerance, then the iteration scheme has converged to a stationary value. That is, the assumed frequency and initial velocity perturbation are such that oscillation is self-sustaining at a steady amplitude and frequency.

## 3.7. Iteration Scheme.

At this point some iteration scheme is necessary to select the values of the variable parameters for the next pass through the loop described in the previous section. There are two variables to adjust: the frequency and the initial perturbation velocity and two criteria to satisfy: equality of the magnitude and the phase of the input and output perturbation velocity. Since the phase reference is the input velocity, it automatically has zero phase angle. The second criterion is, thus, that the phase of the output velocity be zero.

The results of the simple model are used to help select an appropriate way to pick new values based on the results of the previous iteration. The simple model indicates that the phase relations are strongly dependent on frequency. Therefore, the amplitude of the initial perturbation velocity is held fixed for several iterations while the frequency is adjusted using the secant method (28) until the phase of the response velocity is zero. The secant method is a standard two-point iteration scheme to solve the zero-crossing point of a single function of a single variable. At this point, it is unlikely that the amplitude is correct and so it is necessary to make some kind of change in the perturbation velocity magnitude.

The simple model assumes constant forcing regardless of the amplitude of the initial forcing. If this assumption were exactly true, then simply setting the new value equal to the old would not change the output and the solution would then be converged. This exact behaviour is not expected from the full model, however, the output amplitude is likely change only a small amount for large changes in

the input. This is due to the saturation nature of the shear layer. The approach of just setting the new amplitude equal to the old, while keeping the frequency fixed, works quite well, and is the method used.

As an alternative approach, one is tempted to keep the frequency fixed and use the secant method again to adjust the amplitude until the magnitude of the input and output velocities are the same. In fact this was tried and convergence was obtained, but the process was fairly slow in comparison.

If the magnitude of the new perturbation velocity is set equal to the magnitude of the calculated response, as described above, then one might expect to obtain a quasi-steady growth or decay until the amplitude naturally reaches a constant value. However, from one cycle to the next, the amplitude sometimes increases by an order of magnitude, or more. In the acoustic model, the response has been calculated assuming steady-state driving. The amplitude of the oscillator would require more time than a single cycle for its amplitude to increase by a factor of ten or a hundred. Thus, the quasi-steady approximation is violated.

An alternative approach involved fixing the frequency and letting the freestream velocity vary (again using the secant method) to satisfy the phase criterion. It was found that the phase is too sensitive a function of this parameter and divergence was often a problem. When a solution was obtained using this approach, it gave results consistent with the method used above.

An evaluation of the model will be made in the next chapter in which its predictions are compared with results of the experiments.

# Chapter 4
# RESULTS AND DISCUSSION

In this chapter, the results of the experiments are presented and compared with the predictions of the mathematical models discussed in the previous chapter.

## 4.1. Acoustic Properties of the Duct.

The measured natural frequency of the duct is 295Hz. When baffles are installed, this resonant frequency is reduced about 20Hz depending upon the location of the baffles with respect to the velocity antinodes. This effect of an obstacle on the acoustic resonances of a duct is investigated theoretically by El-Raheb and Wagner (29). They conclude that for a given size obstruction the frequency is reduced most when that object is near the velocity antinode. If the object is placed near a velocity node instead, there is a slight increase in the natural frequency, but the variation is much less than for the former case.

The section of the model that deals with the acoustic properties of the duct does not account for the baffles in any way. It gives a natural frequency of 295Hz in excellent agreement with the measured value without baffles. This suggests that the end conditions are correctly modeled by the piston function approach discussed in Appendix D.

If the duct resonator is assumed to behave like a damped linear oscillator, one can determine the associated quality factor, Q, a measure of how strongly an oscillator responds to excitation at its resonant frequency. This quantity, measured using three different techniques, is found to be on the order of 20 for each case. The Q measured for the fundamental frequency of the response curve predicted by the acoustic section also yields a value just slightly greater than 20, confirming that the end impedances correctly account for the energy radiated from the ends of the duct.

The first method of measuring Q is simply to use a loudspeaker driven by a sweep signal generator to pick off the frequencies at which the amplitude is $2^{-1/2}$ multiplied by the peak value. The definition of Q is then used:

$$Q = \frac{f_o}{f_2 - f_1} \qquad (4.1)$$

The measurement was made with and without flow. With no baffles in the duct, Q gradually decreases from about 22 with no flow to about 18 for the maximum velocity of 40 m/s, thus the end conditions do not significantly change with mean flow. With baffles installed, Q was found to be about 20 with no flow. With flow, self-excited resonance occurred, as usual, so a fairly high speed had to be used to eliminate it. The background noise level due to the flow past the baffles was then sufficiently high that the speaker power was insufficient to produce a well defined peak as the frequency was swept through resonance. The second technique for measuring Q involves using a random noise generator to excite the loudspeaker rather than the sinewave used above. The width of the spectral peak can

then be used to infer Q. The third method makes use of a result of the simple model described in Appendix B. Equation B.12 contains Q as a factor which can be determined from the slope of the plot of frequency versus baffle spacing, or $\tau$, at the point of greatest response. That this last method yields the same value for Q is evidence that the the simple model is realistic.

The Q used above is for the response of the oscillator to an external driving force at different frequencies. The peak of the self-excited resonance curves which occur when the mean velocity or baffle spacing are varied bear some resemblance, but measuring the analogous quantity has no meaning. In fact the width of the response peak versus baffle spacing is essentially independent of Q. This is discussed further in Section 4.4.

The time records of the pressure oscillations during self-excited resonance appear very sinusoidal when displayed on an oscilloscope, although the amplitude does not remain completely steady. Frequency spectra of the same signals yield very sharp peaks up to 100dB above the background noise. The content in the harmonics is quite low. The first harmonic is typically 60dB below the fundamental although the location of the microphone is at the duct midpoint, which is a pressure antinode for this frequency, so it will be somewhat higher than indicated.

The measured distribution of acoustic pressure within the duct is plotted in Figure 4.1. The mode shape is very similar to a sinewave as predicted by classical acoustics. From the corresponding theoretical curve in the same figure, it can be seen that the ends are well represented in the Acoustic Model of Appendix C.

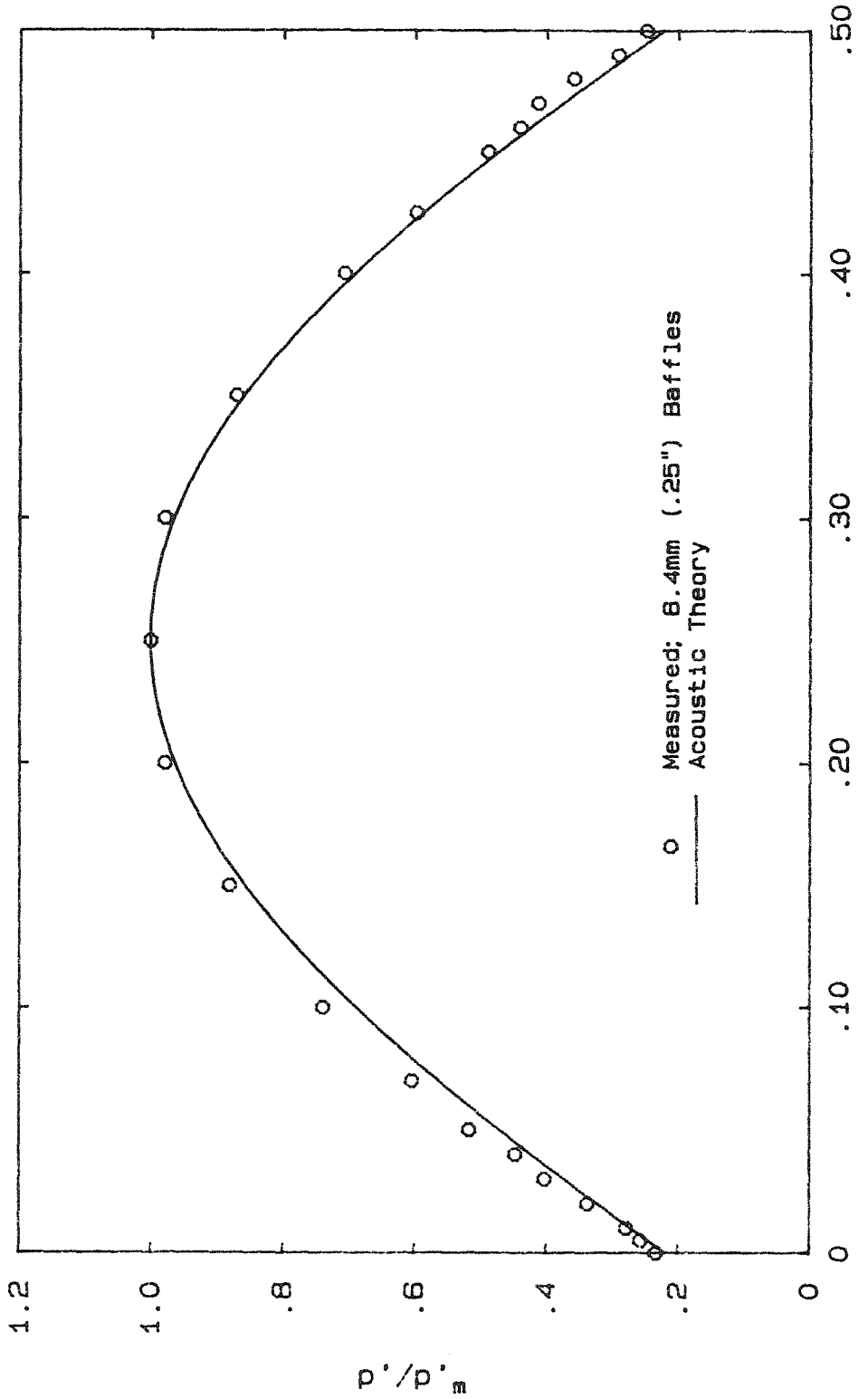


Figure 4.1 Acoustic Pressure Distribution with Baffles at Inlet

The effect of the baffles is seen to be small in Figure 4.2 which graphs the measured mode shape for four different baffle sizes, the greatest difference being caused by the largest baffles (15.2mm, 0.6in). That these acoustic distributions are measured during self-excited resonance demonstrates that the mode shape is largely unaffected by the presence of the mean velocity and the vortices. This is not surprising since changes should be on the order $1 - M^2$, where M is the Mach number of the mean flow. Mean velocities in the duct are on the order of 5 to 10 m/s and perhaps three times that between the baffles; thus the Mach number is certainly less than 0.1 everywhere in the duct.

## 4.2. Velocity Profiles.

Velocity profiles measured well downstream of the baffle set show a distinct bistable asymmetry. The profile plotted in Figure 4.3 and its mirror image occur with equal likelihood depending upon disturbances present in the air entering the duct. Deflecting the flow near the inlet can cause the flow to switch from one side to the other. The explanation is that the jet issuing from between the baffles attaches to one wall or the other due to the Coanda effect. The negative values in the plot indicate reverse flow, but their magnitudes are meaningless since pitot probes cannot measure reverse flow.

Similar profiles taken with baffles of different sizes indicate that the flipping of the mean flow from side to side, described above, occurs only with the taller baffles. With short baffles (6.4mm, .25in), a symmetric velocity profile is obtained as shown in Figure 4.4. The acoustic

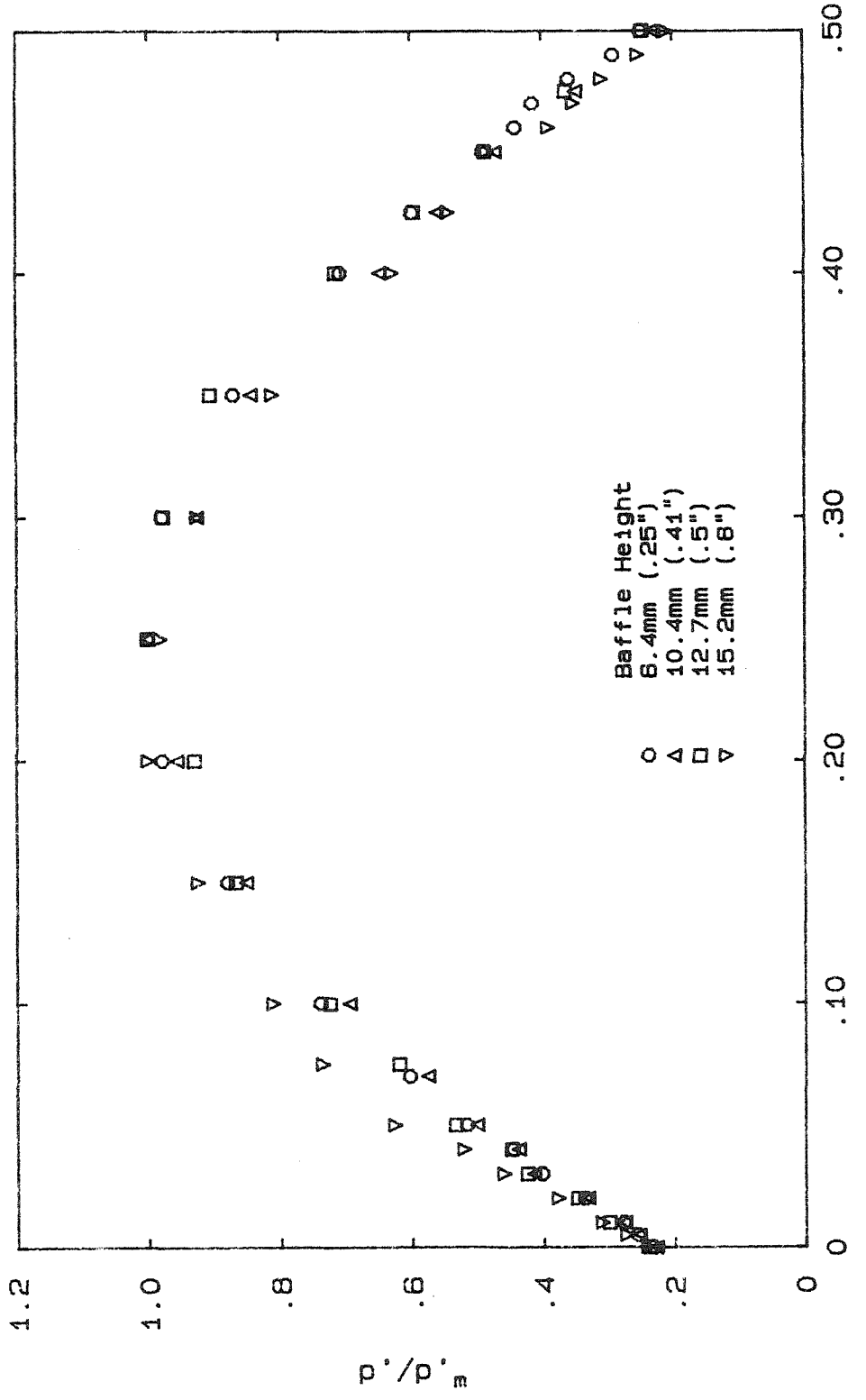


Figure 4.2 Acoustic Pressure Distribution with Baffles at Inlet

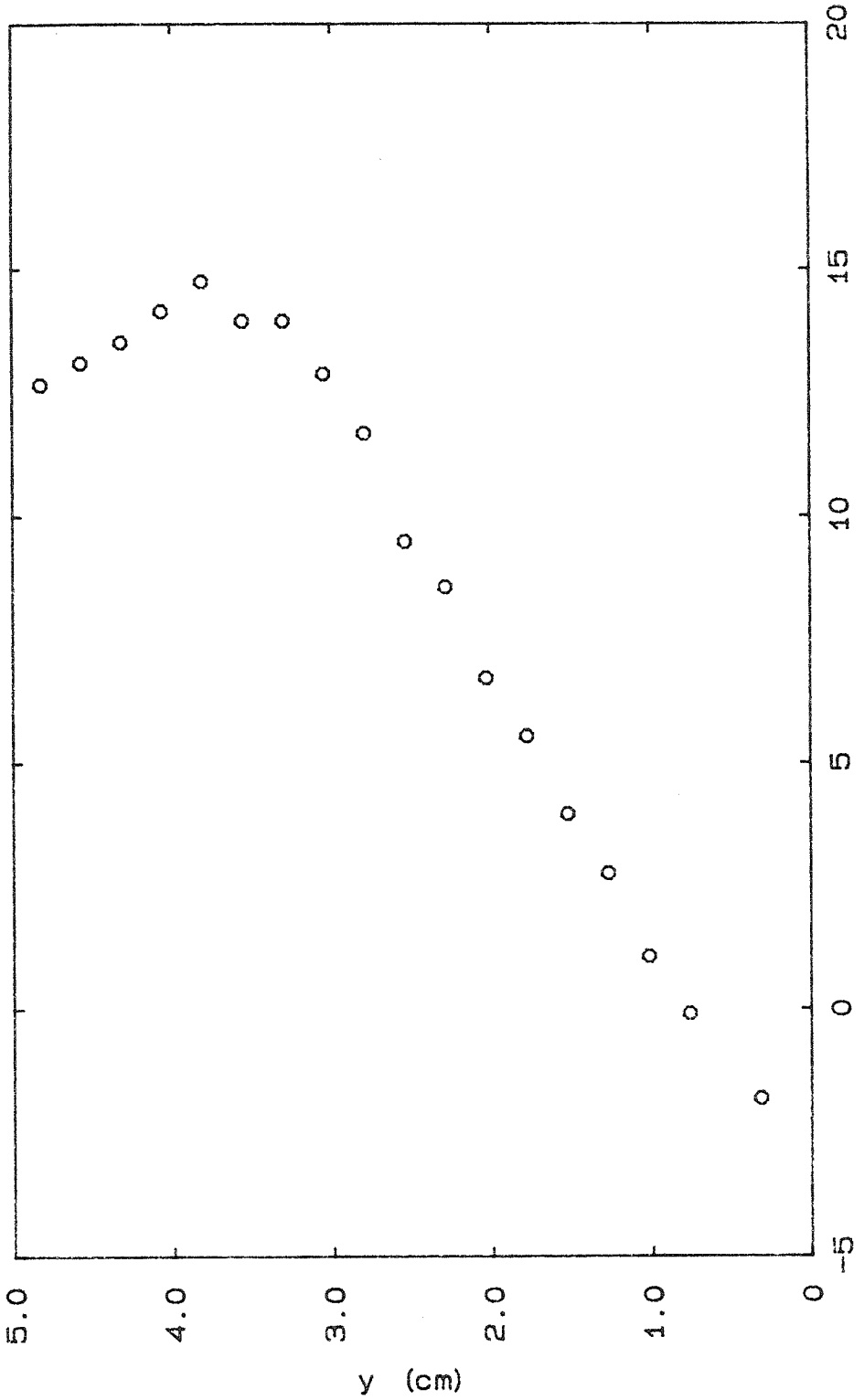


Figure 4.3 Asymmetric Velocity Profile far Downstream

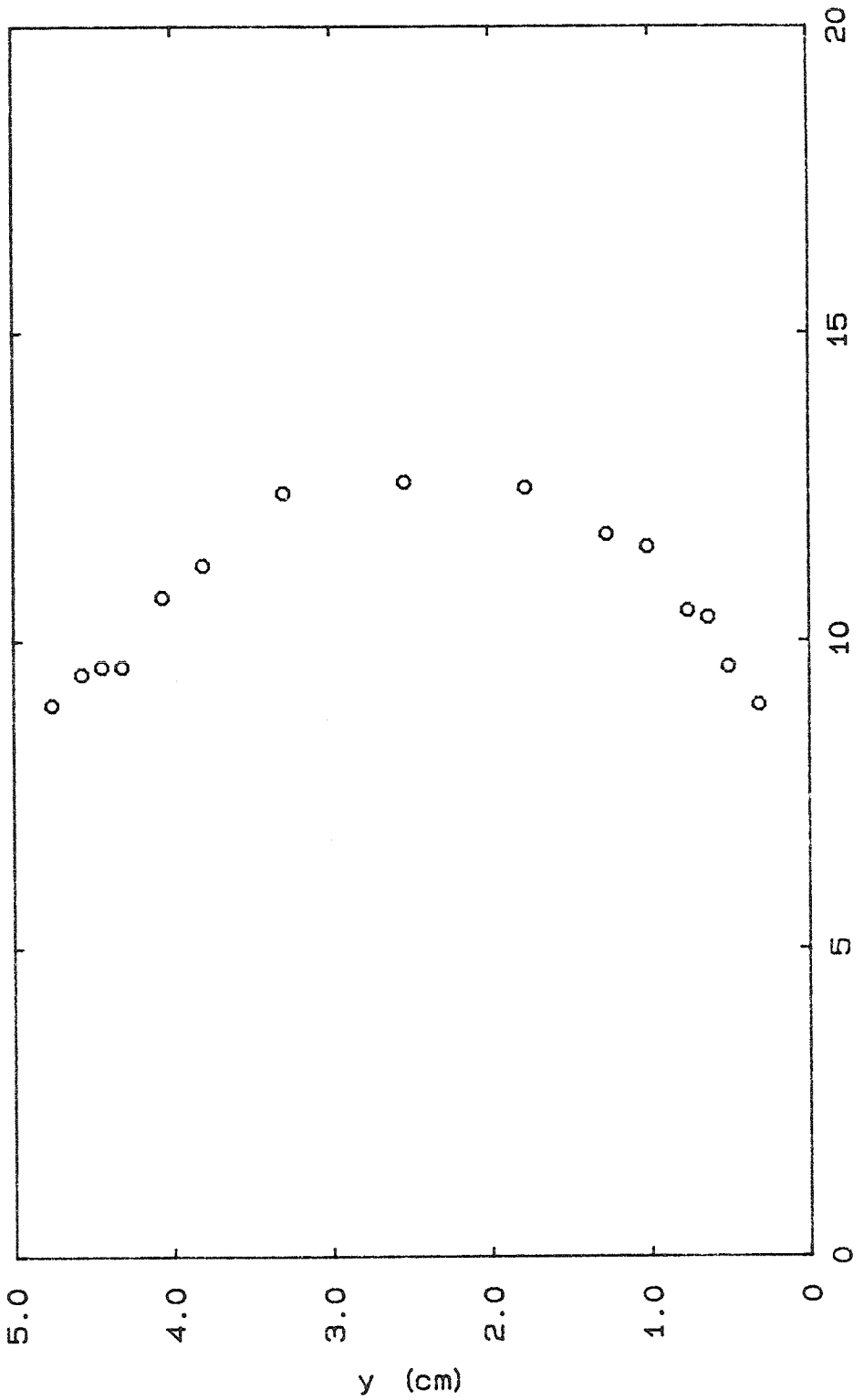


Figure 4.4 Symmetric Velocity Profile far Downstream

pressure distributions for the different size baffles (Figure 4.2) show no influence of this mean flow asymmetry.

With the set of baffles 10.4mm (0.41in) tall installed, for which the mean flow appears symmetric, a velocity profile taken just downstream of the first baffle indicates some evidence of asymmetry nonetheless. This profile, measured using a hotwire anemometer in order to determine the shear layer thickness, $\theta$, is plotted in Figure 4.5. In the plot, two profiles appear to be superimposed with a slight offset. While the measurements were being made, it seemed that at any particular point in the shear layer, the anemometer output would assume one of two values on the average and would randomly switch from one to the other. Perhaps the fluctuations from one value to the other are due to a minor form of the gross asymmetry which occurs with the larger baffles and simply does not make itself evident in the mean velocity profiles taken using the pitot probe with its longer time constant. Due to the double value phenomenon, integration of the shear layer profiles to determine momentum thicknesses leads to values with too much scatter to be useful.

In order to solve this problem, profiles are taken with baffles on only one side of the duct rather than with two pairs symmetrically placed. A significant amplitude is obtained with this configuration only for tall baffles. A set 25.4mm (1in) tall extending half way across the duct gives satisfactory results. Profiles with these baffles are shown in Figures 4.6, 4.7 and 4.8. The momentum thickness calculation based on these measurements will be discussed in the next section. The profile in Figure 4.6 is for a single baffle one inch tall installed in the duct, therefore any effects due to acoustic oscillations and due

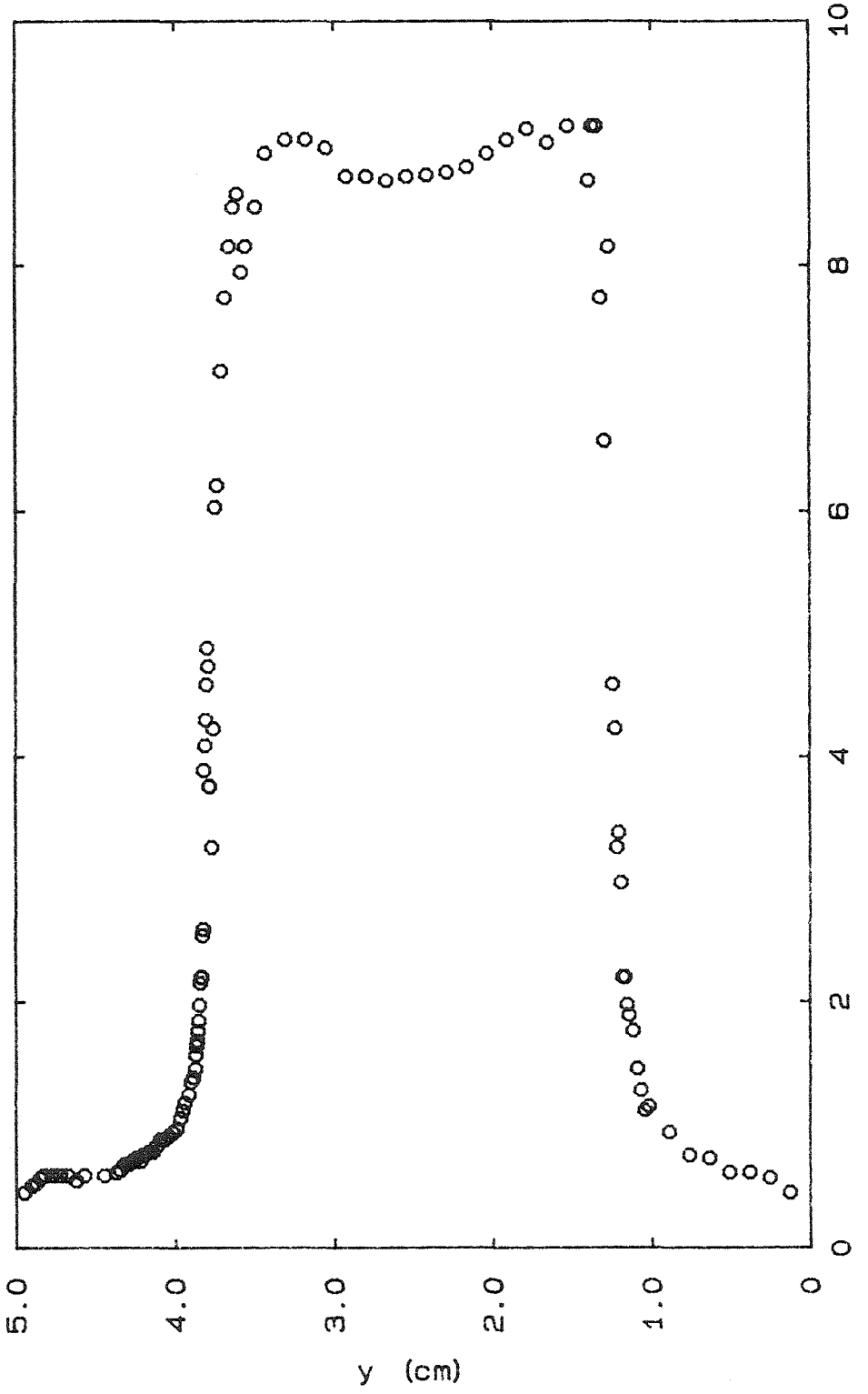


Figure 4.5 Velocity Profile at Upstream Baffle

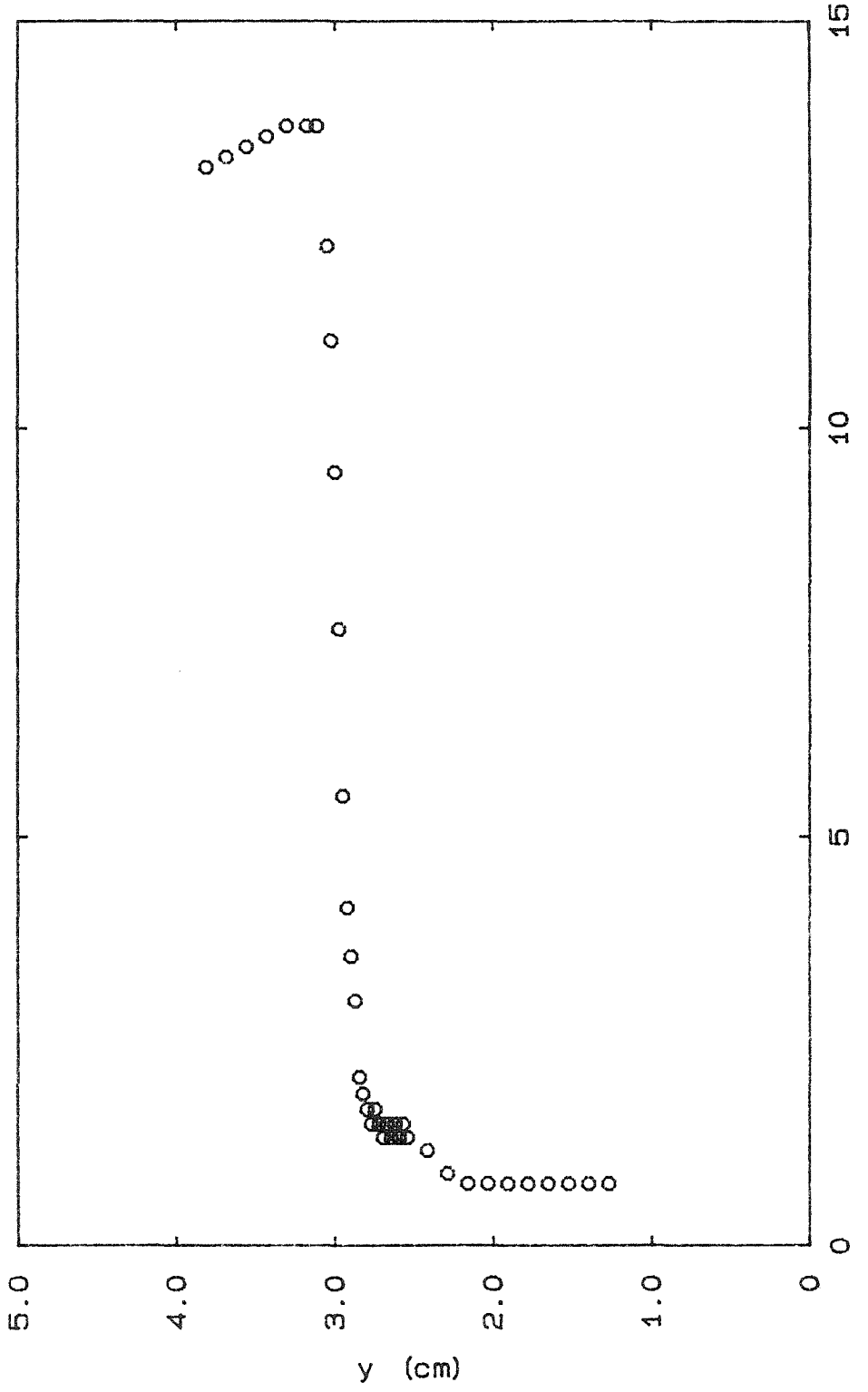


Figure 4.6 Velocity Profile with single Half-Width Baffle

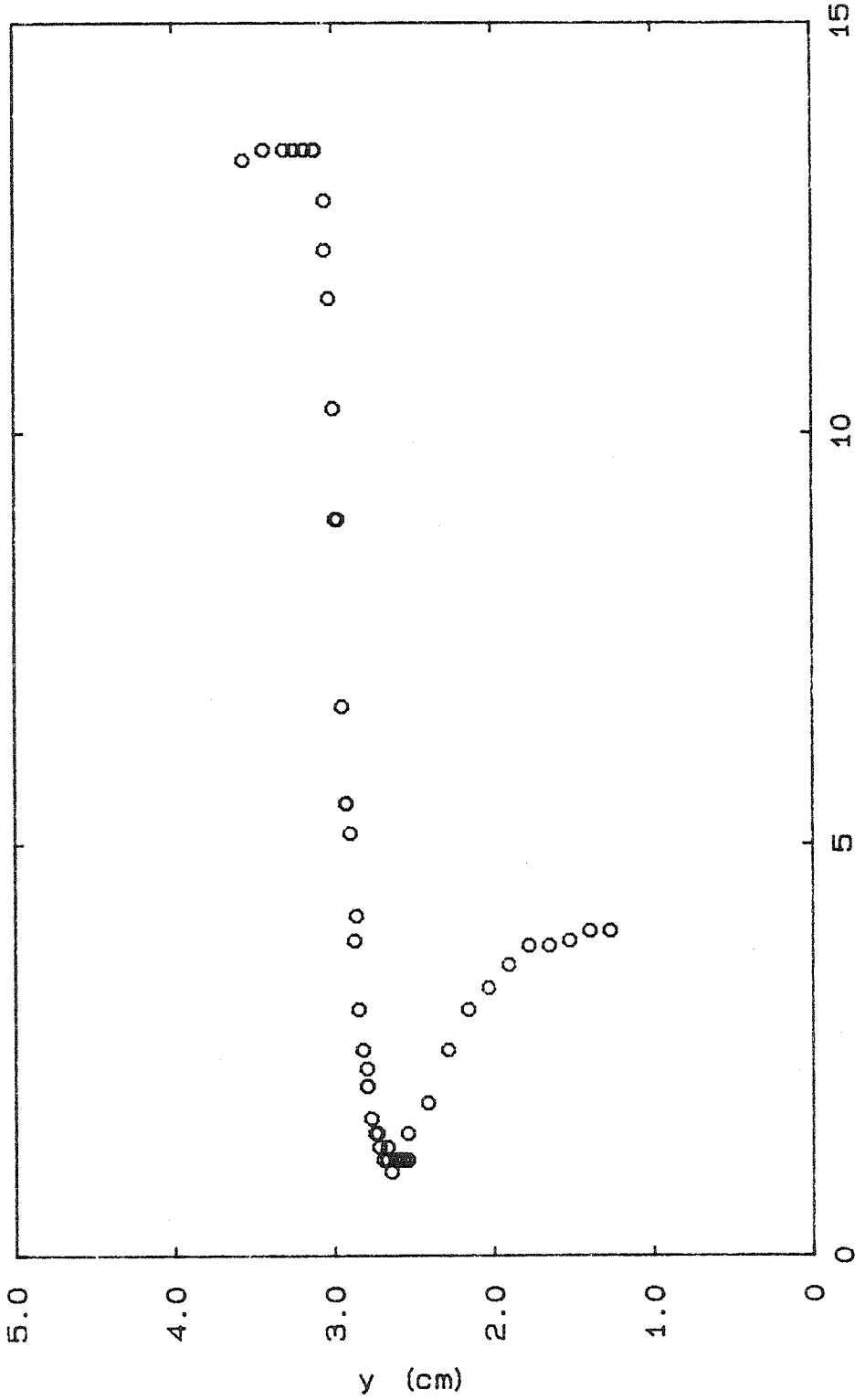


Figure 4.7 Effect of Downstream Baffle

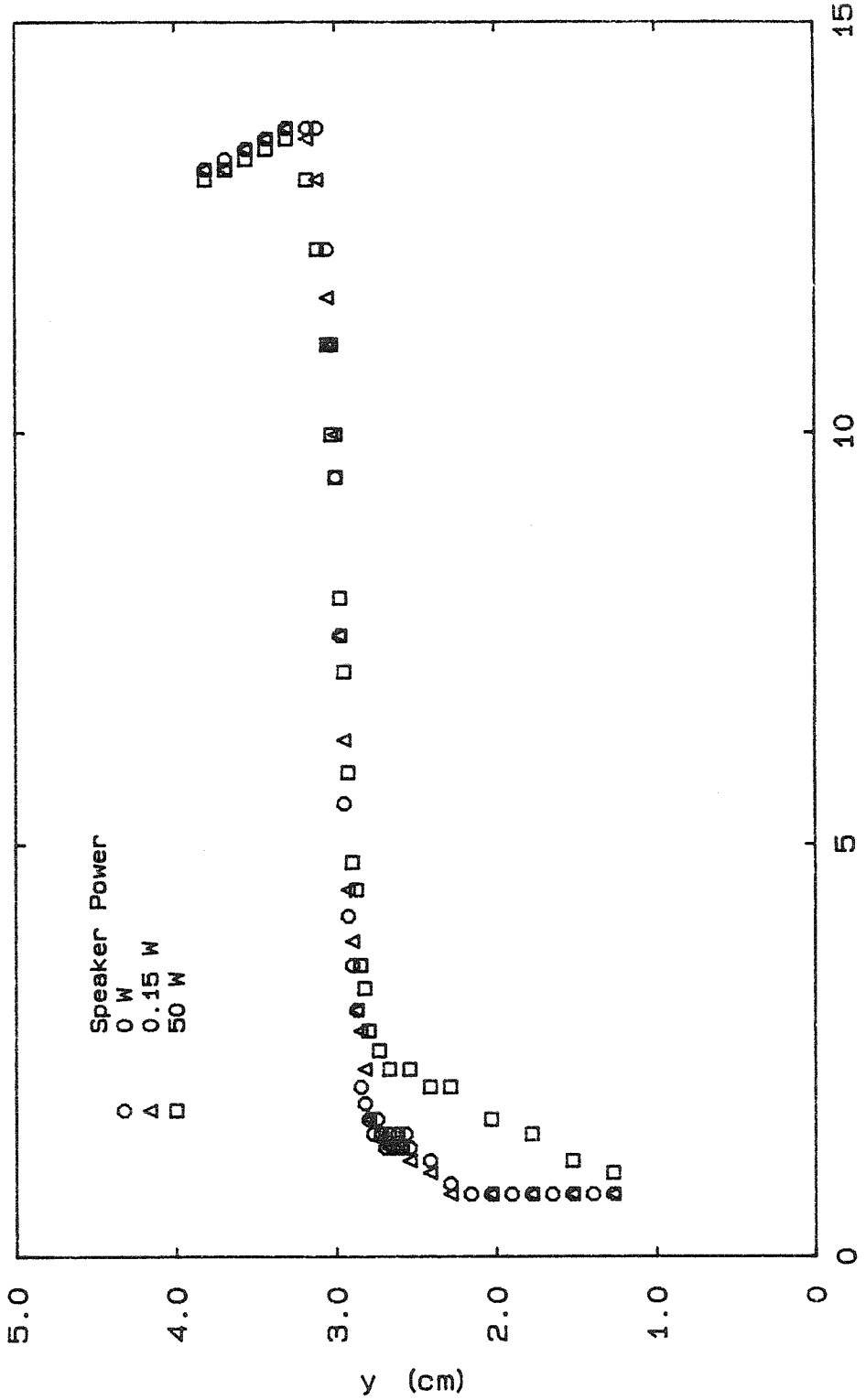


Figure 4.8 Effect of External Acoustic Driving

to the physical presence of the second baffle are absent. In Figure 4.7, a second baffle is installed at the downstream location yielding the strongest oscillation using the same velocity. The profile measured at the same location just downstream of the first baffle shows considerable influence due to recirculation associated with the downstream baffle. However, the shear layer itself is relatively unaffected by the additional baffle.

With substantial acoustic driving using the loudspeaker, it is possible to affect the mean properties of the shear layer, although for levels equivalent to those occurring naturally, such effects are negligible. This is illustrated in Figure 4.8 which shows the effect of different levels of driving using the loudspeaker with a single baffle installed. With the speaker power equal to 0.15 Watts, the acoustic pressure in the duct is the same as for the self-excited resonance occurring when the profile in Figure 4.7 was measured. There is no appreciable difference between the curves with driving at this level and with no driving. Even when the maximum power of the amplifier is used, the thickening of the shear layer is barely perceptible.

## 4.3. Momentum Thickness Measurements.

The momentum thickness is defined as

$$\theta = \int_{-\infty}^{\infty} \frac{(u-U_1)(U_2-u)}{(U_2-U_1)^2}\, dy \qquad (4.2)$$

This is calculated by numerically integrating the experimentally measured data. The momentum thickness calculation depends quite strongly on which points are used as the real limits of integration in calculating the momentum thickness. If the lower limit is taken well behind the baffle, then the velocity is substantially increased from its minimum near the lip of the baffle due to recirculation and it is possible to obtain a negative momentum thickness, which has no physical meaning. Furthermore, it is likely that the increased velocity behind the baffle is not parallel to the freestream, but is rather directed up the rear face of the baffle since a single hotwire anemometer cannot distinguish directions.

Due to the acceleration of the flow in the neighborhood of the baffle tip, there is a reduction in the mean velocity far out in the freestream. If this point were used as the upper limit of integration, unrealistically high values would be obtained for the parameter being calculated.

Generally, the minimum and maximum velocity points are used, although judgement is exercised when such a point is unrepresentative of the velocity in the vicinity. Using this approach, the momentum thickness for the case with two baffles is found to be 0.470mm (0.0185in) compared with 0.434mm (0.0171in) for the single baffle. Considering the amount of variation that can be obtained from a single set of measurements by changing just the limits of integration, the agreement between the two cases is very good, indicating that the mean properties of the shear layer are largely unaffected by the resonance. For the case with self-excited resonance the frequency is 273Hz and the velocity difference across the layer is 12.3 m/s. Thus the Strouhal

number is $S_\theta$ = 0.010 which is close to the Strouhal number with the greatest saturated amplitude (Figure 3.3).

## 4.4. Effect of Baffle Spacing at Constant Mean Velocity.

If the freestream velocity is held constant and the baffle spacing is varied, it is found that the amplitude of the self-excited resonance varies as indicated in Figure 4.9. For some baffle spacing the maximum acoustic pressure is obtained and the amplitude falls off as the spacing is increased or decreased from this point. Also plotted in Figure 4.9 is the predicted response due to the simple model of Appendix B. The curve is adjusted to match only at the maximum point, showing that the trend is well predicted by this cosine.

The same cosine-shaped response to changes in the baffle spacing as the predicted by the simple model can be found using the following result: If the response velocity for any damped linear oscillator is cross-plotted against the phase difference, $\phi$, between the constant forcing function and the response velocity, the result is proportional to $\cos\phi$ regardless of Q. Assume the shear layer can amplify an infinitesimal disturbance enough that it saturates before reaching the downstream baffle. The forcing amplitude is thus constant regardless of the response amplitude. Rockwell and Schachenmann (22), using a long tube terminated with a hole-tone, find that for maximum response there is a phase difference of $2n\pi$ between the centerline velocity fluctuations at separation and impingement. If the convection velocity is constant, then changing the baffle spacing will change the phase difference proportionally. The response velocity plotted versus

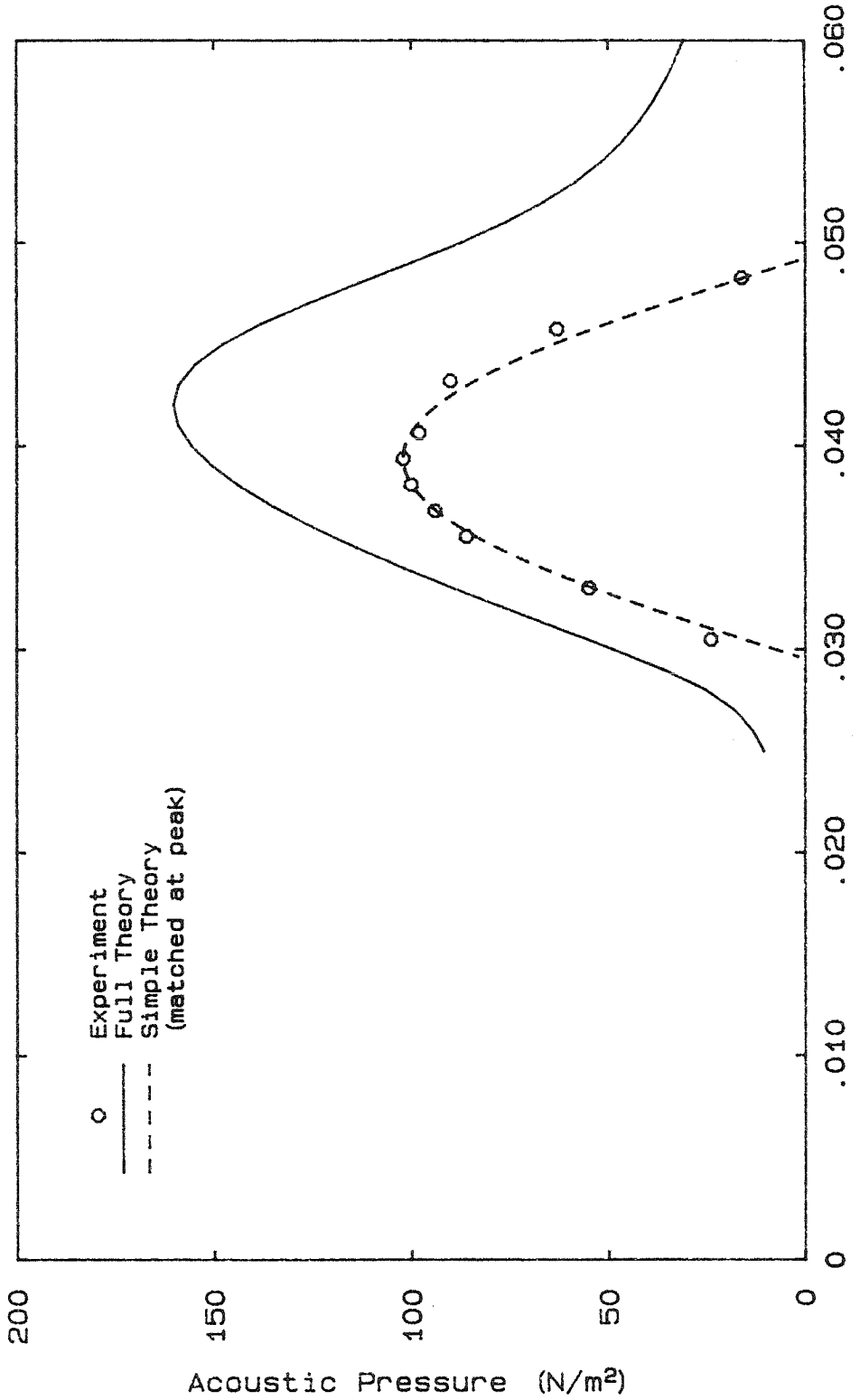


Figure 4.9 Effect of Baffle Spacing on Amplitude

baffle spacing must, then, also have a cosine shape since the baffle spacing is proportional to the phase difference.

The phase difference between the response velocity and the driving force must be in the range -90° to +90° in order for energy to be added to the system. This implies that the variation from the tuned condition mentioned above can be up to 90°. The corresponding baffle spacing must therefore be in the range $(n - 0.25)\Delta x_m$ to $(n + 0.25)\Delta x_m$, where n is the stage number, the integer closest to the number of wavelengths from separation to impingement and $\Delta x_m$ is the spacing that yields maximum response for the first stage of operation, n = 1. Naturally, for a real shear layer the initial disturbance must be of some finite value in order for saturation to occur before the second baffle is reached. For a resonator with a high Q, this reduces the theoretical limits given above only slightly. As can be seen in Figure 4.9, the agreement between these predicted limits and those observed experimentally is excellent.

The more detailed model (Appendix C) is able to predict amplitudes (Figure 4.9), although it does not predict the variation quite as well as the simple model. The shape of the curve near the peak is correct, but the inflection points on either side are not evident in the measured data and indicate a deficiency in some part of the model. Nonetheless, the amplitude is within a factor of two and the peak occurs at a baffle spacing very near to the experimental value. With the assumptions made in the model this is considered to be excellent agreement.

The associated response frequency, while remaining close to the resonant frequency, does increase with decreasing baffle spacing as depicted in Figure 4.10. Once again, the simple model does a remarkable job in predicting the variation. Since the simple model assumes that a natural frequency is given, the curve is matched to the data at the point used in the previous figure. Furthermore, it is also necessary to fit the slope of the tangent to the data here. From the value of this slope, the quality factor of the resonator can be inferred using equation B.12, and is found to be about 20, the same as the value measured experimentally for the first acoustic mode of the duct.

The acoustic model in the full theory overpredicts the natural frequency of the duct since it does not account for the effect of the baffles. The shift between the frequency curve and the measured data in Figure 4.10 corresponds exactly to the difference between the natural frequencies measured with and without the baffles installed.

## 4.5. Effect of Baffle Location within the Duct.

The baffles induce resonance effectively only when they are positioned in the neighbourhood of a velocity antinode. This is demonstrated experimentally in Figure 4.11 in which the maximum acoustic pressure is plotted versus the location of the center of the baffle pair within the duct. The height of the baffles is 15.2mm (0.6in) and the spacing between them is 25.4mm (1.0in). The mean velocity, which is adjusted at each station to produce the largest response, is nearly constant for all locations, increasing from about 13.5 m/s at either extremity to about

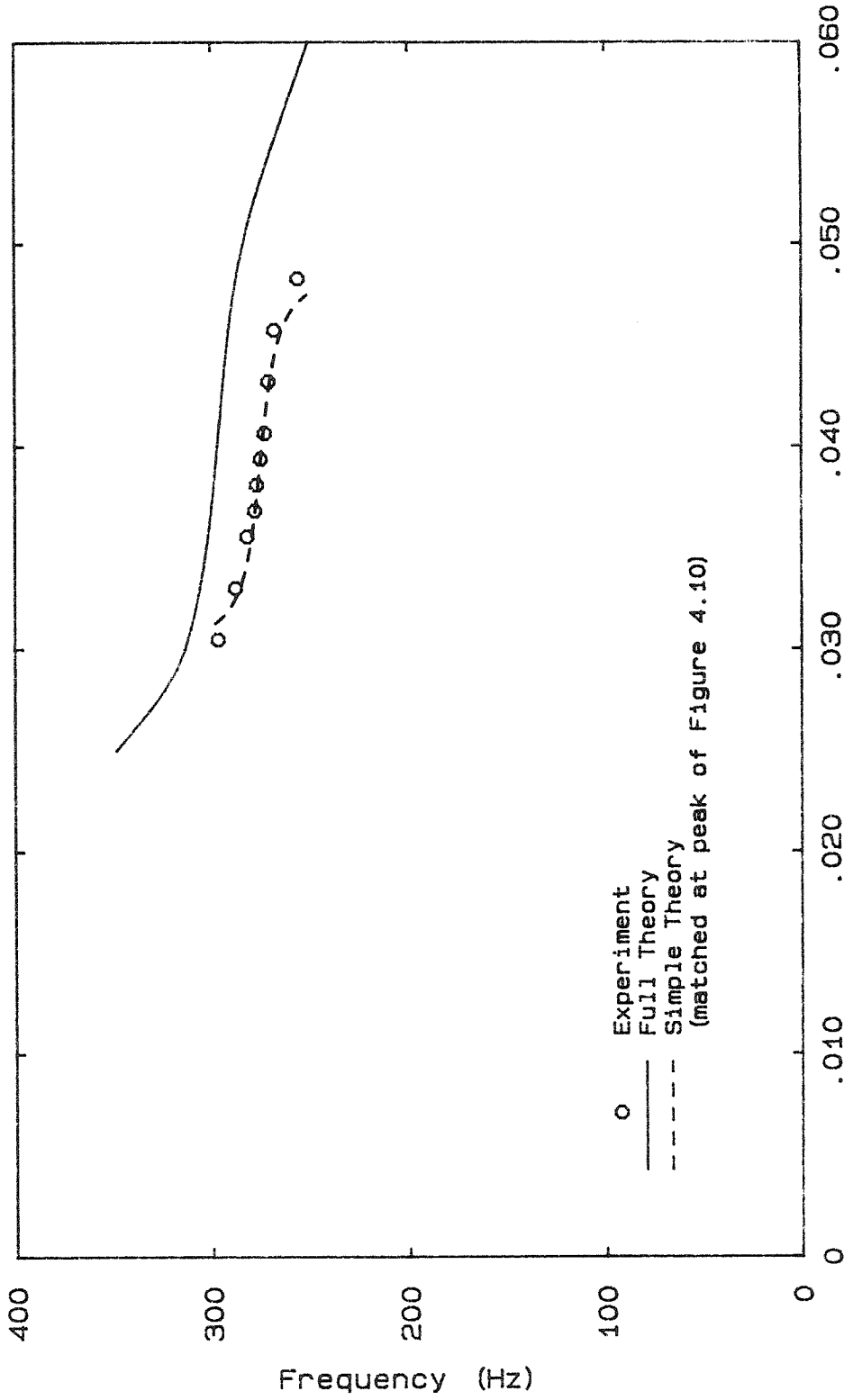


Figure 4.10 Effect of Baffle Spacing on Frequency

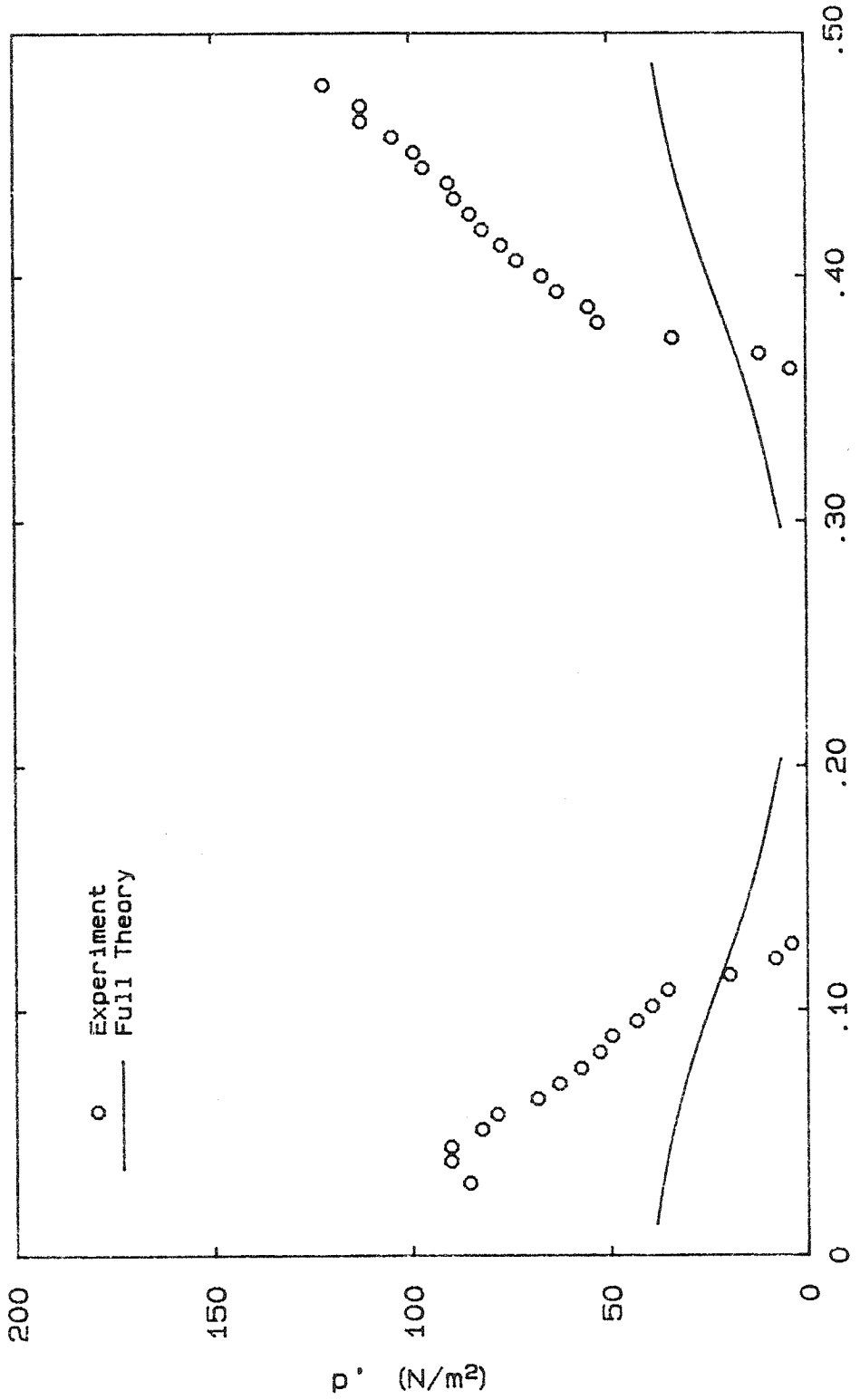


Figure 4.11 Effect of Baffle Location on Amplitude

14.5 m/s towards the center. The frequency also increases slightly, from 270Hz at the ends to 280Hz towards the interior. Although the amplitudes are not exactly the same at each end, the basic characteristics are symmetric with respect to the midpoint of the duct.

The mathematical model discussed in Appendix C gives exactly symmetric results for the two ends. Here, the velocity is equal to 14 m/s throughout. Again, the maximum response occurs at the velocity antinodes and suggests that the assumption that the acoustic response of the duct acts as the initial perturbation to the shear layer is correct. An important conclusion that can be drawn from this observation is that a shear layer responds to fluctuations in the velocity and not in the pressure.

An argument counter to this claim is that perhaps the shear layer does respond to pressure fluctuations but that oscillation are not observed since the duct does not respond strongly to forcing due to the impingement of vortices on a baffle at its pressure antinodes.

The counter argument is shown to be incorrect using smoke flow visualization and a strobe light triggered by the output of a microphone at the pressure antinode. A single baffle is placed in the duct at various locations and the resonance is driven by the loudspeaker. If the formation of the vortices was being triggered by the pressure oscillations, then the strength of the vortices would be greatest with the baffle at the pressure antinode. In fact, vortices form only with the baffle away from this location and their strengths are greatest toward the pressure nodes (velocity antinodes). In addition, for the fundamental acoustic mode of the open/open duct, the

oscillating pressure is essentially in phase at all points along the duct, whereas the velocity is 180° out of phase at opposite ends of the duct. Since the position of the vortex is frozen with respect to the pressure signal, it should appear at the same location relative to the baffle for all points in the duct if vortex formation is triggered by the pressure. Instead, the vortex location is seen to be 180° out of phase when the baffles are located at opposite ends of the duct, further demonstrating that the shear layer responds to oscillations in the velocity and not in the pressure.

Plotted in Figure 4.12 is the variation in frequency as the baffles are moved along the duct. The model indicates a very slight reduction in frequency towards the center, while the experimental points rise a little. This is attributed to holding the velocity constant in the model whereas in the experiments the velocity was increased somewhat to maintain maximum pressure amplitude as the baffles were moved towards the center of duct. Also, the effect of the blockage (29) due to baffles is to reduce the resonant frequency when they are near velocity antinodes (at the ends of the duct), an effect ignored in the model. Once again the vertical offset is due to this same effect of the baffles on the natural frequency.

## 4.6. Changes with Mean Velocity.

When the mean velocity flowing past an edgetone system is varied, the frequency varies proportionately. In the present apparatus, this is not the case due to the effect of the coupled resonator, the duct. When the speed is increased, the frequency does rise slightly, but it remains

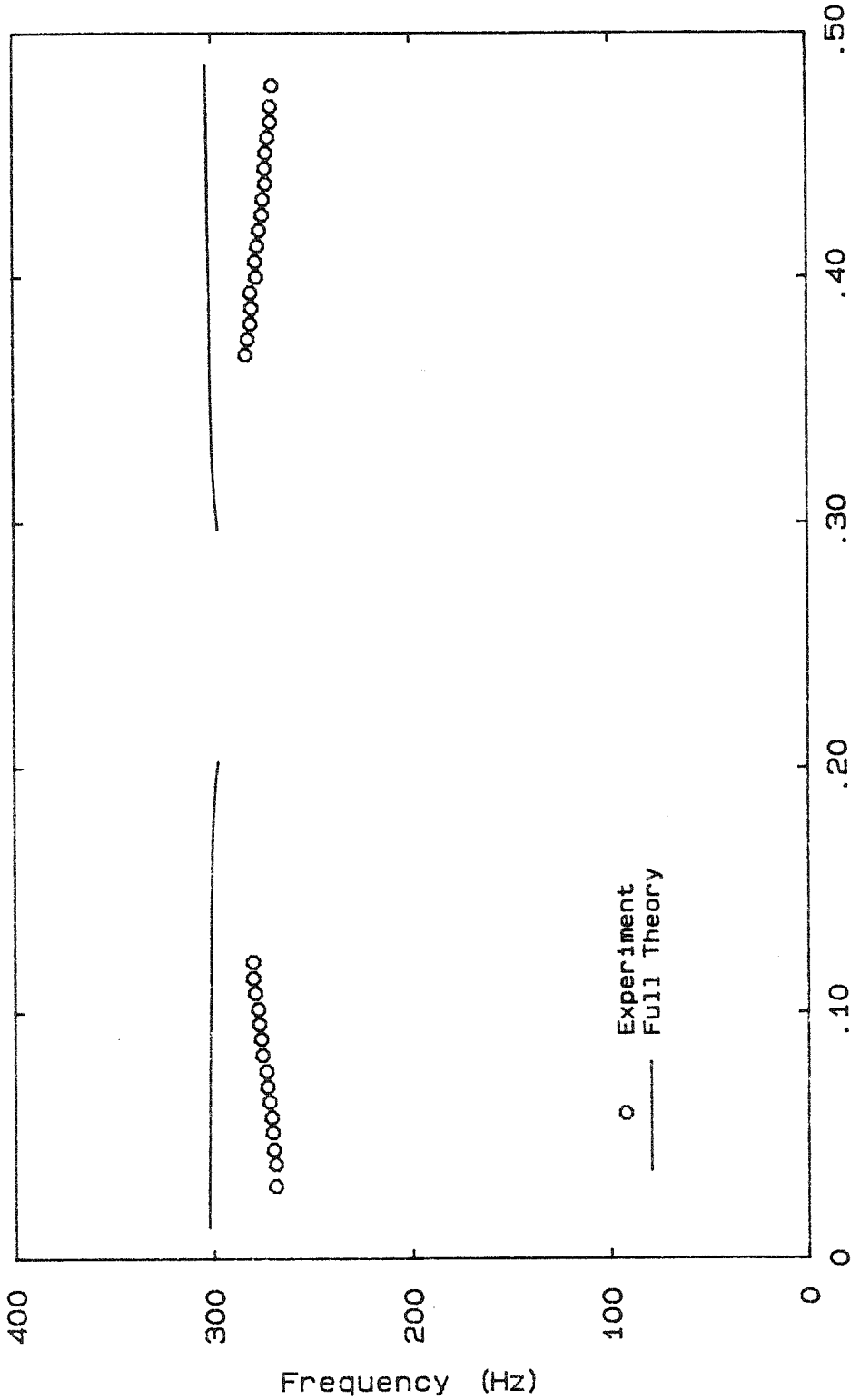


Figure 4.12 Effect of Baffle Location on Frequency

very close to the resonant frequency of the duct, as observed by Nomoto (7). The greatest response occurs for the first acoustic mode and the first edgetone stage of operation in the apparatus used. This condition occurs for some speed depending mostly upon the baffle spacing. If the speed is reduced gradually from this point, the amplitude drops until resonance no longer occurs. As the speed is reduced further, the second stage begins to operate, peaking at roughly a half of the velocity at which the first stage reached its peak. As the velocity is reduced further, the second stage dies and is replaced by the third at one third of the original speed, and then the fourth stage appears and has its peak at a quarter of the speed of the first stage maximum. This succession does not persist indefinitely since reducing the velocity increases the Strouhal number and eventually the shear layer can no longer respond at the resonant frequency of the duct.

The progression of peaks with changing velocity is shown in Figure 4.13. The ratios of the velocities of successive peaks does not exactly follow the progression described above due to the convection velocity's dependence on Strouhal number. The amplitude calculated by the model agrees quite well with the experimental results. More important is the good agreement in the location of the peak since the amplitude is only expected to agree within an order of magnitude on account of the approximations made in the model. For both the experimental and the theoretical cases, the baffle spacing is held fixed at 26.7mm (1.5in). The frequency variation is also modeled well, as shown in Figure 4.14. Again, the vertical difference between the prediction and measurements is attributed to the reduction in the natural frequency of the duct by the physical presence of the baffles.

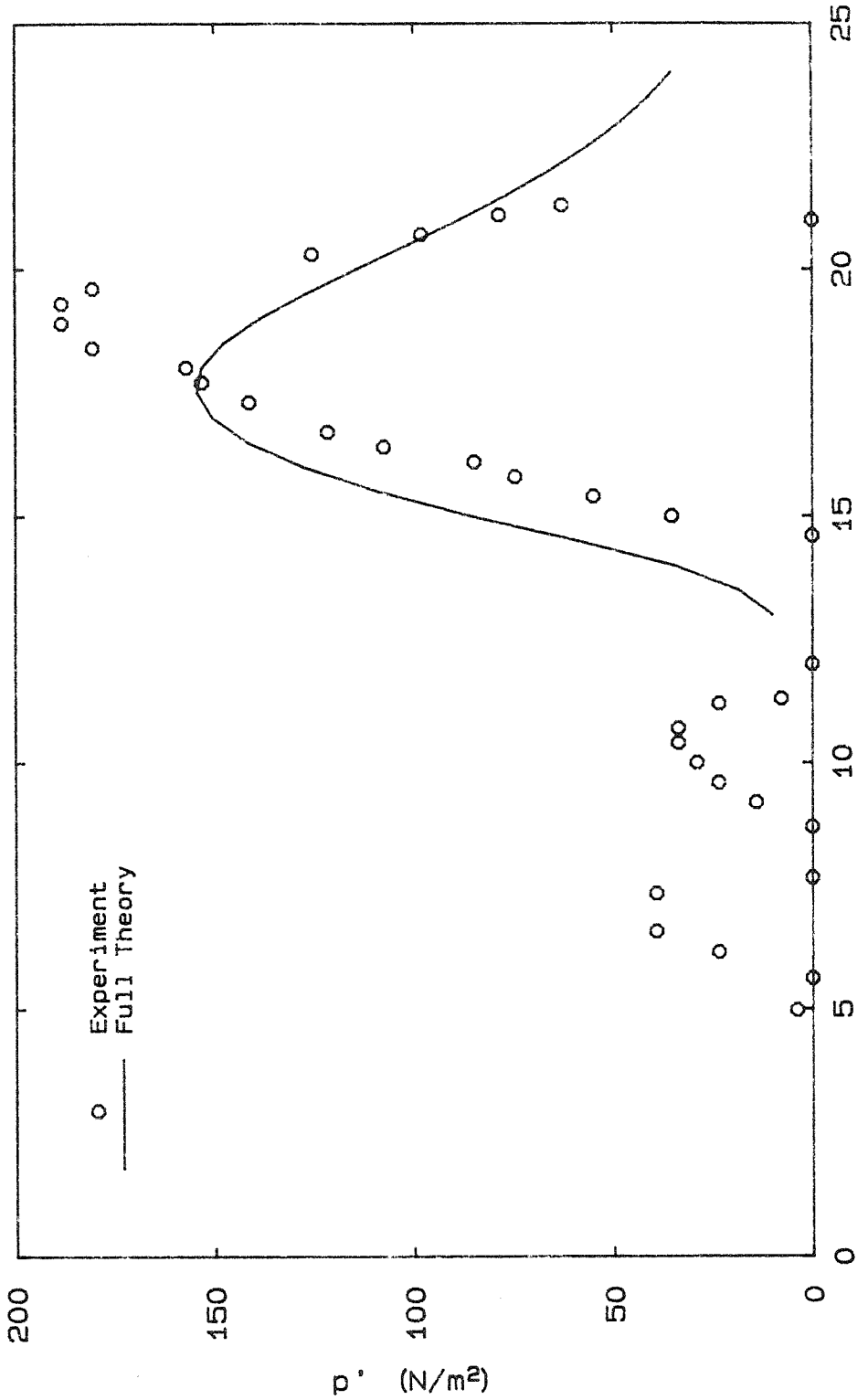


Figure 4.13 Effect of Mean Velocity on Amplitude

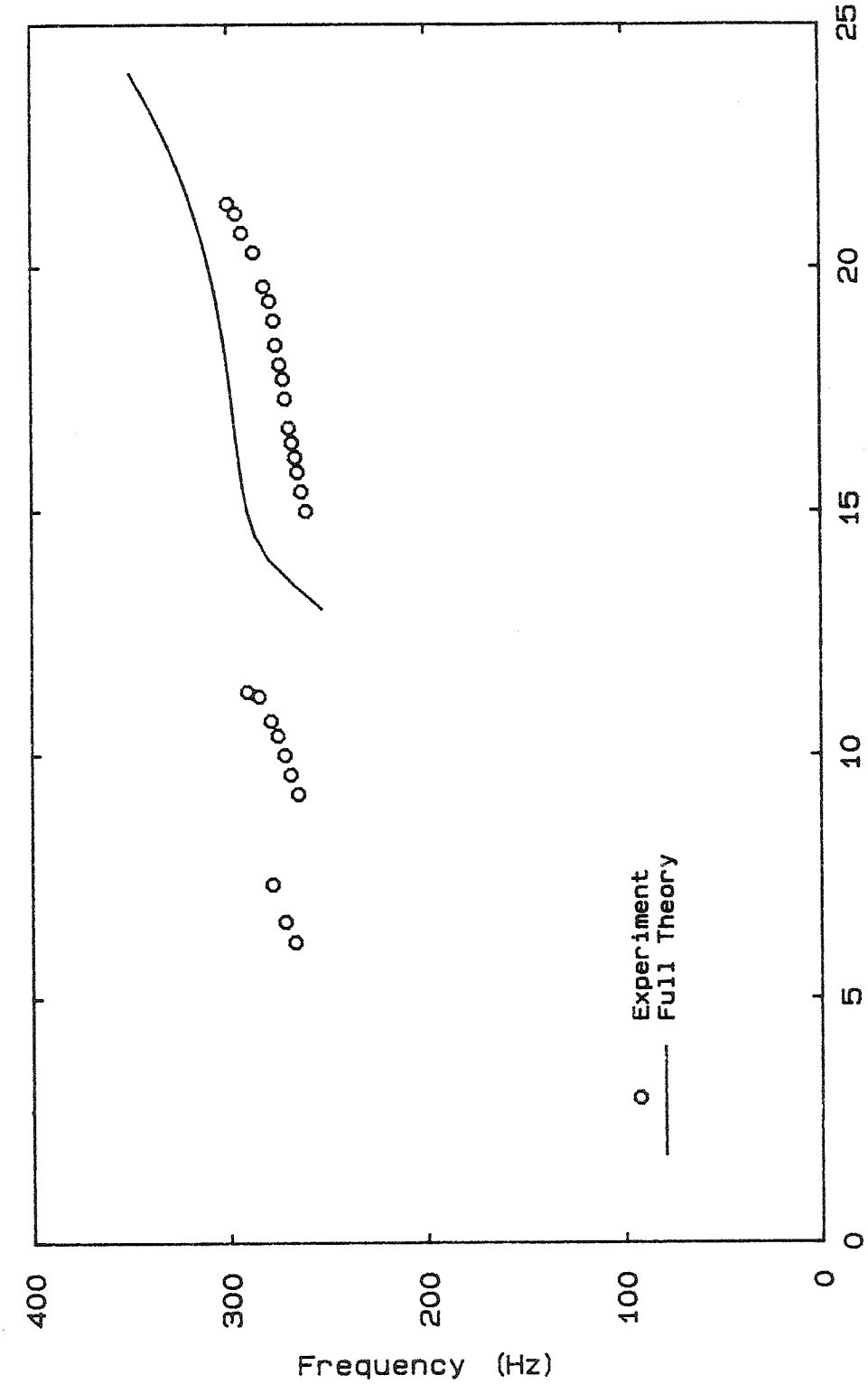


Figure 4.14 Effect of Mean Velocity on Frequency

The model agrees well with the measured data for variations in mean velocity, baffle spacing and baffle location within the duct. This agreement confirms that the postulated mechanism is correct.

# Chapter 5
# CONCLUSIONS

Based on laboratory experiments and results quoted in the literature, a mechanism has been postulated which explains the interaction between an edgetone system and an acoustic resonator. This mechanism is believed to be a contributor to undesirable low frequency tones in segmented solid propellant rockets.

Two key elements required for the mechanism to operate are a shear layer in which vortices grow and an obstruction downstream. The most important idea leading to an understanding of the edgetone and resonator system is that the acoustic response velocity acts as the perturbation which triggers the formation of the vortices in the shear layer. These vortices, in turn, drive the acoustic resonance by interacting with the obstacle downstream. The hydrodynamically-induced velocity fluctuations due directly to the interaction of the vortices with the obstruction, which trigger the vortex growth in an isolated edgetone, are negligible when compared with the acoustic velocity.

Since the vortices are initiated in phase with the acoustic response, changing the distance from separation to impingement or changing the mean velocity changes the phase between the forcing and response of the acoustic resonance. Due to rapid variations with frequency in the phase between driving and response of any lightly damped resonator near its natural frequency, the frequency remains essentially constant and equal to one of the acoustic resonances of the chamber for all operating conditions that produce

oscillations. The larger the quality factor, Q, is, the greater the amplitude will be and the less the frequency will vary. Over large ranges of velocity and large ranges of distance from separation to impingement, an edgetone and resonator system produces significant spontaneous vibrations.

The amplitude of oscillation is limited by the saturation of the strength of the shear layer vortices; therefore it is not possible for the sound level to increase without bound. Generally, the level reached will be quite low compared, for example, with oscillations due to combustion instabilities. Nonetheless, the energy associated with the mechanism is concentrated in narrow frequency bands which could lead to vibration problems with components having resonant frequencies in those bands.

An important parameter is the Strouhal number based on the momentum thickness at separation. Oscillation will not occur if the resonant frequencies correspond to Strouhal numbers outside the amplified range (0 to 0.04). The strongest fluctuations exist when the resonant peak corresponds to the Strouhal number with the maximum saturated amplitude (0.01).

Based on the physical description given above, a model has been developed which behaves in a manner similar to that of the experimental apparatus used to investigate these self-excited oscillations. Amplitudes can only be predicted within an order of magnitude with any degree of confidence due to some coarse assumptions in the model. Therefore, the actual agreement, which is within a factor of two for most cases, is probably fortuitous. The good agreement in the observed trends, however, is very

important and confirms that the proposed mechanism is correct.

Armed with an understanding of this mechanism, designers should be able to anticipate the occurrence of oscillations due to the phenomenon described and either enhance or weaken them as desired by adjusting the geometry or flow characteristics. The most obvious way to eliminate these self-excited acoustic oscillation is to remove the edgetone. Separation should be avoided so shear layers cannot form. When geometries which place obstacles in the path of vortices are unavoidable, an effort to increase the momentum thickness at separation may force the Strouhal number beyond the value of 0.04, the upper limit for which the shear layer is unstable.

# 1. References

[1] Flandro, G. A., Jacobs, H. R., "Vortex-Generated Sound in Cavities," Progress in Astronautics and Aeronautics: Aeroacoustics: Jet and Combustion Noise: Duct Acoustics, vol 37 (1975)

[2] Freymuth, P., "On transition in a separated laminar boundary layer," JFM 25,683-704 (1966)

[3] Michalke, A., "On the inviscid instability of the hyperbolic tangent velocity profile," JFM 19,543-556 (1964)

[4] Michalke, A., "On spatially growing disturbances in an inviscid shear layer," JFM 23,521-544 (1965)

[5] Michalke, A., Freymuth, P., "The Instability and the Formation of Vortices in a Free Boundary Layer," AGARD-CP-4 Separated Flow Part II (1966)

[6] Culick, F. E. C., Magiawala, K., "Excitation of Acoustic Modes in a Chamber by Vortex Shedding," J. Sound and Vib 64,455-457 (1979)

[7] Nomoto, H., "Acoustic Waves Generated by Vortex Shedding," Aeronautics Engineer's thesis, CIT, Pasadena (1980)

[8] Brown, R. S., Dunlap, R., Young, S. W., Flandro, G. A., Isaacson, L. K., Beddini, R. A., Culick, F. E. C., "Vortex Shedding Studies," AFRPL TR-80-13 (1980)

[9] Brown, R. S., Dunlap, R., Young, S. W., Waugh, R. C., "Vortex Shedding as a Source of Acoustic Energy in Segmented Solid Rockets", J. Spacecraft 18,312-319 (1981)

[10] Dunlap, R., Brown, R. S., "Exploratory Experiments on Acoustic Oscillations Driven by Periodic Vortex Shedding," AIAA J. 19,408-409 (1981)

[11] Nomoto, H., Culick, F. E. C., "An Experimental Investigation of Pure Tone Generation by Vortex Shedding," in a Duct, J. Sound and Vib. 84,247-252 (1982)

[12] Andronow, A. A., Chaikin, C. E., "Theory of Oscillations," Princeton Univ. Press, New Jersey (1949)

[13] Stoker, J. J., "Nonlinear Vibrations in Mechanical and Electrical Systems," Interscience Publishers, Inc., New York (1950)

[14] Rockwell, D., "Oscillations of Impinging Shear Layers," Invited lecture, 20th Aerospace Sciences Meeting, AIAA (1982)

[15] Rockwell, D., Naudascher, E., "Self-Sustained Oscillations of Impinging Free Shear Layers," Ann. Rev. Fl. Mech. 11,67-94 (1979)

[16] Rossiter, J. E., "Wind-Tunnel Experiments on the Flow over Rectangular Cavities at Subsonic and Transonic Speeds," R.& M. 3438, London (1966)

[17] Gharib, M., "The Effect of Flow Oscillations on Cavity Drag, and a Technique for Their Control," Ph D thesis, Caltech, Pasadena (1983)

[18] Ziada, S., Rockwell, D., "Oscillations of an unstable mixing layer impinging upon an edge," JFM 124,307-334 (1982)

[19] Kinsler, L. E., Frey, A. R., "Fundamentals of Acoustics," Wiley (1962)

[20] Flandro, G. A., Finlayson, P. A., "Nonlinear Interactions Between Vortices and Acoustic Waves in a Rocket Combustion Chamber," Preprint. U. Utah (1984)

[21] Schachenmann, A., Rockwell, D., "Self-sustained oscillations of turbulent pipe flow terminated by an axisymmetric cavity," J. Sound and Vib. 73,61-72 (1980)

[22] Rockwell, D., Schachenmann, A., "Self-generation of organized waves in an impinging turbulent jet at low Mach number," JFM 117,425-441 (1982)

[23] Rockwell, D., Schachenmann, A., "The organized shear layer due to oscillations of a turbulent jet through an axisymmetric cavity," J. Sound and Vib. 85(3),371-382 (1982)

[24] Kryloff, N., Bogoliuboff, N., "Introduction to Non-Linear Mechanics," Princeton University Press (1943)

[25] Holger, D. K., Wilson, T. A., Beavers, G. S., "Fluid mechanics of the edgetone," J. Acoust. Soc. Am. 62(5),1116-1128 (1977)

[26] Holger, D. K., Wilson, T. A., Beavers, G. S., "The amplitude of edgetone sound," J. Acoust. Soc. Am. 67(5),1507-1511 (1980)

[27] Panaras, A. G., "Pressure pulses generated by the interaction of a discrete vortex with an edge," JFM (to be published, 1985)

[28] Ralston, A. "A First Course in Numerical Analysis," McGraw-Hill, New York (1965)

[29] El-Raheb, M., Wagner, P., "Acoustic propagation in rigid ducts with blockage," J. Acoust. Soc. Am. (72),1046-1055 (1982)

[30] Bogoliubov, N. N., Mitropolsky, Y. A., "Asymptotic Methods on the Theory of Non-Linear Oscillations," Hindustan Publishing Corp., Delhi (1961)

[31] Culick, F. E. C., "Nonlinear behaviour of acoustic waves in combustion chambers-I," Acta Astronautica(3),715-734 (1976)

[32] Culick, F. E. C., "Nonlinear behaviour of acoustic waves in combustion chambers-II," Acta Astronautica(3),735-757 (1976)

[33] Culick, F. E. C., "Non-Linear Growth and Limiting Amplitude of Acoustic Oscillations in Combustion Chambers," Comb. Sc. and Tech. 3,1-16 (1971)

[34] Milne-Thomson "Theoretical Hydrodynamics," Fourth edition, MacMillan Co. NY (1960)

[35] Tang, Y. P., Rockwell, D., "Instantaneous pressure fields at a corner associated with vortex impingement," JFM 126,187-204 (1983)

## Appendix A

## METHOD OF TIME AVERAGING

In this appendix, the method of time averaging will be reviewed in order to use the results in solving the equation connected with the simple mathematical model in Appendix B. This approximate technique is due to Kryloff and Bogoliuboff (24), although the notation has been changed a little. A more rigorous treatment can be found in Bogoliubov and Mitropolsky (30). Further discussion and application of the method of time averaging to problems of acoustics in combustion chambers can be found in several papers by Culick (31,32,33).

Consider an oscillator governed by the equation

$$\ddot{\eta} + \omega_o^2 \eta + f(\dot{\eta}) = 0 \qquad (A.1)$$

where dots denote differentiation with respect to time. If $f = 0$, then the solution is

$$\eta = A \sin(\omega_o t + \phi) \qquad (A.2)$$

$$\dot{\eta} = \omega_o A \cos(\omega_o t + \phi) \qquad (A.3)$$

If $f(\dot{\eta})$ is small compared with the other terms, then it is expected that a solution of the form

$$\eta = A(t) \sin(\omega_o t + \phi(t)) \qquad (A.4)$$

will hold, where $A(t)$ and $\phi(t)$ are slowly varying functions

of time. Differentiating gives

$$\dot{\eta} = \omega_o A \cos(\omega_o t+\phi) + \dot{\phi}A \cos(\omega_o t+\phi) + \dot{A} \sin(\omega_o t+\phi) \tag{A.5}$$

The second two terms are much smaller than the first, and following the approach of Kryloff and Bogoliuboff (24) the combination is required to be identically zero.

$$\dot{\phi}A \cos(\omega_o t+\phi) + \dot{A} \sin(\omega_o t+\phi) = 0 \tag{A.6}$$

This leaves (A.5) in the form of (A.3), which when differentiated yields

$$\ddot{\eta} = -\omega_o^2 A \sin(\omega_o t+\phi) - \omega_o \dot{\phi}A \sin(\omega_o t+\phi) + \omega_o \dot{A} \cos(\omega_o t+\phi) \tag{A.7}$$

Substituting (A.4) and (A.7) into (A.1) gives

$$-\omega_o \dot{\phi}A \sin(\omega_o t+\phi) + \omega_o \dot{A} \cos(\omega_o t+\phi) + f(\dot{\eta}) = 0 \tag{A.8}$$

(A.6) and (A.8) can be solved simultaneously to give

$$\omega_o \dot{A} + f(\dot{\eta}) \cos(\omega_o t+\phi) = 0 \tag{A.9}$$

$$\omega_o \dot{\phi}A - f(\dot{\eta}) \sin(\omega_o t+\phi) = 0 \tag{A.10}$$

or

$$\frac{d}{dt}A(t) = \frac{f(\dot{\eta}) \cos(\omega_o t+\phi)}{\omega_o} \tag{A.11}$$

$$\frac{d}{dt}\phi(t) = - \frac{f(\dot{\eta}) \sin(\omega_o t+\phi)}{\omega_o A(t)} \qquad (A.12)$$

Averaging over a period of oscillation at $\omega_o$, $T = 2\pi/\omega_o$, and assuming $A(t)$ and $\phi(t)$ are constant throughout the period of integration gives

$$\frac{d}{dt}A(t) \approx - \frac{1}{\omega_o T} \int_o^T f(\dot{\eta}) \cos(\omega_o t+\phi)dt \qquad (A.13)$$

$$\frac{d}{dt}\phi(t) \approx \frac{1}{\omega_o AT} \int_o^T f(\dot{\eta}) \sin(\omega_o t+\phi)dt \qquad (A.14)$$

Use will be made of these equations in Appendix B which deals with the simple model. Note that $\frac{d\phi}{dt}$ equals a constant represents a shift in frequency.

As an example, consider the case when $f(\dot{\eta})$ is proportional to $\dot{\eta}$. The resulting equation

$$\ddot{\eta} + \frac{\omega_o}{Q}\dot{\eta} + \omega_o^2\eta = 0 \qquad (A.15)$$

represents the response of a damped linear oscillator with no forcing. In this case, $f(\dot{\eta})$ represents just the damping term. The exact solution is

$$\eta = Ce^{\alpha t}\cos(\omega_d t + \phi_d) \qquad (A.16)$$

where

$$\alpha = - \frac{\omega_o}{2Q} \qquad (A.17)$$

$$\omega_d^2 = \omega_o^2 \left(1 - \frac{1}{4Q^2}\right) \qquad (A.18)$$

C and $\phi_d$ are determined by the initial conditions and are unimportant here.

In order to apply the method of time averaging we use

$$f(\dot{\eta}) = \frac{\omega_o}{Q} \dot{\eta} = \frac{\omega_o^2}{Q} A \cos(\omega_o t + \phi) \qquad (A.19)$$

where $\dot{\eta}$ has been replaced by $\omega_o A \cos(\omega_o t + \phi)$. When this is substituted into equations (A.13) and (A.14) the results are

$$\frac{dA}{dt} \approx - \frac{\omega_o}{2Q} A, \text{ that is, } \alpha = - \frac{\omega_o}{2Q} \qquad (A.20)$$

$$\frac{d\phi}{dt} \approx 0 \qquad (A.21)$$

The approximate method incorrectly predicts zero shift in frequency; however, to the order of approximation in the model the result is correct. The correction term, $- \frac{1}{4Q^2}$ is second order, and for Q = 20, a typical value for the duct used in the experiments, this correction is negligible. The model gives the exact value for the growth rate given in equation (A.17) (negative value means decay).

## Appendix B

## Simple Mathematical Model

In the simple model, the important idea is that the forcing function, analogous to the oscillating drag on the downstream baffle, is related to the acoustic velocity at an earlier time, $\tau$, determined by the time of flight of the vortices from one baffle to the next.

$$\tau = \frac{\Delta x}{U_c} \qquad (B.1)$$

where $\Delta x$ is the baffle spacing and $U_c$ is the convection velocity of the vortices. It is desired to calculate the response for two cases. For the first case, the forcing is assumed to be directly proportional to the velocity at the earlier time. Continuing with the notation of Appendix A

$$f(\dot{\eta}) = \frac{\omega_o}{Q}\dot{\eta} - B\dot{\eta}(t-\tau) \qquad (B.2)$$

where the first term is the damping and the second term is the forcing. B is the constant of proportionality between the response velocity and the driving force.

For the second case, the forcing amplitude is saturated but its phase is determined by the velocity at the earlier time. Thus,

$$f(\dot{\eta}) = \frac{\omega_o}{Q}\dot{\eta} - \frac{B_s\dot{\eta}(t-\tau)}{\dot{\eta}_{o-p}(t-\tau)} \qquad (B.3)$$

where $\dot{\eta}_{o-p}(t-\tau)$ is the amplitude of $\dot{\eta}(t-\tau)$. $B_s$ is the saturated value of the forcing function amplitude.

Returning to the first case, we substitute (A.3) into (B.2)

$$f = \frac{\omega_o^2}{Q}A\cos(\omega_o t+\phi) - B\omega_o A\cos\omega_o\tau \qquad (B.4)$$

This is substituted into (A.13)

$$\frac{dA}{dt} \approx -\frac{A\omega_o}{QT}\int_o^T \cos^2(\omega_o t+\phi)dt$$

$$+\frac{BA}{T}\int_o^T \cos(\omega_o t+\phi)\cos(\omega_o(t-\tau)+\phi)dt \qquad (B.5)$$

$$\frac{dA}{dt} \approx -\frac{A\omega_o}{2Q} + \frac{BA}{2}\cos\omega_o\tau \qquad (B.6)$$

This means the exponential growth rate is

$$\alpha \approx \frac{B}{2} \cos\omega_o\tau - \frac{\omega_o}{2Q} \qquad (B.7)$$

Note there is only growth when the forcing is greater than the damping. When (B.4) is substituted into (A.13) and the integrals are evaluated, the result is

$$\Delta\omega = \frac{d\phi}{dt} \approx - \frac{B}{2} \sin\omega_o\tau \qquad (B.8)$$

(B.7) and (B.8) imply that there is exponential growth with a frequency shift ($\omega = \omega_o + \Delta\omega$) determined entirely by the baffle spacing which fixes $\tau$. When $\tau$ is an integral multiple of the period, T, then the greatest growth rate occurs.

The saturated case yields results with some essential differences. When (B.3), with $\dot{\eta}$ replaced by (A.3), is substituted into (A.13) and the integral is evaluated, the following equation results:

$$\frac{dA}{dt} \approx - \frac{A\omega_o}{2Q} + \frac{B_s}{2\omega_o} \cos\omega_o\tau \qquad (B.9)$$

This equation corresponds to an exponential approach to a constant amplitude given by

$$A = \frac{B_s Q}{\omega_o^2} \cos\omega_o \tau \qquad (B.10)$$

The maximum amplitude occurs when $\tau = nT$ as expected, where n is an integer, and the amplitude is also greater for lightly damped systems (high Q). The frequency shift is found by substituting (B.3) into (A.14) and evaluating the integral

$$\Delta\omega = \frac{d\phi}{dt} \approx - \frac{B_s}{2\omega_o A(t)} \sin\omega_o \tau \qquad (B.11)$$

As the amplitude, A(t), grows, the frequency shift decreases to its final value when A(t) reaches the quantity given by (B.10):

$$\Delta\omega = - \frac{\omega_o}{2Q} \tan\omega_o \tau \qquad (B.12)$$

It can be seen that the frequency shift is less for high Q (low damping) systems. Thus, for such a system, the frequency remains close to the natural frequency of the oscillator in the absence of forcing. When $\tau = nT$, there is no frequency shift and the self-excited resonance occurs at the natural frequency of the oscillator.

# Appendix C

## ACOUSTIC MODEL

In this model, the acoustic response of the duct to a forcing function sinusoidal in time and localized in space is calculated using one-dimensional acoustics. The location at which the forcing is concentrated corresponds to the position of the downstream baffle. As vortices convect past this point, they induce pressures on the faces of the baffle resulting in a fluctuating force in the streamwise direction. By reaction, the baffles exert an equal and opposite force on the fluid. This force, which is calculated independently in Appendix E, is then assumed to act uniformly on the cross-sectional area of the duct. El-Raheb and Wagner (29) theoretically investigate the effect of blockage on the acoustic propagation in finite cylindrical cavities. They find that the resonant frequency is reduced most when the obstruction is located near a velocity antinode, as is the case in the present experiments. However, with the area ratio and blockage length used in the experiments, the maximum reduction is only about 5 per cent. Here, the geometric effect of the baffles on the acoustic response is completely ignored, although a more detailed calculation could include the effect.

C.1. Wave Equation.

The wave equation is found by starting with the one-dimensional continuity and momentum equations

$$\frac{\partial \rho}{\partial t}+\rho\frac{\partial u}{\partial x}+u\frac{\partial \rho}{\partial x} = 0 \qquad (C.1)$$

$$\frac{\partial u}{\partial t}+u\frac{\partial u}{\partial x} = -\frac{1}{\rho}\frac{\partial p}{\partial x}+\frac{1}{\rho}F \qquad (C.2)$$

where the effect of viscosity is neglected and $F/\rho$ is the force per unit mass acting in the x-direction. The variables are now replaced by mean and fluctuating values

$$\rho = \bar{\rho} + \rho' \qquad (C.3)$$

$$p = \bar{p} + p' \qquad (C.4)$$

$$u = \bar{u} + u' \qquad (C.5)$$

These are substituted into (C.1) and (C.2) with $\bar{u} = 0$ and terms of first order are retained

$$\frac{\partial \rho'}{\partial t} + \bar{\rho}\frac{\partial u'}{\partial x} = 0 \qquad (C.6)$$

$$\frac{\partial u'}{\partial t} + \frac{1}{\bar{\rho}}\frac{\partial p'}{\partial x} = -\frac{1}{\bar{\rho}}F'(x,t) \qquad (C.7)$$

The wave equation is now formed by substituting the following expressions for p', u', $\rho'$ in terms of the particle displacement, $\xi$, as in (19)

$$p' = -\bar{\rho}c^2\frac{\partial \xi}{\partial x} \qquad (C.8)$$

$$u' = \frac{\partial \xi}{\partial t} \qquad (C.9)$$

$$\rho' = -\bar{\rho}\frac{\partial \xi}{\partial x} \qquad (C.10)$$

where c is the speed of sound. When (C.9) and (C.10) are substituted, the continuity equation, (C.6), is satisfied identically. The momentum equation, (C.7), becomes

$$\frac{\partial \xi^2}{\partial t^2} - c^2\frac{\partial \xi^2}{\partial x^2} = \frac{1}{\bar{\rho}}F'(x,t) \qquad (C.11)$$

which is a wave equation with forcing.

The forcing function is idealized as acting at a point, $x_2$, corresponding to the location of the second baffle and is taken to be sinusoidal in time

$$F'(x,t) = F\delta(x-x_2)e^{i\omega t} \qquad (C.12)$$

where use is made of the complex notation to represent oscillating quantities and $\delta$ is the Dirac delta function.

C.2. Solution.

It is noted that the unforced wave equation holds except at the ends of the duct, $x = 0$ and $x = L$, and at the location of the forcing, $x = x_2$. Except at these points, the solution is just the sum of a right travelling wave (RTW) and a left travelling wave (LTW). Thus, there are four unknown (complex) amplitudes which must be determined. Two conditions are specified by the impedances of the duct endpoints. This is done by modeling the ends as pistons and calculating the effective impedance due to the radiation of acoustic energy. This is discussed briefly in Appendix D. At the location of the forcing, the two remaining conditions are determined by the continuity of the displacement, $\xi$, and the balance between the force and the jump in pressure which occurs since the force is a delta function.

The region between $x = 0$ and $x = x_2$ is labelled region 1, and that between $x = x_2$ and $x = L$, region 2. This is shown in Figure C.1. With the exception of $x_2$, subscripts 1 and 2 refer to regions 1 and 2. To take advantage of symmetry, the solutions in the two regions are written in terms of the distance from their respective ends towards the point $x_2$. Furthermore, in region 2, the variable y is defined as $y = L-x$ to make the notation simpler. The steady-state solution is thus

$$\xi_1 = A_1 e^{i(\omega t - kx)} + B_1 e^{i(\omega t + kx)} \qquad (C.13)$$

$$\xi_2 = A_2 e^{i(\omega t - ky)} + B_2 e^{i(\omega t + ky)} \qquad (C.14)$$

The 'A's are the amplitudes of waves travelling inward from the ends toward $x_2$. $A_1$ corresponds to a RTW, $A_2$, a LTW.

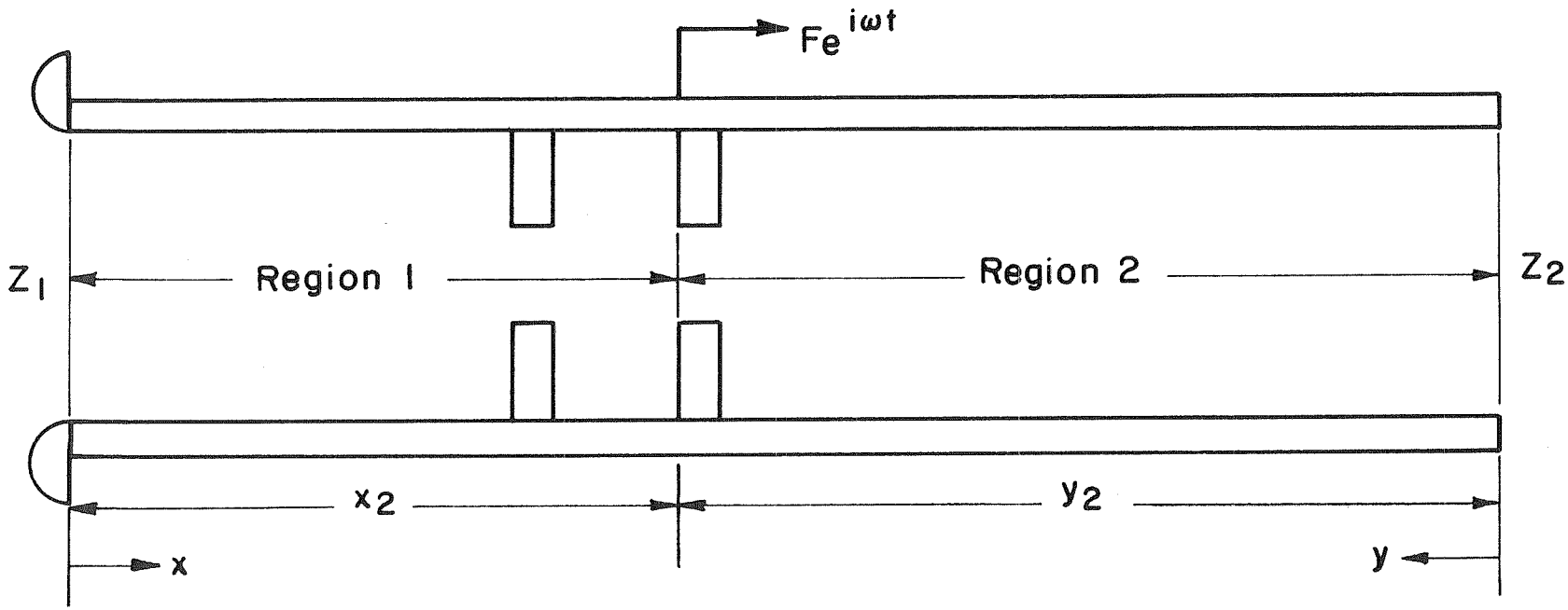


RTW: $A_1 e^{i(\omega t - kx)}$ →

LTW: $A_2 e^{i(\omega t - ky)}$ ←

LTW: $B_1 e^{i(\omega t + kx)}$ ←

RTW: $B_2 e^{i(\omega t + ky)}$ →

FIGURE C.1 ACOUSTIC MODEL CALCULATION REGIONS

Similarly, the 'B's correspond to waves travelling away from $x_2$.

## C.3. End Conditions.

The dimensionless impedance is defined by

$$Z = \frac{p'}{\bar{\rho}cu'} \qquad (C.15)$$

Thus, at x = 0,

$$Z_1 = \frac{p_1'}{\bar{\rho}cu_1'} \qquad (C.16)$$

The expression for $\xi_1$ (C.13) is substituted into (C.8) and (C.9), giving

$$p_1' = -\bar{\rho}c^2[-ikA_1e^{i(\omega t-kx)} + ikB_1e^{i(\omega t+kx)}] \qquad (C.17)$$

$$u_1' = i\omega[A_1e^{i(\omega t-kx)} + B_1e^{i(\omega t+kx)}] \qquad (C.18)$$

These are substituted into (C.16) and evaluated at x = 0 to give the condition

$$Z_1 = \frac{A_1-B_1}{A_1+B_1} \qquad (C.19)$$

where use has been made of the relation $\omega = kc$.
(C.19) is easily manipulated to give

$$B_1 = A_1 \frac{1-Z_1}{1+Z_1} \qquad (C.20)$$

A similar procedure at x = L gives

$$B_2 = A_2 \frac{1+Z_2}{1-Z_2} \qquad (C.21)$$

## C.4. Conditions at $x = x_2$.

The first condition at $x = x_2$ is that the displacement be continuous there $\xi_1(x_2) = \xi_2(x_2)$. That is,

$$A_1 e^{-ikx_2} + A_1 \frac{(1-Z_1)}{(1+Z_1)} e^{ikx_2} = A_2 e^{-iky_2} + A_2 \frac{(1-Z_2)}{(1+Z_2)} e^{iky_2} \qquad (C.22)$$

where $B_1$ and $B_2$ have been replaced by (C.20) and (C.21) and $Y_2 = L-x_2$. Use is made of the relation

$$e^{i\theta} = \cos\theta + i\sin\theta \qquad (C.23)$$

in order to simplify (C.22) to

$$\frac{A_1(2\ \cos kx_2 - 2iZ_1\ \sin kx_2)}{(1+Z_1)} = \frac{A_2(2\ \cos ky_2 + 2iZ_2\ \sin ky_2)}{(1-Z_2)} \qquad (C.24)$$

Rearrangement gives

$$A_2 = A_1 \frac{(1-Z_2)}{(1+Z_1)} \frac{(\ \cos kx_2 - iZ_1\ \sin kx_2)}{(\ \cos ky_2 + iZ_2\ \sin ky_2)} \qquad (C.25)$$

The second condition at $x = x_2$ is the balance between the force and the jump in pressure there:

$$p_2(x_2,t) - p_1(x_2,t) = \frac{F}{S}e^{i\omega t} \qquad (C.26)$$

F is the total force acting on the cross-sectional area of the duct, S. A non-dimensional force is defined in the following way

$$G \equiv \frac{F}{\bar{\rho}c^2 S} \qquad (C.27)$$

Using this and equation (C.8), the force balance condition becomes

$$G = \frac{\partial \xi_1}{\partial x} + \frac{\partial \xi_2}{\partial y} \qquad (C.28)$$

Performing the differentiation on (C.13) and (C.14) and evaluating at $x = x_2$ gives

$$G = -ik[A_1 e^{-ikx_2} - B_1 e^{ikx_2} + A_2 e^{-iky_2} - B_2 e^{iky_2}] \qquad (C.29)$$

After substituting for $B_1$ and $B_2$ in (C.20) and (C.21) and again making use of (C.23), this expression reduces to

$$G = \frac{-2kA_1(\sin kx_2 + iZ_1 \cos kx_2)}{(1+Z_1)} - \frac{2kA_2(\sin ky_2 - iZ_2 \cos ky_2)}{(1-Z_2)} \qquad (C.30)$$

$A_2$ is now replaced by (C.25) and the expression is multiplied by the denominator and expanded:

$$-\frac{G}{2k}(1+Z_1)(\ \cos ky_2 + iZ_2\ \sin ky_2) =$$
$$A_1(\ \sin kx_2+iZ_1\ \cos kx_2)(\ \cos ky_2+iZ_2\ \sin ky_2)$$
$$+\ A_1(\ \sin ky_2-iZ_2\ \cos ky_2)(\ \cos kx_2-iZ_1\ \sin kx_2) \qquad (C.31)$$

Recognizing the sine and cosine sum and difference expressions and using $x_2 + y_2 = L$, the right hand side of (C.31) simplifies to

$$A_1(1-Z_1Z_2)\sin kL + iA_1(Z_1-Z_2)\cos kL \qquad (C.32)$$

Thus, $A_1$ is given by

$$A_1 = G\frac{(1+Z_1)\quad(\ \cos ky_2 + iZ_2\ \sin ky_2)}{2k\quad((Z_1Z_2-1)\sin kL+i(Z_2-Z_1)\cos kL)} \qquad (C.33)$$

and the solution is completed when this is replaced in the expression for $\xi_1$ (C.13):

$$\xi_1 = \frac{Ge^{i\omega t}\ (\ \cos ky_2 + iZ_2\ \sin ky_2)}{k[(Z_1Z_2-1)\sin kL+i(Z_2-Z_1)\cos kL]}\ (\cos kx-iZ_1\sin kx) \qquad (C.34)$$

An entirely analogous procedure gives

$$\xi_2 = \frac{Ge^{i\omega t}\ (\ \cos kx_2 - iZ_1\ \sin kx_2)}{k[(Z_1Z_2-1)\sin kL+i(Z_2-Z_1)\cos kL]}\ (\cos ky+iZ_2\sin ky) \qquad (C.35)$$

valid in region 2.

The expressions (C.8) to (C.10) are used to obtain the corresponding equations for p', u', and $\rho'$.

## Appendix D

## ACOUSTIC RADIATION FROM ENDS OF DUCT

In Appendix C, the conditions at the ends of the duct are idealized as complex impedances. The procedure for finding $Z_1$ and $Z_2$ will be outlined here.

The air in the vicinity of the open ends of the duct moves in and out almost as a unit. The surrounding air outside the duct behaves almost as if the moving mass of air were a solid piston. Sound energy is radiated as would be by a solid piston, thus the pressure and velocity must be phased such that energy is extracted from the moving mass of air. The ratio of these two quantities is the effective impedance of the end of the duct and can be found by calculating the impedance of the equivalent piston.

The pressure at any point on the piston can be calculated by considering all other points on the piston as simple sources which radiate spherical acoustic waves as discussed in (19). By integrating the pressure over the area of the piston, the total force or the average pressure can be obtained. This integration is performed analytically for a circular piston in (19). The impedance of the piston is calculated by dividing the average fluctuating pressure by the fluctuating velocity, both expressed as complex quantities. When this is normalized by dividing by $\rho c$, the non-dimensional impedance, Z, is obtained. Z is a function of the frequency of oscillation and the diameter of the piston

$$Z(2kr_d) = R(2kr_d) + iX(2kr_d) \qquad (D.1)$$

where

$$R(x) = \frac{x^2}{2\cdot 4} - \frac{x^4}{2\cdot 4^2\cdot 6} - \frac{x^6}{2\cdot 4^2\cdot 6^2\cdot 8} - \cdots \qquad (D.2)$$

$$X(x) = \frac{4}{\pi}\left(\frac{x}{3} - \frac{x^3}{3^2\cdot 5} + \frac{x^5}{3^2\cdot 5^2\cdot 7} - \cdots\right) \qquad (D.3)$$

R is known as the piston resistance function and X as the piston reactance function (19). These functions are plotted in Figure D.1. The impedance of the end of an open tube of radius r· is assumed to be the same as the impedance of a piston of radius r·. This impedance is all that is needed to calculate the reflected waves within the tube due to the open end.

In the experimental apparatus, the exit is rectangular, not round. It is simply assumed that the impedance is the same as for a circular cross-section with the same area.

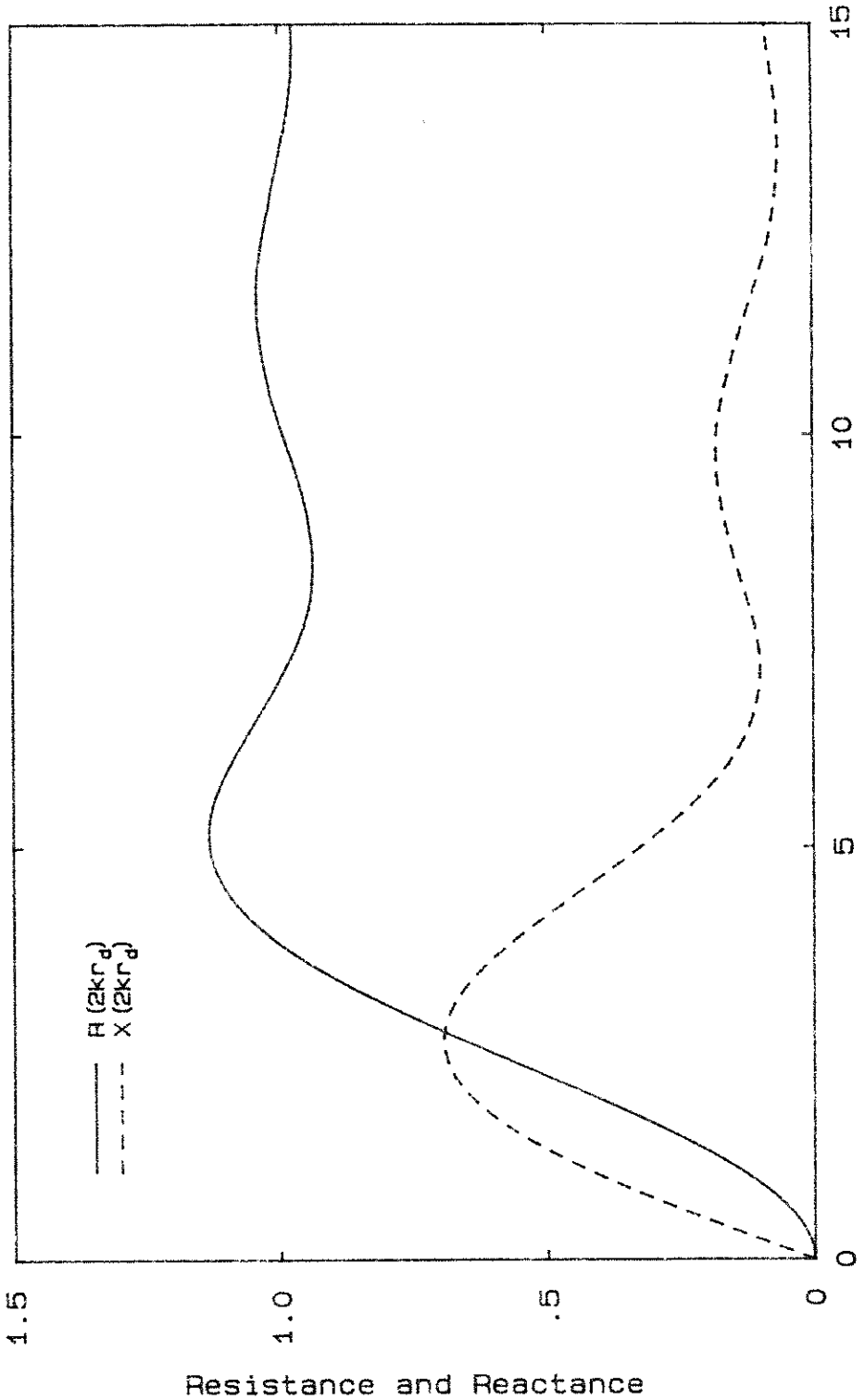


Figure D.1 Piston Functions

## Appendix E

## FORCE ON BAFFLE DUE TO MOTION OF VORTEX

As vortices are convected past, pressures act on the surface of the downstream baffle resulting in a fluctuating force in the streamwise direction. Since the fluid exerts a force on the baffle, by reaction the baffle exerts an equal and opposite force on the fluid. It is this force which is used as the driving function in the Acoustic Model, Appendix A. An analytic expression for this force is obtained here using a two-dimensional potential flow calculation.

In the experiments both rectangular and semi-circular baffles were used. These experiments indicate that the results are not much difference when different shaped baffles are used. Therefore, the calculation was performed only for the half-round configuration. For the rectangular geometry the Schwarz-Christoffel transformation could have been used but the calculation would have been more lengthy. It should be noted that the trajectory of a vortex in one plane does not transform directly into another plane (34). The circular geometry used permits direct use of the circle theorem and no transformation is necessary. This is the main reason for selecting the round configuration rather than the rectanglar shape for the calculation.

The flow field desired is that past a semi-circular hill on an infinite plane. A vortex embedded in the free-stream is carried past the hill, inducing a force on it. The boundary condition of no flow through the ground plane is enforced by calculating the flow in an unbounded fluid

but with two vortices convecting symmetrically past a circular cylinder. This is the standard method of using image vortices. The boundary condition on the cylinder is satisfied by using the circle theorem (34). This results in two more image vortices within the cylinder.

## E.1. Complex Potential Function.

The convention used here is $\bar{U} = \nabla\phi$. The stream function, $\psi$, is defined in the usual way. Letting z be the complex variable representing points in the plane and $z_o$ be the location of the vortex of strength $\Gamma$, the complex potential function is

$$w(z) = U(z+\frac{a^2}{z}) + i\Gamma[\ln(z-z_o)-\ln(z-z_o^*) - \ln(z-\frac{a^2}{z_o^*}) + \ln(z-\frac{a^2}{z_o}) - \ln(\frac{z_o^*}{z_o})] \qquad (E.1)$$

where a is the radius of the circle. The last term is a constant which arises in the manipulation of the preceding two terms from the form given by the application of the Circle Theorem.

## E.2. Blasius Theorem.

The force on the cylinder is obtained by using the Blasius Theorem (34):

$$X-iY = \frac{i}{2}\rho\int_c \left(\frac{dw}{dz}\right)^2 + i\rho\int_c \frac{\partial\phi}{\partial t}dz^* \qquad (E.2)$$

where the sign of the second term has been reversed to account for the difference in the definition of $\phi$ used in Milne-Thompson (34). X is the drag force on the cylinder, and Y is the lift. Due to symmetry, the total lift on the cylinder is zero and will provide a check on the calculation. The second term is cast in a more convenient form by recognizing that the stream function is an instantaneous constant, $\psi = c(t)$, on the contour of integration, the surface of the cylinder. Thus,

$$\frac{\partial w^*}{\partial t} = \frac{\partial\phi}{\partial t} - c'(t) \qquad (E.3)$$

When the instantaneous constant, c', is integrated, the result is zero. The Blasius Theorem then becomes

$$X-iY = \frac{i}{2}\rho\int_c \left(\frac{dw}{dz}\right)^2 dz + i\rho\int_c \frac{\partial w^*}{\partial t}dz^* \qquad (E.4)$$

which can be evaluated more readily.

## E.3. Vortex Velocity.

When the force on the cylinder is evaluated by substituting the complex potential function (E.1) into (E.4), the terms $\frac{dz_o}{dt}$ and $\frac{dz_o^*}{dt}$ will arise. These correspond to the motion of the vortex at $z_o$. The complex velocity of the the vortex is found by using the complex potential function (E.1) with the singularity due to the vortex at $z_o$ subtracted:

$$w_v(z) = w(z) - i\Gamma \ln(z - z_o) \qquad (E.5)$$

$$u_v - iv_v = \frac{dw_v}{dz}\bigg|_{z=z_o} = \frac{dz_o^*}{dt} \qquad (E.6)$$

This is evaluated to be

$$\frac{dz_o^*}{dt} = U - \frac{Ua^2}{z_o^2} + i\Gamma\left[\frac{-1}{(z_o - z_o^*)} - \frac{1}{(z_o - \frac{a^2}{z_o^*})} + \frac{1}{(z_o - \frac{a^2}{z_o})}\right] \qquad (E.7)$$

which depends only on the position of the vortex. The trajectory of the vortex is found by integrating this expression numerically.

## E.4. Evaluation of Force on Cylinder.

The integrands in (E.4) are found by performing the appropriate operations on (E.1). The integrals are then evaluated by using the Residue Theorem. The second integral is evaluated first. The complex conjugate of (E.1) is

$$w^* = U(z^* + \frac{a^2}{z^*}) - i\Gamma[\ln(z^* - z_o^*) - \ln(z^* - z_o) - \ln(z^* - \frac{a^2}{z_o}) + \ln(z^* - \frac{a^2}{z_o^*}) - \ln(\frac{z_o}{z_o^*})] \qquad (E.8)$$

The partial derivative is taken with respect to time to give

$$\frac{\partial w^*}{\partial t} = i\Gamma\left[\frac{-1}{(z^*-z_o)} + \frac{a^2}{z_o^2}\frac{1}{(z^*-\frac{a^2}{z_o})} + \frac{1}{z_o}\right]\frac{dz_o}{dt}$$

$$+ i\Gamma\left[\frac{1}{(z^*-z_o^*)} - \frac{a^2}{z_o^{*2}}\frac{1}{(z^*-\frac{a^2}{z_o^*})} - \frac{1}{z_o^*}\right]\frac{dz_o^*}{dt} \qquad (E.9)$$

The first term in each bracket has poles outside the contour of integration, $|z| = a$, and the last term in each bracket cancel one another. Only the remaining two terms contribute to give the result

$$\int\frac{\partial w^*}{\partial t}dz^* = -2\pi\Gamma\left[\frac{a^2 dz_o}{z_o^2\,dt} - \frac{a^2\,dz_o^*}{z_o^{*2}\,dt}\right] \qquad (E.10)$$

where $\frac{dz_o}{dt}$ is the complex vortex velocity discussed above.

The first integral in (E.4) is now evaluated. Differentiating (E.1) with respect to z gives

$$\frac{dw}{dz} = U-\frac{Ua^2}{z^2} + i\Gamma\left[\frac{1}{(z-z_o)} - \frac{1}{(z-z_o^*)} - \frac{1}{(z-\frac{a^2}{z_o^*})} + \frac{1}{(z-\frac{a^2}{z_o})}\right] \qquad (E.11)$$

The square of (E.11) is:

$$\left(\frac{dw}{dz}\right)^2 = U^2 + \frac{U^2a^2}{z^4} - \frac{\Gamma^2}{(z-z_o)^2} - \frac{\Gamma^2}{(z-z_o^*)^2} - \frac{\Gamma^2}{\left(z-\frac{a^2}{z_o^*}\right)^2} - \frac{\Gamma^2}{\left(z-\frac{a^2}{z_o}\right)^2}$$

$$- \frac{2U^2a^2}{z^2} + 2iU\Gamma\left[\frac{1}{(z-z_o)} - \frac{1}{(z-z_o^*)} - \frac{1}{\left(z-\frac{a^2}{z_o^*}\right)} + \frac{1}{\left(z-\frac{a^2}{z_o}\right)}\right]$$

$$+ 2iU\Gamma a^2\left[\frac{-1}{z^2(z-z_o)} + \frac{1}{z^2(z-z_o^*)} + \frac{1}{z^2\left(z-\frac{a^2}{z_o^*}\right)} - \frac{1}{z^2\left(z-\frac{a^2}{z_o}\right)}\right]$$

$$+ \frac{\Gamma^2}{(z-z_o)(z-z_o^*)} + \frac{\Gamma^2}{(z-z_o)\left(z-\frac{a^2}{z_o^*}\right)} - \frac{\Gamma^2}{(z-z_o)\left(z-\frac{a^2}{z_o}\right)}$$

$$- \frac{\Gamma^2}{(z-z_o^*)\left(z-\frac{a^2}{z_o^*}\right)} + \frac{\Gamma^2}{(z-z_o^*)\left(z-\frac{a^2}{z_o}\right)} + \frac{\Gamma^2}{\left(z-\frac{a^2}{z_o^*}\right)\left(z-\frac{a^2}{z_o}\right)} \qquad \text{(E.12)}$$

None of the first nine terms of the expression above contribute to the integral since their residues are zero or they have no singularity within the contour of the integration. The residues for the last two terms on the second line are $-2iU\Gamma$ and $+2iU\Gamma$ and therefore cancel each other. The four terms on the third line are all of the form requiring the use of partial fraction expansion to establish their residues. This is demonstrated explicitly for only the first of these.

$$\frac{-1}{z^2(z-z_o)} = \frac{A}{z} + \frac{B}{z^2} + \frac{C}{(z-z_o)} \qquad \text{(E.13)}$$

A common denominator is established and the numerators equated:

$$Az(z-z_o) + B(z-z_o) + Cz^2 = -1 \qquad (E.14)$$

Collecting terms:

$$(A + C)z^2 + (B - Az_o)z - Bz_o = -1 \qquad (E.15)$$

Equating coefficients of like powers of z gives

$$B = \frac{1}{z_o}, \quad A = \frac{1}{z_o^2}, \quad C = -\frac{1}{z_o^2} \qquad (E.16)$$

The residue of this term is $2i\mathrm{U}\Gamma a^2 A = 2i\mathrm{U}\Gamma a^2/z_o^2$. The next term has residue $-2i\mathrm{U}\Gamma a^2/z_o^{*2}$. Each of the following two terms has contributions from both A and C in the partial fraction expansion and since A = -C their total contribution is zero.

A two-term partial fraction expansion is used to evaluate the residues of the remaining six terms of (E.12). The first term has no singularity within the contour and the sixth has two residues which cancel. The remaining four each contribute a term to give

$$-\frac{\Gamma^2}{(z_o-\frac{a^2}{z_o^*})} + \frac{\Gamma^2}{(z_o-\frac{a^2}{z_o})} + \frac{\Gamma^2}{(z_o^*-\frac{a^2}{z_o^*})} - \frac{\Gamma^2}{(z_o^*-\frac{a^2}{z_o})} \qquad (E.17)$$

After some manipulation, a common denominator is established and this combination is re-written more compactly as

$$\frac{-\Gamma^2 a^2 (z_o^2 - z_o^{*2})(z_o - z_o^*)}{(z_o^2 - a^2)(z_o^{*2} - a^2)(z_o z_o^* - a^2)} \qquad \text{(E.18)}$$

When all the contributions are collected, the force on the cylinder is given by

$$X - iY = 2\pi a^2 \rho U \Gamma i \left(\frac{1}{z_o^2} - \frac{1}{z_o^{*2}}\right) + \frac{\pi a^2 \rho \Gamma^2 (z_o^2 - z_o^{*2})(z_o - z_o^*)}{(z_o^2 - a^2)(z_o^{*2} - a^2)(z_o z_o^* - a^2)} + 2\pi a^2 \rho \Gamma i \left(\frac{1}{z_o^2}\frac{dz_o}{dt} - \frac{1}{z_o^{*2}}\frac{dz_o^*}{dt}\right) \qquad \text{(E.19)}$$

The first and last terms can be combined to give

$$X - iY = 2\pi a^2 \rho \Gamma i \left(\frac{U + U_v}{z_o^2} - \frac{U + U_v^*}{z_o^{*2}}\right) + \frac{\pi a^2 \rho \Gamma^2 (z_o^2 - z_o^{*2})(z_o - z_o^*)}{(z_o^2 - a^2)(z_o^{*2} - a^2)(z_o z_o^* - a^2)} \qquad \text{(E.20)}$$

It is noted that since anything minus its conjugate is pure imaginary and anything multiplied by its conjugate is pure real the above expression is pure real. The Y force is zero as it should be from symmetry.

The drag on the cylinder depends only on the instantaneous position of the vortex which is found by integrating the vortex velocity, $U_v$, as given by the conjugate of (E.7). This is done numerically, the drag being calculated for each position, and is plotted in figure E.1. Four cases are shown corresponding to differing points of release of the vortex. It can be seen that for trajectories passing closer to the cylinder, the drag force is greater and that the trajectories are symmetric upstream and downstream of the cylinder as expected. The drag on the cylinder is negative when the vortex is upstream and positive when it is downstream. This is associated with the reduction of pressure at the core of a vortex. The magnitude of the drag force is calculated for typical values occurring in the apparatus and agrees well with measurements of pressures on corners due to vortex passage made by Tang (35).

For realistic values, the trajectory of the vortex differs only by about a tenth of a percent from the trajectory that would result if the vortex had zero strength. For a calculation which must be repeated many times, this could lead to considerable savings. Similarly, for realistic values, the second term of the drag force (E.20) is also negligible compared with the first and could easily be omitted.

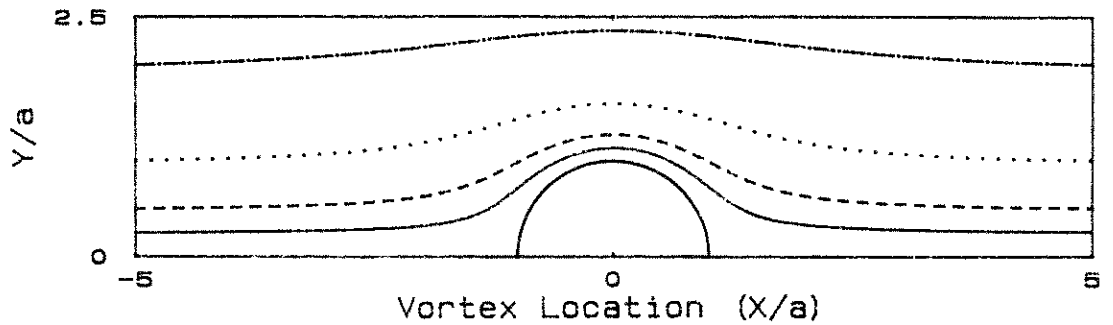


Trajectories of Vortices

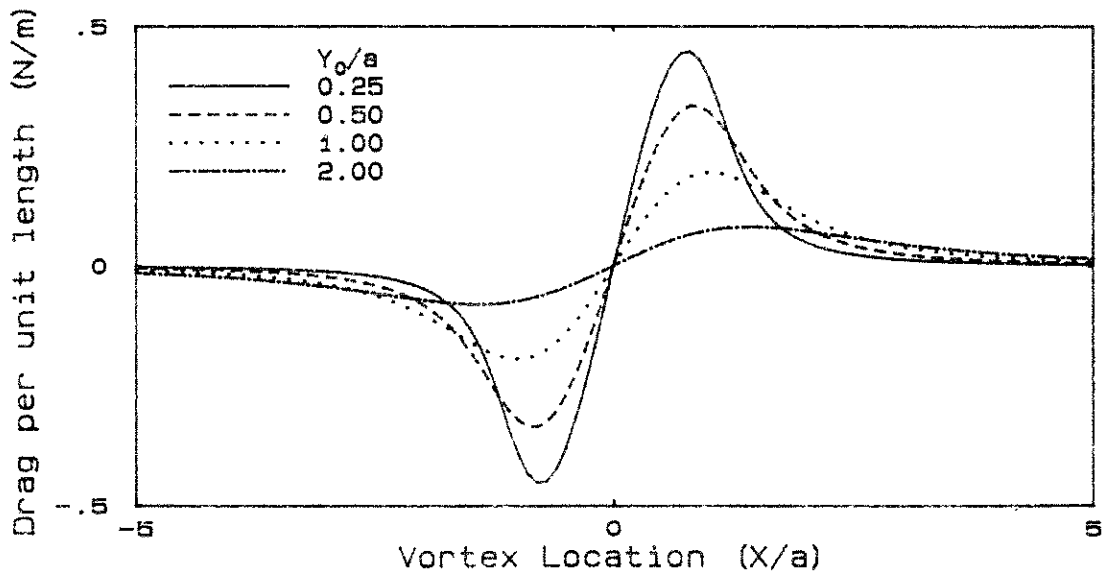


Drag on Baffle due to Vortex

Fig E.1 Effect of Initial Vortex Offset

# Appendix F

## FORTRAN LISTING OF PROGRAM

```
c      Kim Aaron                                          May 1985
c      program to calculate quasi-steady response of duct
c      due to mean flow past baffles internal to duct.
c      mag of perturbation vel is set = response vel.
c      freq is iterated at each step to give zero phase
c      as usual

       complex uout,G
       common x1,x2,Uinf,theta,pi,G,S,istage
       character outfil*15,dummy*1
       outfil='quasi.out'

       pi=4.0*atan(1.0) ! pi ~ 3.14159
       conv=180./pi     ! to convert radians to degrees

       open(unit=4,type='new',name=outfil)
       write(4,*)'        freq              Uinf       ',
      .'G          x1          x2'
       write(4,*)' '
       close (unit=4)

100    write(5,*)'Enter acoustic mode desired, 0 to quit'
       read(5,*) mode ! mode = # half-wavelengths in duct
       if(mode.eq.0)  stop

       write(5,*)'Enter istage (# vortices)'
       read(5,*) istage

c  call model once only to calculate sines and cosines.
c  rest of time use entry point mod.
       call model(295.,0.1,uout)    ! (dummy variables)

       write(5,*)'Enter initial perturbation vel'
       read(5,*) unew

       write(5,*)'Enter initial frequency'
       read(5,*)fguess

       fnew=fguess*float(mode) ! initial guess at freq (Hz)
       write(5,*)'Enter Uinf'
       read(5,*)Uinf
       write(5,*)'Enter x1/m, x2/m'
       read(5,*)x1,x2

       theta=0.0005*SQRT(13./Uinf)
       ! assume 1/sqrt dependence; use experimental values

       open(unit=4,type='old',name=outfil) ! open file
11     read(4,12,end=13)dummy              ! read to end
12     format(a1)                          !
       goto 11                             !
13     continue
```

```
10    write(5,*)'Iterate on freq:'

      fold=0.999*fnew
      call mod(fold,unew,uout)
      aold=arg(uout)

c  use entry point mod in model:
1     call mod(fnew,unew,uout)
      anew=arg(uout) ! phase angle of output velocity

      write(5,40)fnew,anew*conv
40    format('+'f10.4,' arg = ',f11.6,' degrees')

      if (abs(anew).lt.0.0001) goto 2 ! converged

c  secant method to find zero of a function:
      ftemp=fnew
      fnew=(fold*anew-fnew*aold)/(anew-aold)
      if ((fnew-ftemp).gt.10.) fnew=ftemp+10.
      if ((fnew-ftemp).lt.-10.) fnew=ftemp-10.
           ! limit change in freq to 10 Hz
      fold=ftemp
      aold=anew
      goto 1

2     write(5,*)'Update u:'

3     call mod(fnew,unew,uout)  ! use entry point mod

      write(5,50)unew,cabs(uout)
50    format('+',2(f11.6,2x))

      if(cabs(uout-unew).le.0.0005*cabs(uout)) goto 88
c                                (converged within .05%)

      unew=cabs(uout)

4     goto 10

88    write(4,*)fnew,Uinf,cabs(G),x1,x2
      write(4,*)' '
      close(unit=4)
      goto 100        ! do another
      end
```

```
      subroutine model(freq,cin,c2out)

c  DECLARATION STATEMENTS:

      complex cmplx,conjg,i,zv,zo,zos,zo2,dzo,zinit,Uv,Uvs
      complex z1,z2,den,num1,Zimped,c2out,Dequiv,G
      parameter m=100       ! Number of steps per period
      complex circle(0:m)   ! sine and cosine for equivalent
                            ! drag calculation
      real L,Lrd,k,kL,klmx2
      logical satflg
      common x1,x2,Uinf,theta,pi,G,S,istage

c  SET UP SINES AND COSINES FOR EQUIVALENT DRAG CALCULATION:

      rm=float(m)             ! real equivalent of m
      do 5 j=0,m
      rj=float(j)             ! real equivalent of j
      argmnt=2.0*pi*rj/rm     ! arg for sines and cosines
      circle(j)=cmplx(sin(argmnt),cos(argmnt))
5     continue

c  CONSTANTS:

      i=(0.0,1.0)           ! SQRT (-1)
      c=343                 ! speed of sound (m/s)
      rho=1.21              ! density (kg/m**3)
      rb=0.0127             ! radius of downstream baffle (m)
      rb2=rb**2             ! rb squared (m**2)
      L=0.5                 ! duct length (m)
      w=0.15                ! duct width (m)
      h=0.05                ! duct height (m)
      rd=sqrt(w*h/pi)       ! duct radius with same area
      Lrd=L/rd              ! length to radius of duct
      m2s=2*istage*m        ! number of time steps sufficient
                            ! to get vortex well downstream

      return
```

```
      entry mod(freq,cin,c2out)

      c2=cin                ! don't change cin in subroutine
      xv=(x1-x2)            ! initial location of vortex wrt
                            ! downstream baffle (m)
      yv=rb                 ! intital y location of vortex (m)
      zv=cmplx(xv,yv)       ! initial vortex position (m,m)
      omega=2*pi*freq       ! angular freq (rad/s)
      tau=1./freq           ! period of oscillation (s)
      dt=tau/float(m)       ! time increment (s)
      k=omega/c             ! wavenumber (rad/m)
      kL=k*L                ! k x duct length (radians)
      zo=zv                 ! initial vortex location
      S=freq*theta/Uinf     ! Strouhal Number
      call poly(S,4,alpha,cmax,c1c2,ucuinf)
      csatn = Uinf*10.**(cmax)  ! satn value of c2 (m/s)
      Uc=Uinf*ucuinf        ! Convection velocity (m/s)
      Dequiv=0.0            ! reset Drag accumulator
      G=(0.0,0.0)           ! reset forcing amplitude
      jcirc=-1              ! reset counter
      satflg = .FALSE.      ! flag = true when c2 saturates
      gamc=Uc/(freq*pi*pi) ! constant for gamma calculation

c SHEAR LAYER DEVELOPMENT AND DRAG ON BAFFLE AT X2

      do 10 j=0,m2s
      jcirc=jcirc+1
      if (jcirc.eq.m) jcirc=jcirc-m
      c1=c1c2*c2            ! Velocity peak on lo speed side
      Gam=gamc*(c1+c2)/2.   ! Vortex strength
      zo2=zo*zo             ! zo**2
      xo=real(zo)           ! Vortex location (m)
      yo=aimag(zo)          !                 (m)
      zos=conjg(zo)
      r1=2.*pi*rb2*rho*Gam  ! Constants used in drag calc.
      r2=pi*rb2*rho*Gam*Gam !
      Uvs=Uc*(1.0-rb2/zo2)  ! approximate version;
c   remove comment on next line for full version:
c*    Uvs=Uc*(1.0-rb2/zo2)+i*Gam*(1.0/(zo-rb2/zo)
c*   .-1.0/(zo-rb2/zos)-1.0/(zo-zos))     ! full version
      Uv=conjg(Uvs)         ! velocity of vortex (m/s)
      D1=-r1*(2.*aimag((Uc+Uv)/zo2))  ! major portion
      D2=0.0    ! approximate version
c*    D2=-r2*(2*aimag(zo2)*(2.*yo))/  ! correction term
c*   .       ((cabs(zo2-rb2))**2*(cabs(zo2)-rb2))
      D=D1+D2           ! Total Drag           (N/m)
      Dequiv=Dequiv+D*circle(jcirc)
```

```
c  Calculate new values:

      dzo=Uv*dt
      zo=zo+dzo                    ! New vortex location (m,m)
      dx=real(dzo)
      if (satflg) goto 10 ! if saturated before, skip section

      c2=c2*exp(alpha*dx/theta) ! (m/s) growth ratio per dx
      if (c2.le.csatn) goto 10  ! amplitude saturated?

c Saturated for first time:

      satflg=.TRUE.
      c2=csatn

10    continue

c  ACOUSTIC SECTION:

c Non-dimensional complex force; includes phase wrt t=0:
      G=2.0*Dequiv/(rm*h*rho*c*c)
      z2=Zimped(2.0*k*rd) ! duct exit acoustic impedance
      z1=-z2              ! duct entrance acoustic impedance
      klmx2=k*(L-x2)
      den=(z1*z2-1.0)*sin(kL) + i*(z2-z1)*cos(kL)
      num1=G*(cos(kLmx2) + i*z2*sin(kLmx2))
      c2out=c*(z1*sin(k*x1)+i*cos(k*x1))*num1/den

      return
      end
```

```
      subroutine poly(x,m,y)
      dimension a(7,4),y(4)

c  FREYMUTH'S DATA:

c  Matrix of coefficients of 4 polynomials fit
c  to Freymuth' data:
c  1) growth rate; 2) c2 sat'n ampl.; 3) c1/c2;
c  4) phase velocity (Uc/Uinf)

      data a/-5.0388277e-4,4.281727,1159.177,-120072.9,
     +4566421.0,-8.0925136e7,5.5069203e8,
     +-1.674993,317.6765,-31970.39,1243078.0,-1.9311138e7,2*0.0,
     +7.9464465e-2,4.53495,996.4305,4*0.0,
     +0.9025712,-38.00021,1193.581,-12376.64,3*0.0/

      do 1 j=1,m
1     y(j)=0.0              ! initialize ys
      xj=1.0                ! x**0
      do 3 i=1,7            ! 7=#coefs in polynomial fits
      do 2 j=1,m            ! m=#polynomials being evaluated
2     y(j)=y(j)+a(i,j)*xj   ! coef*power of x
3     xj=xj*x               ! next power of x
      return
      end




      function arg(z)
      complex z
      arg=atan2(aimag(z),real(z))  ! find argument of complex
      return                       ! quantity
      end
```

```
      function Zimped(y)

c  Piston impedance function.  Z=R+iX  Series solution in
c  Kinsler and Frey, Fundamentals of Acoustics (ref 19)
c  page 178

      complex Zimped,cmplx
      integer rflag,xflag

      y2=y*y                  ! square of argument
      pi=4.0*atan(1.0)

      rflag=0
      xflag=0

      R=y2/8.0                ! Resistance
      X=4.0*y/3./pi           ! Reactance

      j=1

      Rterm=R                 ! term in series approx.
      Xterm=X                 ! term in series approx.

1     j=j+1

      if (abs(Rterm).lt.0.01) Rflag=1   !
      if (Rflag.eq.1) goto 5            ! R series converged

      den=float(4*j*(j+1))
      Rterm=-Rterm*y2/den   ! Previous x Rterm/den = present
      R=R+Rterm             ! sum

5     if (abs(Xterm).lt.0.01)Xflag=1    !
      if (Xflag.eq.1) goto 10           ! X series converged

      den=float((2*j-1)*(2*j+1))
      Xterm=-Xterm*y2/den
      X=X+Xterm

      goto 1                      ! X series not yet converged

10    if (Rflag.eq.0) goto 1      ! R series not yet converged

      Zimped=cmplx(R,X)
      return                      ! Both series converged
      end
```